UNIVERSITY OF CALIFORNIA
SANTA CRUZ

MODELING OF COASTAL PROCESSES AND LAGRANGIAN TRANSPORT AROUND THE MONTEREY PENINSULA

A dissertation submitted in partial satisfaction
of the requirements for the degree of

DOCTOR OF PHILOSOPHY

in

OCEAN SCIENCES

by

Anna B. Lowe

September 2020

The Dissertation of Anna B. Lowe is approved:

_____
Professor Christopher A. Edwards, chair

_____
Professor Mark H. Carr

_____
Professor Andrew M. Moore

_____
Quentin Williams
Acting Vice Provost and Dean of Graduate Studies

TABLE OF CONTENTS

ABSTRACT

MODELING OF COASTAL PROCESSES AND LAGRANGIAN TRANSPORT AROUND THE MONTEREY PENINSULA

by Anna B. Lowe

The Monterey Peninsula is an ecologically important area, highlighted by numerous marine protected areas (MPAs), but little is known about the specific circulation processes that support its species-rich ecosystems. This suite of research used the Regional Ocean Modeling System (ROMS) to simulate the circulation during the 2014 and 2015 spring/summer upwelling seasons through a series of nested grids to resolve the circulation on the central California coast at approximately 120 m resolution. A particle tracking model, OpenDrift, calculated Lagrangian trajectories to identify source water and simulate near-surface larval transport. We examine the circulation patterns and temperature structure in Carmel Bay, a small embayment in the lee of the Monterey Peninsula. We explore mechanisms driving local population connectivity: self-recruitment and connectivity between populations ~10 km apart by simulating transport of kelp rockfish (*Sebastes atrovirens*) larvae from populations in southwest Monterey Bay and Carmel Bay. We characterize submesoscale sea surface temperature (SST) fronts off the southern edge of the Monterey Peninsula by strain, that generate different Lagrangian transport patterns. Collectively, these results demonstrate that nearby populations (and thus MPAs) do

not have homologous recruitment or exchange, which has important implications for MPA management, and how this heterogeneity results from dynamic circulation processes.

ACKNOWLEDGEMENTS

I want to thank my committee for your mentorship, and transforming me from a book-smart student into an oceanographer and modeler

- A very special thank you to, Chris, for always being a wonderful advisor and person, for your commitment to detail and eagerness to teach. Thank you for your kindness, assurance, and gracefully pushing me. When I applied to UCSC years ago, I had no idea how lucky I would be to learn from you.
- Thank you, Mark, for your positive energy and contagious enthusiasm. I left every meeting jazzed about our research and with a multitude of ideas for future projects.
- Thank you, Andy, for helpful discussion and constant cheer.

Thank you to the UCSC Modeling Group for your support, interesting discussion, and community. In particular, thank you, Jann Paul Mattern, for your friendship and SCUBA diving adventures, mentorship, and teaching Python coding to me.

Thank you to my unexpected best friend, Elisha Henry, for your understanding kindness, laughter, and encouragement. I am grateful that we were able to support one another throughout this PhD process, even from opposite coasts.

Thank you to my family.
Thank you, Zach, for your easy-going demeanor and putting things in perspective.
Thank you, Haley, for your unwavering support and many phone calls over the years.
Thank you, Mom, for your ‘go-getter’ attitude mixed with compassion and understanding. Thank you for all the experiences you have given me and encouraged me to pursue.
Thank you, Dad, for showing your steadfast belief in me and active encouragement of my dreams.

CHAPTER ONE
INTRODUCTION

Physical processes transporting larvae span spatial scales of meters to hundreds of kilometers and temporal scales of hours to years (reviewed in Carr et al., 2011). At the larger and longer end of this spectrum, propagules may be transported by oceanographic currents resulting from the large scale mean flow and transient motions associated with eddies, wind-driven upwelling, and tides. In addition, propagules may encounter small-scale currents, fronts, and turbulence that locally modify transport. During the pelagic phase, the unique blend of coastal transport processes leads to a diverse set of larval trajectories and, in turn, potential settlement locations.

The geographic settlement distribution is often embodied statistically by a dispersal kernel, which provides the probability that a propagule settles at various distances from its origination location. Dispersal kernels may vary between species depending on differing larval traits and behavioral strategies that utilize different processes for transport and delivery to suitable habitat (Largier 2003). For example, larvae released in winter generally inhabit different ocean conditions (e.g., currents, mixed layer depth) than those that spawn in summer. Substantial vertical shear in ocean currents causes naturally buoyant larvae (or those that swim toward the surface) to experience quite different transport directions than those that reside beneath the surface mixed layer or deeper. Some organisms may be adapted to utilize behavior that reduces dispersal distances and increase local recruitment (Miller and Morgan 2013; Morgan 2014; Drake et al. 2018). While the suitable habitat criteria and distribution are largely known for many species, questions prevail about how the

recruits develop and are transported by coastal processes during the pelagic phase. Dispersal distance matters because it directly relates to connectivity between near and far habitat regions.

The state of California uses a network of marine protected areas (MPAs) for marine conservation. This network is designed to make the entire marine ecosystem more resilient by protecting small, biologically-rich segments of the coast. To do this, the MPA network protects source populations and relies on self-recruitment and connectivity between MPAs to sustain populations. Some of the larvae released within MPAs settle outside in non-protected areas, commonly referred to as the "spillover effect". The proportion of self-recruitment, connectivity between neighboring MPAs, and the "spillover effect" remains unknown. This dissertation investigates coastal processes that influence larval transport and thereby settlement distribution on the US west coast.

As an eastern boundary upwelling system, wind-driven coastal upwelling along the U.S. west coast from Point Conception through Oregon is the dominant process driving circulation during spring and summer (e.g., Huyer 1983; Hickey 1998). Yet the region experiences considerable alongshore heterogeneity associated with variations in that wind forcing and, more importantly, alongshore bathymetry and coastline shape. Enhancement of upwelling near promontories such as Cape Blanco, Cape Mendocino, and Point Sur are well known (Hickey 1998; Breaker and Mooers 1986; Rosenfeld et al. 1994), but less well studied are circulation features associated with embayments in the coastline.

On the central California coast, Carmel Bay is located between two coastal promontories: (1) Monterey Peninsula and (2) Point Lobos. Chapter 2 describes the circulation within and just outside this small, but species-rich embayment. Extending only about 3 km in the alongshore direction and even less cross-shore, Carmel Bay experiences strong surface forcing that is strongly influenced by the local terrain. The rocky reefs and kelp forest ecosystems within Carmel Bay have been chosen for numerous studies on macroalgae (e.g., Reed and Foster 1984; Graham 1997), invertebrates (e.g. Wobber 1975; Kenner 1992; Clark et al. 2004), and fishes (e.g., Hallacher and Roberts 1985; Carr 1991; Johnson 2006a,b; Johnson 2007; Green and Starr 2011; Green et al. 2014). Despite numerous ecologically-focused studies, only one study (Carroll 2009) documents the physical environment supporting these ecosystems. This chapter describes the circulation patterns driven by the alongshore wind and semidiurnal tides, and source waters to the bay.

Chapter 3 builds on the previous chapter and investigates larval transport between southwest Monterey Bay and Carmel Bay. Compiling the rich-literature on larval transport and connectivity, indicates the paradigm has shifted (reviewed in Levin 2006; Cowen and Sponaugle 2009). Marine populations that were thought to be 'open' with ubiquitous exchange of larvae has largely shifted towards 'closed' populations that rely primarily on self-recruitment and nearby sources of larvae to sustain that population (Cowen et al. 2000; Drake, Edwards, and Barth 2011; Morgan et al. 2018). Although marine habitats receive larvae from near and distant sources, this study is designed to investigate local connectivity between larval sources separated by only a few kilometers, similar to the network of MPAs. This study

enables multiple spatial scales by using a model that covers a large spatial domain to allow potentially faraway transport to return to the region and recruit, but with grid dimensions that resolve submesoscale and coastal dynamics that transport larvae.

Lastly, chapter 4 investigates submesoscale fronts off the Monterey Peninsula. Fronts describe the interface between two water masses often defined by a large gradient between water properties (e.g., temperature or salinity). Observational studies often describe fronts as biological oases (Lévy et al. 2012; Woodson et al. 2012; Woodson and Litvin 2015; Lévy et al. 2018) because the circulation aggregates plankton (Wolanski and Hamner 1988; Russell et al. 1999) and larvae with limited swimming abilities (Bjorkstedt et al. 2002; Genin et al. 2005), which then attracts larger predators (Snyder et al. 2017; Sims and Quayle 1998; Russell et al. 1999; Siegelman et al. 2019). Submesoscale fronts are sharp, rapidly morphing, ephemeral features about 0.1-10 km long that last hours to days (McWilliams 2016). Therefore, modeling studies enable detailed investigation of these features that observational studies cannot. Despite being aggregation features associated with enhanced larval recruitment (Woodson et al. 2012), fronts are also known for high current velocities and to transport material (Dauhajre et al. 2017; Gula et al. 2014; Romero et al. 2016; Harrison et al. 2013). Through the biophysical lens of this dissertation, this chapter focuses on near-surface transport of material near fronts. Fronts are separated into two categories by their strain squared percentage, which result in different Lagrangain transport patterns that have important implications for larval recruitment and connectivity.

This suite of research delves into the details of the coastal circulation processes that have an impact on larval transport near the Monterey Peninsula. For this research, we built a realistically configured, high resolution numerical model that simulates the circulation during the spring and summers of 2014 and 2015.

REFERENCES

Bjorkstedt, Eric P., Leslie K. Rosenfeld, Brian A. Grantham, Yehoshua Shkedy, and Joan Roughgarden. 2002. "Distributions of Larval Rockfishes Sebastes Spp. across Nearshore Fronts in a Coastal Upwelling Region." *Marine Ecology Progress Series*. https://doi.org/10.3354/meps242215.

Breaker, Laurence C., and Christopher N.K. Mooers. 1986. "Oceanic Variability off the Central California Coast." *Progress in Oceanography*. https://doi.org/10.1016/0079-6611(86)90025-X.

Carr, Mark H. 1991. "Habitat Selection and Recruitment of an Assemblage of Temperate Zone Reef Fishes." *Journal of Experimental Marine Biology and Ecology* 146: 113–37. https://doi.org/10.1016/0022-0981(91)90257-W.

Carr, Mark H., Clifton B. Woodson, Olivia M. Cheriton, Daniel Malone, Margaret A. McManus, and Peter T. Raimondi. 2011. "Knowledge through Partnerships: Integrating Marine Protected Area Monitoring and Ocean Observing Systems." *Frontiers in Ecology and the Environment*. https://doi.org/10.1890/090096.

Carroll, Dustin. 2009. "Carmel Bay : Oceanographic Dynamics and Nutrient Transport in a Small Embayment of the Central California Coast ." *Master's Thesis*. California State University, Monterey Bay.

Clark, R. P., M. S. Edwards, and M. S. Foster. 2004. "Effects of Shade from Multiple Kelp Canopies on an Understory Algal Assemblage." *Marine Ecology Progress Series* 267: 107–19. https://doi.org/10.3354/meps267107.

Cowen, Robert K., Kamazima M.M. Lwiza, Su Sponaugle, Claire B. Paris, and Donald B. Olson. 2000. "Connectivity of Marine Populations: Open or Closed?" *Science*. https://doi.org/10.1126/science.287.5454.857.

Cowen, Robert K., and Su Sponaugle. 2009. "Larval Dispersal and Marine Population Connectivity." *Annual Review of Marine Science*. https://doi.org/10.1146/annurev.marine.010908.163757.

Dauhajre, Daniel P., James C. McWilliams, and Yusuke Uchiyama. 2017. "Submesoscale Coherent Structures on the Continental Shelf." *Journal of Physical Oceanography*. https://doi.org/10.1175/JPO-D-16-0270.1.

Drake, Patrick T., Christopher A. Edwards, and John A. Barth. 2011. "Dispersion and Connectivity Estimates along the U.S. West Coast from a Realistic Numerical Model." *Journal of Marine Research*. https://doi.org/10.1357/002224011798147615.

Drake, Patrick T., Christopher A. Edwards, Steven G. Morgan, and Erin V. Satterthwaite. 2018. “Shoreward Swimming Boosts Modeled Nearshore Larval Supply and Pelagic Connectivity in a Coastal Upwelling Region.” *Journal of Marine Systems* 187: 96–110. https://doi.org/10.1016/j.jmarsys.2018.07.004.

Genin, Amatzia, Jules S. Jaffe, Ruth Reef, Claudio Richter, and Peter J. S. Franks. 2005. “Swimming Against the Flow: A Mechanism of Zooplankton Aggregation.” *Science* 308 (5723): 860–62.

Graham, Michael H. 1997. “Factors Determining the Upper Limit of Giant Kelp, Macrocystispyrifera Agardh, along the Monterey Peninsula, Central California, USA.” *Journal of Experimental Marine Biology and Ecology* 218 (1): 127–49. https://doi.org/10.1016/S0022-0981(97)00072-5.

Green, Kristen M., Ashley P. Greenley, and Richard M. Starr. 2014. “Movements of Blue Rockfish (Sebastes Mystinus) off Central California with Comparisons to Similar Species.” *PLoS ONE*. https://doi.org/10.1371/journal.pone.0098976.

Green, Kristen M., and Richard M. Starr. 2011. “Movements of Small Adult Black Rockfish: Implications for the Design of MPAs.” *Marine Ecology Progress Series*. https://doi.org/10.3354/meps09263.

Gula, Jonathan, Jeroen J. Molemaker, and James C. Mcwilliams. 2014. “Submesoscale Cold Filaments in the Gulf Stream.” *Journal of Physical Oceanography*. https://doi.org/10.1175/JPO-D-14-0029.1.

Hallacher, Leon E., and Dale A. Roberts. 1985. “Differential Utilization of Space and Food by the Inshore Rockfishes (Scorpaenidae: Sebastes) of Carmel Bay, California.” *Environmental Biology of Fishes*. https://doi.org/10.1007/BF00002762.

Harrison, Cheryl S., David A. Siegel, and Satoshi Mitarai. 2013. “Filamentation and Eddy-Eddy Interactions in Marine Larval Accumulation and Transport.” *Marine Ecology Progress Series*. https://doi.org/10.3354/meps10061.

Hickey, Barbara M. 1998. “Coastal Oceanography of Western North America from the Tip of Baja California to Vancouver Island.” In *The Sea*, edited by Allan R. Robinson and Kenneth H. Brink, 11th ed., 345–93. John Wiley & Sons, Inc. https://books.google.com/books?hl=en&lr=&id=-uhTulqFRIgC&oi=fnd&pg=PA345&ots=17YWMPqbCw&sig=TptPd-1kvWE38CKRdz4M5NtEDXo#v=onepage&q&f=false.

Huyer, Adriana. 1983. “Coastal Upwelling in the California Current System.” *Progress in Oceanography*. https://doi.org/10.1016/0079-6611(83)90010-1.

Johnson, Darren W. 2006a. “Density Dependence in Marine Fish Populations Revealed at Small and Large Spatial Scales.” *Ecology* 87 (2): 319–25. https://doi.org/10.1890/04-1665.

———. 2006b. “Predation, Habitat Complexity, and Variation in Density-Dependent Mortality of Temperate Reef Fishes.” *Ecology* 87 (5): 1179–88. https://doi.org/10.1890/0012-9658(2006)87[1179:PHCAVI]2.0.CO;2.

———. 2007. “Habitat Complexity Modifies Post-Settlement Mortality and Recruitment Dynamics of a Marine Fish.” *Ecology* 88 (7): 1716–25. https://doi.org/10.1890/06-0591.1.

Kenner, M. C. 1992. “Population Dynamics of the Sea Urchin Strongylocentrotus Purpuratus in a Central California Kelp Forest: Recruitment, Mortality, Growth, and Diet.” *Marine Biology* 112 (1): 107–18. https://doi.org/10.1007/BF00349734.

Largier, John L. 2003. “Considerations in Estimating Larval Dispersal Distances from Oceanographic Data.” *Ecological Applications*. https://doi.org/10.1890/1051-0761(2003)013[0071:cieldd]2.0.co;2.

Levin, Lisa A. 2006. “Recent Progress in Understanding Larval Dispersal: New Directions and Digressions.” In *Integrative and Comparative Biology*, 282–97. https://doi.org/10.1093/icb/icj024.

Lévy, Marina, Raffaele Ferrari, Peter J.S. Franks, Adrian P. Martin, and Pascal Rivière. 2012. “Bringing Physics to Life at the Submesoscale.” *Geophysical Research Letters*. https://doi.org/10.1029/2012GL052756.

Lévy, Marina, Peter J.S. Franks, and K. Shafer Smith. 2018. “The Role of Submesoscale Currents in Structuring Marine Ecosystems.” *Nature Communications*. https://doi.org/10.1038/s41467-018-07059-3.

McWilliams, James C. 2016. “Submesoscale Currents in the Ocean.” *Proceedings of the Royal Society A: Mathematical, Physical and Engineering Sciences*. https://doi.org/10.1098/rspa.2016.0117.

Miller, Seth H., and Steven G. Morgan. 2013. “Interspecific Differences in Depth Preference: Regulation of Larval Transport in an Upwelling System.” *Marine Ecology Progress Series*. https://doi.org/10.3354/meps10150.

Morgan, Steven G. 2014. “Behaviorally Mediated Larval Transport in Upwelling Systems.” *Advances in Oceanography*. https://doi.org/10.1155/2014/364214.

Morgan, Steven G., Seth H. Miller, Matt J. Robart, and John L. Largier. 2018.

"Nearshore Larval Retention and Cross-Shelf Migration of Benthic Crustaceans at an Upwelling Center." *Frontiers in Marine Science*. https://doi.org/10.3389/fmars.2018.00161.

Reed, Daniel C., and Michael S. Foster. 1984. "The Effects of Canopy Shadings on Algal Recruitment and Growth in a Giant Kelp Forest." *Ecology*. https://doi.org/10.2307/1938066.

Romero, Leonel, David A. Siegel, James C. McWilliams, Yusuke Uchiyama, and Charles Jones. 2016. "Characterizing Storm Water Dispersion and Dilution from Small Coastal Streams." *Journal of Geophysical Research: Oceans*. https://doi.org/10.1002/2015JC011323.

Rosenfeld, Leslie K., Franklin B. Schwing, Newell Garfield, and Dan E. Tracy. 1994. "Bifurcated Flow from an Upwelling Center: A Cold Water Source for Monterey Bay." *Continental Shelf Research*. https://doi.org/10.1016/0278-4343(94)90058-2.

Russell, Robert W., Nancy M. Harrison, and George L. Hunt. 1999. "Foraging at a Front: Hydrography, Zooplankton, and Avian Planktivory in the Northern Bering Sea." *Marine Ecology Progress Series*. https://doi.org/10.3354/meps182077.

Siegelman, Lia, Malcolm O'Toole, Mar Flexas, Pascal Rivière, and Patrice Klein. 2019. "Submesoscale Ocean Fronts Act as Biological Hotspot for Southern Elephant Seal." *Scientific Reports*. https://doi.org/10.1038/s41598-019-42117-w.

Sims, David W., and Victoria A. Quayle. 1998. "Selective Foraging Behaviour of Basking Sharks on Zooplankton in a Small-Scale Front." *Nature*. https://doi.org/10.1038/30959.

Snyder, Stephanie, Peter J. S. Franks, Lynne D. Talley, Yi Xu, and Suzanne Kohin. 2017. "Crossing the Line: Tunas Actively Exploit Submesoscale Fronts to Enhance Foraging Success." *Limnology and Oceanography Letters*. https://doi.org/10.1002/lol2.10049.

Wobber, Don R. 1975. "Agonsim in Asteroids." *The Biological Bulletin* 148 (3): 483–96.

Wolanski, Eric, and William M. Hamner. 1988. "Topographically Controlled Fronts in the Ocean and Their Biological Influence." *Science*. https://doi.org/10.1126/science.241.4862.177.

Woodson, C. B., M. A. McManus, J. A. Tyburczy, J. A. Barth, L. Washburn, J. E. Caselle, M. H. Carr, et al. 2012. "Coastal Fronts Set Recruitment and

Connectivity Patterns across Multiple Taxa." *Limnology and Oceanography*. https://doi.org/10.4319/lo.2012.57.2.0582.

Woodson, C. Brock, and Steven Y. Litvin. 2015. "Ocean Fronts Drive Marine Fishery Production and Biogeochemical Cycling." *Proceedings of the National Academy of Sciences* 112 (6): 1710–15.

CHAPTER TWO
A MODEL DESCRIPTION OF THE CIRCULATION PATTERNS WITHIN CARMEL BAY, A SMALL EMBAYMENT ON THE CENTRAL CALIFORNIA COAST

A model description of the circulation patterns within Carmel Bay, a small embayment on the central California coast

Key Points:

- Due to the small spatial scale of Carmel Bay, supertidal and tidal variability alter circulation patterns
- Tidal residual circulation develops a headland eddy that is enhanced by downwelling-favorable alongshore winds
- Upwelling in the lee of the Monterey Peninsula and weak canyon upwelling provide cold, nutrient-rich water to Carmel Bay

Abstract

Carmel Bay is an important ecological area, highlighted by four marine protected areas (MPAs) within and just outside, but little is known about its circulation and temperature structure that drive nutrient availability, larval connectivity, and other processes that support its rich ecosystems. This study describes the temperature structure and circulation patterns within Carmel Bay, considering specifically the wind-driven and tidally driven components. We use the Regional Ocean Modeling System (ROMS) to simulate the circulation during the 2014 and 2015 spring/summer upwelling seasons using a series of nested grids to resolve the circulation on the central California coast at approximately 120 m resolution. Energy of the circulation within the bay is roughly equally partitioned between subtidal, tidal, and higher frequencies. During upwelling favorable wind conditions, surface waters strongly flow southward across the face of Carmel Bay with weak velocities within Carmel Bay. In contrast, during downwelling-favorable wind conditions offshore surface waters reverse, flowing northward, and develop stronger cross-shore circulation into Carmel Bay. The wind-driven circulation develops a temperature gradient outside the

entrance to Carmel Bay that separates warmer offshore waters from the colder, bay water that strengthens and weakens during upwelling- and downwelling-favorable winds, respectively. Tidal velocities are relatively weaker in northern Carmel Bay and stronger in the southern part of the bay, which is dominated by a tidal-residual headland eddy. Upwelling occurs in the lee of the Monterey Peninsula immediately outside and north of Carmel Bay, cooling the bay's temperature relative to the larger region. The combination of wind- and tidally driven circulation provide a nutrient-rich environment that supports the species-rich coastal ecosystems within Carmel Bay.

1 Introduction

The central California coast is a well-known eastern boundary upwelling system in which equatorward winds along the coast drive near surface Ekman transport offshore, replaced by cold, nutrient-rich water from depth. The dominant alongshore winds are interrupted by periods of wind relaxation or reversal, causing transport in the reverse pattern and typically rendering warmer surface temperatures nearshore. Equatorward winds exhibit a seasonal structure along the coast (Strub et al. 1987), and wind-driven coastal upwelling is the predominant process driving circulation along the US west coast from Oregon to Point Conception in California (e.g., Huyer 1983; Hickey 1998).

Yet the region experiences considerable alongshore heterogeneity associated with variations in wind forcing and, more importantly, alongshore bathymetry and coastline shape. Enhancement of upwelling near promontories such as Cape Blanco,

Cape Mendocino, Año Nuevo, and Point Sur are well known (Hickey 1998; Breaker and Mooers 1986; Rosenfeld et al. 1994). Embayments along the coastline also influence the circulation that results in local variability in ocean properties. As the largest open embayment on the US west coast, Monterey Bay's circulation is well studied (e.g., Rosenfeld et al. 1994; Breaker and Broenkow 1994; Graham and Largier 1997). Less well understood are circulation features associated with small embayments in the coastline. Immediately to the south of Monterey Bay and about two orders of magnitude smaller by area, lies Carmel Bay, a small, open embayment located between two coastal promontories (Figure 1). Like Monterey Bay, Carmel Bay bathymetry is noteworthy for its deep submarine canyon that enters its southern half.

The productive and species rich coastal ecosystems of Carmel Bay have attracted numerous, primarily ecological, studies. Many observational and experimental studies of benthic macroalgae (e.g., Reed and Foster 1984; Graham 1997), invertebrates (e.g. Wobber 1975; Kenner 1992; Clark et al. 2004) and fishes (e.g., Hallacher and Roberts 1985; Carr 1991; Johnson 2006a,b; Johnson 2007; Green and Starr 2011; Green et al. 2014) associated with rocky reefs and kelp forests have been conducted within the bay. Very close to shore, a suite of observational and modeling studies investigated the effect of surf zone hydrodynamics on plankton and larval transport off Carmel River State Beach (Shanks et al. 2014, 2015; Morgan et al. 2017; Fujimura et al. 2017). Geological studies have focused on sediment transport along the Monterey Peninsula that separates Carmel from Monterey Bay (Storlazzi and Field 2000) and Monastery Beach, located near the head of the Carmel Canyon

(Dingler 1981; Dingler and Anima 1989). Carroll (2009) documented temperature, velocity, and nutrient patterns from moorings within Carmel Bay spanning June 2006 to February 2008 and three ship cruises. However, to date, there has not been an investigation of the broader physical circulation and water properties of Carmel Bay as a whole.

The circulation within and around Carmel Bay supports a biologically rich environment, highlighted by multiple marine protected areas (MPAs), including two state marine reserves that do not allow fishing and two state marine conservation areas that allow limited fishing (https://wildlife.ca.gov/Conservation/Marine/MPAs/Network/Central-California). The patchy mosaic of hard and soft-bottom marine habitats characteristic of the central coast of California suggest that local features such as changes in bathymetry, undulations in the coastline, and smaller scale forcing impact marine communities (Young and Carr 2015a,b). These patchily distributed species populations and communities interact with and are strongly influenced by one another through the dispersal of propagules (algal spores and animal larvae), the patterns of which are determined by coastal currents. Likewise, the contribution of populations within MPAs to the replenishment of other populations along the coast are influenced by coastal ocean currents (Baetscher et al. 2019; White et al. 2019). Therefore, management of living marine resources along the coast should benefit from understanding the local circulation patterns on these scales.

This study uses a numerical model to investigate the circulation within Carmel Bay and its vicinity during spring and summer of 2014 and 2015. We aim to describe

the circulation processes within Carmel Bay that support the rich ecosystems housed within. In particular, we characterize its mean circulation and thermal structure, investigate their variations as they relate to tidal and winds stress forcing and the degree to which Carmel Bay properties are coherent with nearby oceanic conditions. In a companion paper, Lowe et al. (2020b) uses this model to understand marine connectivity of rockfish populations within and between Carmel Bay and southern Monterey Bay.

2 Materials and Methods

For this study, we used an implementation of the Regional Ocean Modeling System (ROMS) (Shchepetkin and McWilliams 2005; https://myroms.org), with 4 telescoping grids to achieve the high resolution required to resolve ocean dynamics in the immediate region around Monterey Bay and Carmel Bay (Figure 1). The outermost domain extends meridionally from 30^{o}N to 48^{o}N, the middle of the Baja Peninsula, Mexico to just south of Vancouver Island, Canada, and offshore to 134^{o}W at 1/30^{o} horizontal resolution and includes 42 terrain-following s-levels in the vertical. At the ocean surface, the model is forced by atmospheric fields derived from the Coastal Ocean/Atmosphere Mesoscale Prediction System (COAMPS) (Hodur 1997), and lateral boundary conditions are climatological, from the 2005 version of the World Ocean Atlas (Locarini et al. 2006; Antonov et al. 2006). This outer domain

is a higher resolution version of that described in Veneziani *et al.*, (2009), and has been documented in Drake *et al*., (2011, 2013, and 2015).

The series of nests span sequentially smaller domains with horizontal resolutions of 1/90^{o}, 1/270^{o}, and 1/810^{o} (roughly 1.1 km, 350 m, and 120 m, respectively). For convenience, we will refer to these nests as the a-, b-, and c-nest. Realistic bathymetry was obtained from ETOPO 1, refined to values (where available) from the USGS 3 arc second bathymetry product (Amante and Eakins 2009). A minimum bottom depth of 10 m was imposed in the outer three domains, and a value of 2 m was applied in the c-nest. Bathymetry was smoothed to limit the Haidvogel and Beckman number ($\delta h/2h$) to a maximum of 0.25, 0.2, 0.17, and 0.17 in the coarsest to finest grids, respectively. Surface forcing for each nest is derived from the same COAMPS source as the outermost grid. Daily average oceanic files from the outermost domain and hourly snapshots from each nested domain were used to produce lateral boundary conditions for each refined grid, thus coupling all domains in a one-way, offline fashion. Chapman and Flather boundary conditions were used on all grids for the barotropic motion, radiation (with nudging) boundary conditions (Marchesiello *et al*., 2001) were used in the outermost grid and a-nest, and clamped boundary conditions were applied for the b- and c-nests. Tidal forcing was introduced in the a-nest and drawn from TPXO8-Atlas (Egbert *et al*., 1994) using 9 tidal constituents. Tidal information propagated directly through the clamped boundary

conditions to the b- and c-nests. Estuaries (including San Francisco Bay and Elkhorn Slough) and riverine input were not included in this configuration.

All model domains used a nonlinear equation of state, the k-ω vertical mixing scheme, a quadratic bottom drag with a drag coefficient of 0.0025, and harmonic horizontal viscosity with a value of 1 m^2/s. The outermost grid was initialized from climatology, run for 6-years with climatological forcing, and then run for 17 years with realistic forcing from 1999 through 2015. The a-nest was initialized with conditions for January 1, 2014 and run through September 2015, and the b- and c-nests were initialized for January 1, 2014 and January 1, 2015 and run through September of each year.

To analyze the wind-driven circulation, we estimate an alongshore wind direction as the leading empirical orthogonal function (EOF1) obtained from a time-series of COAMPS 10 m wind velocities spatially averaged over the coastal region near Carmel Bay (Figure 1b). This direction is alongshore (-12.3° counterclockwise from North) and nearly parallel to the broad strike of the central California coast. We removed high frequency variability and focused on subtidal frequencies using a wind-intermittency index following Giddings et al. (2014) with a 3.0 day exponentially-weighted running mean of the EOF1 amplitude, hereafter called the alongshore wind. We defined upwelling-favorable conditions as negative amplitudes of this dominant mode with wind projections onto the leading mode exceeding -5 m/s, and

downwelling-favorable conditions were defined having positive wind projections exceeding 5 m/s.

To analyze the tidal component of the circulation, we use the *ttide* Python package, which is based on the T_TIDE toolbox in MATLAB by Pawlowicz *et al*. (2002), and conducts harmonic analysis to separate the signal of multiple tidal constituents. For this analysis, we specify the same nine tidal constituents used to force the model: Q_1, O_1, P_1, K_1, N_2, M_2, S_2, K_2, M_4. Harmonic analysis on a time-series of sea surface height (SSH) separates the surface tidal signal from other SSH fluctuations; harmonic analysis on a time-series of complex velocity calculates tidal ellipse parameters of how the velocity at a location rotates over the tidal period due to each tidal constituent.

3 Results

3.1 Comparison of model and HF radar velocities

The near-surface circulation of the model was compared with estimates of surface velocities derived from the high frequency (HF) radar network along the California coast (Terrill et al., 2006). Model velocities and data were processed in a manner similar to that described in Drake et al. (2018). Radar-derived velocities were downloaded from the Coastal Observing Research and Development Center website (http://cordc.ucsd.edu/projects/mapping) at the highest resolution for which substantial temporal and spatial coverage was available, 6 km. This resolution allows for a detailed comparison with the b-nest. Both the hourly HF radar and surface model velocities were daily averaged. To produce the most direct comparison, the

daily-averaged model surface velocities were also spatially averaged onto the HF radar's 6 km grid. Model and data were compared over the period of April 1 – September 27, for 2014 and 2015, with the two years concatenated to form one extended spring and summer "season." Only grid cells with at least 50 percent temporal coverage over this extended season of 360 days were included. Mean eddy speeds were calculated as the square root of twice the eddy kinetic energy ($\sqrt{2}$EKE), where $EKE = 0.5[u'^2 + v'^2]$, and u' and v' are deviations from the time mean fields of eastward and northward velocity. The complex correlation between radar-derived and modeled velocities was calculated (Kundu 1976), and significance levels were computed assuming perfect covariance between the alongshore and cross-shore components of the currents (Kaplan et al. 2005). To account for temporal autocorrelation, the effective degrees of freedom for significance levels was determined using the integral time scale (Emery and Thomson 2001).

The spring and summer mean flow shows a similar overall spatial pattern in both the model and data (Figure 2a and 2b). The flow is primarily southward, strongest offshore of the mouth of Monterey Bay, and much weaker inside the bay. The velocity mean is stronger in the model and southeastward at its largest magnitude, whereas the HF radar mean is consistently southwestward offshore. Principal axes of current variance show a large range of orientations in both the model and data but are often not well-aligned (Figure 2c). HF radar mean velocities and eddy speeds are relatively weak around the mouth of Carmel Bay. The model overestimates eddy speeds in this area by a factor of 1.5-2 (Figure 2d), but underestimates them inside Monterey Bay. The complex correlation between radar-

derived and modeled velocities is significant only near the mouth of Carmel Bay (not shown).

We compared our ROMS model to several tidal stations along the coast using NOAA's tidal prediction tables for 2014 and 2015. Root mean square error (RMSE) ranged from 0.06-0.20 m for tidal stations at San Simeon, Monterey, Santa Cruz, and Año Nuevo Island. At Carmel Cove tidal station, the RMSE was 0.06 m (Figure 3).

3.2 Description of the circulation within Carmel Bay

We start with a brief description of Carmel Bay because the basin geometry plays a critical role in the circulation. Carmel Bay is approximately 4 km across at the ocean entrance and roughly 2 km wide (onshore-offshore axis). The bathymetry is dominated by Carmel Canyon, whose head lies in southern Carmel Bay. Since the temperature structure and circulation vary across Carmel Bay, we divide the bay at Carmel Point (36.54°N) into northern and southern halves (black line in Figure 1c). Northern Carmel Bay is shallow, with an average modeled depth of 34 m, and southern Carmel Bay has an average depth of 95 m. The dichotomy between the shelf and canyon in the northern and southern halves of the bay modifies their circulations. The energy spectrum helps to quantitatively identify the partitioning of Carmel Bay into tidally or wind-driven components. In this study, we calculate the cumulative power spectral density of temperature and velocity time-series from a depth of 10 m within northern and southern subparts of Carmel Bay (Figure 4) and, for comparison, from the modeled M1 buoy site (Figure 1b) which lies in the center of the much larger Monterey Bay and is more exposed to open ocean dynamics of the central

California Coast. The fractional cumulative energy is reported in three categories: low frequency variability defined by a period greater than 13 hours (e.g., alongshore winds, diurnal tides, sea breezes, mesoscale eddies), semidiurnal tidal frequency variability with a period between 12-13 hours (e.g., M_2 tides), and high frequency variability with a period shorter than 12 hours. At M1 the vast majority (89.7%) of temperature variability occurs at low frequencies, only 3.5% of the energy occurs in the semidiurnal tidal frequency band, and 6.8% of the energy occurs at higher frequencies. The power spectral densities of temperature in Carmel Bay closely mirror those at M1. Southern Carmel Bay has more than double that proportion of energy (11.9%) at semidiurnal tidal frequencies and slightly less energy (79.5%) at lower frequencies. Notably, more than 50% of the energy associated with the temperature fluctuations in Carmel Bay and offshore occurs at timescales longer than 10 days, emphasizing the importance of changes over time scales longer than wind-variability (Allen 1980; Checkley and Barth 2009), and including the seasonal cycle. These calculations support the idea that temperature fluctuations offshore and within Carmel Bay are driven by similar mechanisms at low frequencies.

In contrast, forcing mechanisms that determine the circulation within Carmel Bay largely differ from those at M1. At the Monterey Bay buoy, the overwhelming majority (88.0%) of the energy in velocity is due to low frequency variability, with only 5.6% and 6.4% of the energy occurring in semidiurnal tidal and higher frequency bands, respectively. At M1, the energy spectra from temperature and velocity are quite similar. In contrast, the energy of the velocity fluctuations within Carmel Bay is more distributed among these three frequency bands. In northern

Carmel Bay, low frequency variability accounts for 51.5% of the energy, semidiurnal tides constitute 21.2%, and 27.3% of the energy occurs at higher frequencies. Compared to northern Carmel Bay, the southern region has nearly double the proportion of energy (38.2%) attributed to semidiurnal tides, resulting in a smaller proportion (33.9%) of energy in low frequency variability. While not reported explicitly, the fraction of energy in velocity associated with diurnal tides around one day is visible as a small slope discontinuity in Figure 4b and forms about 10% of the total. Variability in temperature and velocity at M1 is dominated by low frequency forcing mechanisms, as are temperature changes in Carmel Bay, but the circulation in Carmel Bay is strongly influenced by forcing across the spectrum from 1 hour to more than 10 days.

Temperature variability within Carmel Bay over the study period exhibits fluctuations uniform through the water column as well as changes in its stratification (Figure 5a). To characterize this variability, we calculate a spatial mean temperature, defined from the surface up to 100 m deep including all grid points from the coast to the bay mouth (Figure 1). The mean bay temperature ranges from 10.20 to 14.71°C, with an overall average of 12.25°C. The time-series of spatial average anomalies relative to this mean is shown as the green line in Figure 5c and 5d. After the spatial mean time-series is removed, bulk (top to bottom) stratification is represented by the first Empirical Orthogonal Function (EOF1) of the remaining 3-dimensional temperature field; the amplitude time-series of EOF1 is shown as blue lines in Figure 5c and 5d, and its vertical structure at a single central grid point in Figure 5b, representative of many locations within the bay. When EOF1 is positive, the upper

water column is anomalously warmer and the lower portion of the water column is anomalously cooler than the mean temperature profile, indicating a stronger temperature gradient. EOF1 accounts for up to 3.8°C temperature difference from the surface to 100 m depth. A negative EOF1 implies weaker stratification which occurs if the water column is more well-mixed or through advection of more homogenous temperatures at the mouth. EOF1 accounts for 67% of the temperature variance remaining once the mean is removed. Although Figure 5 presents profiles at one location, profiles of EOF1 throughout Carmel Bay show similar structure, though with zero crossings at depths ranging from 22.6 to 26.9 m. The second mode (EOF2) has two zero crossings in the vertical and represents a shallowing or deepening of the pycnocline; it is not shown because it accounts for only 14% of the variability. For simplicity in description, we refer to the spatial mean structure and EOF1 as the two modes of variability, although we recognize that the spatial mean does not derive from EOF analysis.

The time-series in Figure 5 reveal the seasonal cycle of overall cooler bay temperatures and weaker stratification in the spring to early summer months and warmer temperatures and stronger stratification during the late summer. The transition between these two phases is around July 1 in both summers. On top of the seasonal cycle, there are large amplitude changes on timescales of several days to weeks. The two modes of temperature variability in the bay defined above are in phase with a statistically significant coefficient of determination of 0.54 ($p<0.01$) between the two records. We also include the alongshore wind velocity in the region surrounding Carmel Bay for reference. Neither mode of temperature variability is

statistically related to the local alongshore wind (shown as the black line in Figure 5c,d) nor offshore wind (not shown). Additionally, both modes include oscillations due to the spring/neap tidal cycle and semidiurnal tides (not seen in the smoothed time-series). Temperature changes within Carmel Bay are highly correlated with the advective heat flux through the mouth of the bay (not shown), revealing that surface heating is locally negligible and that circulation strongly governs the temperature field.

During the spring-summer upwelling seasons, alongshore winds are the dominant forcing on the circulation in the CCS with the variance in local wind alongshore component 2.3 times that of the local cross-shore component. During the study period, alongshore wind conditions are roughly equally partitioned, with upwelling- and downwelling-favorable winds (with alongshore wind amplitude exceeding +/-5 m/s) occurring 19.2% and 18.9% of the time, respectively. The mean circulation and temperature anomaly (calculated by subtracting the daily spatial mean temperature from each daily field) resulting from these wind conditions is shown at 10 m depth in Figure 6. Offshore, upwelling-favorable alongshore wind results in surface waters south/southwestward at ~10 cm/s. During these wind conditions, the Monterey Peninsula shelters Carmel Bay from this stronger alongshore motion, resulting in much weaker velocities within and immediately outside the bay. During downwelling-favorable winds, offshore flow reverses transporting fluid poleward along the coastline. As expected from a classic upwelling region, the temperature gradient between offshore and near-coast water is stronger during upwelling-favorable winds and weaker during downwelling-favorable conditions. Within

Carmel Bay, the structure of the mean circulation structure is similar regardless of the alongshore wind direction though the amplitude changes noticeably. Water flows into the bay near the center of its mouth. In northern Carmel Bay, the circulation is weak, with outflow at the northern edge moving poleward along the peninsula. The strongest outflow from Carmel Bay is on the southern edge, moving southward around Point Lobos during upwelling-favorable wind conditions and northwestward joining the offshore circulation during downwelling-favorable winds.

In southern Carmel Bay is found an anticyclonic vortex, a headland eddy resulting from asymmetric flow over a tidal cycle. The headland eddy in the mean circulation is an artifact of strong tidal residual circulation within Carmel Bay (e.g. Pingree and Maddock 1977, 1979; Geyer and Signell 1990). During flood tidal conditions, northward transport along the outer edge of Point Lobos generates negative relative vorticity from the frictional torque associated with the shoaling bathymetry, leading to a negative vorticity flux into the bay. Then, stretching of the water column over the submarine canyon further enhances the relative vorticity, and, thus, the center of the headland eddy lies in the lee of Point Lobos over Carmel Canyon. During ebb tidal conditions, flow roughly reverses, and westward then southward motion along Point Lobos generates a positive relative vorticity flux out of the bay, though no subsequent enhancement occurs because no canyon exists to the south. The tidal motion creates an asymmetric dipole of relative vorticity off Point Lobos in the time mean. As seen in Figure 6, the headland eddy is stronger during downwelling-favorable winds compared to other conditions. This enhancement occurs because the wind-driven poleward motion near Point Lobos provides an

additional source of negative relative vorticity flux into Carmel Bay, strengthening the vortex. In this system, the headland eddy is generated by asymmetric flow over the tidal cycle and modulated by alongshore, wind-driven transport.

Off the central California coast, the M_2 tidal constituent dominates the tidal signal (Jachec et al. 2006). The horizontal circulation of the M_2 tidal constituent is summarized in Figure 7, which depicts the tidal velocity as ellipses with a red stick indicating the velocity direction and amplitude during high tide; green and blue ellipses denote clockwise or counterclockwise rotation of the velocity vector over the tidal cycle. Bathymetry impacts the barotropic tide, visible by the orientation and rotational direction of the ellipses. The M_2 tidal ellipses located along the northern and southern walls of Carmel Canyon rotate in opposite directions and align approximately parallel to the bathymetry. These opposing ellipses meet at the head of Carmel Canyon in southern Carmel Bay. Due to this canyon enhancement, the ellipses show a stronger tidal signal in southern Carmel Bay than the northern region. This gradient in ellipse size is consistent with the power spectral density results showing a stronger tidal signal in southern Carmel Bay compared to northern Carmel Bay. The tidal excursion length measures the distance a particle would travel solely due to the local Eulerian tidal velocity over half a tidal cycle. In this region, the strongest tidal transport occurs off Point Lobos. Within Carmel Bay, the maximum distance a particle may travel due to the M_2 tide is 1.3 km over half a tidal cycle, or 24% of the north-south length of Carmel Bay. This Eulerian calculation is helpful in that it translates a velocity into a scale of transport if no spatial variations in a field existed. In practice, floats experience high velocities (e.g., near Point Lobos) only for

a portion of a tidal cycle, and thus do not travel the full distance indicated. The spatial mean tidal excursion length within Carmel Bay is about 0.25 km or about 4.6% of the north-south extent.

While tidal ellipses and the tidal excursion length summarize some M_2 tidal properties, snapshots of the circulation during particular tidal phases visually reveal how the tidal velocity adds to the overall circulation, and two phases of the M_2 tidal flow are shown in Figure 8. Circulation during low and high tides depend meaningfully on the terrain: the strongest horizontal velocity and transport occurs in deeper water and tidal velocity is negligible in shallow areas. During low tide, transport is generally southward along isobaths of the canyon, generally into central Carmel Bay along the northern edge of the canyon and outward velocities along its southern edge near Point Lobos. During high tides the reverse pattern is found. In northern Carmel Bay, M_2 tidal velocities are small during high and low tidal conditions. Circulation in the shallow regions becomes non-negligible during other phases of the tide. For example, the flood tide circulation includes meaningful velocities in depths shallower than 50 m, transporting water into Carmel Bay along its northern and southern edges and out in the center. Ebb tides transport water in the reverse pattern. Note that in Figure 8, arrows represent the depth-averaged tidal velocity, and color represents the transport of the water column at that location. The strongest transport is into and out of the bay near Point Lobos during flood and ebb tides. In our model, the M_2 tide constitutes on average 17.9% of the velocity variance within Carmel Bay.

As an open embayment, exchange between Carmel Bay and the open ocean also influences the local circulation. Figure 9 presents the velocity into and out of the bay using a depth section across its mouth. The depth section clearly reveals the deep canyon and a shallow offshoot into the northern part of the bay. The mean velocity at the entrance to Carmel Bay (Figure 9a) shows inflow at the center from the surface to about 20 meters above the bottom with a maximum value of 4.6 cm/s. Outflow spans the water column at the northern and southern edges of the bay. Within the canyon, below about 90 m, weak inflow occurs at the center and outflow is found along the walls. Mean outflow near Point Lobos reaches 9.5 cm/s, the strongest value into or out of the bay. The most dramatic shift from the mean circulation under different alongshore wind forcing occurs in the upper water column. Near surface water flows out of the bay at ~2.7 cm/s during upwelling-favorable wind conditions and into the bay at ~4.1 cm/s during downwelling-favorable winds. During upwelling-favorable winds, flow below 10 m is anomalously outward in the northern half and inward in the southern half of Carmel Bay. The anomaly during downwelling-favorable conditions is nearly opposite that during upwelling-favorable wind conditions (Figure 9b,c). Note that under both wind conditions, the northern half of the bay flows similarly to the surface, whereas flow below 10 m is opposite to the surface motion in southern Carmel Bay. These figures indicate that the circulation and exchange between Carmel Bay and the open ocean responds meaningfully to the alongshore winds. Because upwelling- or downwelling-favorable winds, as defined here, are present almost 40% of the time and are normally sustained for a few days, this wind-forcing enables substantial exchange into and out of Carmel Bay.

Transport into and out of Carmel Bay due to the M_2 tide occurs on a faster timescale than the circulation's response to lower frequency wind changes. During M_2 low tide, inflow occurs over the northern part of the section, with strong outflow reaching 12.4 cm/s near the southern edge of Carmel Bay (Figure 9d). Net transport is 166.4 m^3/s into the bay. During M_2 high tide, flow moves northward in the reverse pattern. Flood and ebb tidal cycles are dominated by vertical shear flow with inflow at depth especially within the canyon and outflow mostly above about 60 m depth (Figure 9e). At flood tide, net transport is 647.1 m^3/s into the bay. Exchange with the coastal ocean flows in the reverse pattern at ebb tide (not shown). Since the M_2 tide cycles through these phases almost twice daily, the induced lateral exchange is only with the immediate coastal ocean.

To identify source water to Carmel Bay, three-dimensional, backward-in-time Lagrangian particle tracking was employed using OpenDrift (Dagestad et al. 2018). Particles were released daily during the Spring (April 1 – June 30) in 2014 and 2015 from a sample of gridpoints within Carmel Bay at a distribution of depths centered on 30 m (mean = 29.2 m, standard deviation = 3.9 m/s). Particle trajectories were calculated for 5 days backwards in time. Of the 24,915 particles analyzed, 60.1% were at depths 0-50 m, 29.6% were 50-100 m, 7.9% were 100-150 m, and 2.5% were below 150 m five days before arriving at their release location within Carmel Bay. Probability maps of trajectories for particles that originated in the upper water column (0-50 m depths) and deep (below 150 m) are shown in Figure 10. The probability maps show the geographic extent of 5-day source locations feeding Carmel Bay. Source water from the upper water column (0-50 m) spans the northern limit of

Monterey Bay to south of Point Sur and 60 km offshore; before entering Carmel Bay, the majority of these particles move along a narrow strip of the coast just south of the bay. The spatial footprint gets smaller and smaller for particles from deeper in the water column. The deepest particles (from below 150 m) originated mostly deep within the Carmel Canyon and a few come from further south. Although the majority of particles were transported by near surface waters, a significant number originated deeper indicating that a portion of Carmel Bay's upper water column comes from cold, deep water masses.

Carmel Bay is typically colder than Monterey Bay and the greater region offshore surrounding the bay. Over the study period, the mean surface temperature in Carmel Bay is 14.3°C, which is 1.5°C colder than Monterey Bay on average. Carmel Bay lies in the lee of the Monterey Peninsula, a local coastal headland. The two nearest recognized upwelling centers are Año Nuevo to the north and Point Sur to the south. Over the spring-summer study period, comparable mean temperatures of 14.3, 14.3, and 13.7°C are found in the lees of Año Nuevo, the Monterey Peninsula, and Point Sur, respectively. Figure 11 maps the correlation coefficient between the mean SST anomaly within Carmel Bay and SST anomalies at all other points in the model domain; SST anomalies calculated each timestep relative to the spatial-mean SST of the domain to remove the seasonal cycle. Temperature fluctuations within Carmel Bay are surprisingly distinct from those off Año Nuevo and Point Sur. The mean SST within Carmel Bay lags SST in the lee of Point Sur by three days (r^2=0.32) and Año Nuevo by five days (r^2=0.25). Within Carmel Bay, net vertical transport at 10 to 50 m depth is related to the local alongshore wind with coefficients of determination

ranging from 0.34 to 0.24, significant to the 99% level. Additionally, SST in the northern half of Carmel Bay is slightly colder than its southern half. The evidence indicates that cool surface temperatures in Carmel Bay likely result more from local upwelling than advection of cold water from an upwelling center further south.

4 Discussion

This study describes analysis of realistically configured, numerical model output from a telescoped, nested domain reaching ~120 m horizontal resolution to investigate the circulation within and around Carmel Bay that sits along the central California coast. The energy spectrum for near-surface temperature and velocity time-series within the bay shows that temperature changes occur primarily on the order of several days or longer, whereas variability in velocity is more evenly spread across the scale from days to hours. Temperature energy spectra within the bay and those near the mouth of Monterey Bay are similar, whereas velocity spectra in Carmel Bay exhibits finer time-scale variability. Temperature within Carmel Bay is almost exclusively driven by the advective heat flux through the mouth of Carmel Bay. The area surrounding the bay experiences classic upwelling dynamics in response to changes in the alongshore wind, and there is a distinct upwelling plume off the Monterey Peninsula separate from the nearby Point Sur upwelling center. Wind forcing impacts exchange between the bay and open ocean with the strongest signal in the circulation near the surface. The M_2 tidal constituent dominates the tidal signal, and the tidal circulation is strongly influenced by the submarine canyon. In southern Carmel Bay, a headland eddy develops due to tidally driven vorticity flux past Point

Lobos that is enhanced and weakened during downwelling- and upwelling favorable alongshore winds, respectively.

The close proximity of Carmel Bay to well-studied Monterey Bay merits comparison. As adjacent bays, both experience similar large-scale forcing (atmospheric winds and offshore mesoscale conditions). Generally, Monterey Bay experiences a wind-driven cyclonic near-surface circulation in its interior (Breaker and Broenkow 1994). An upwelling shadow zone of slower velocity and warmer temperature develops in the northern part of the bay (Graham and Largier 1997). Monterey Bay is roughly an order of magnitude larger in each horizontal dimension than Carmel Bay, whose small physical scale alters its forcing response, and thus its properties, considerably. In the time-mean, Carmel Bay's near-surface circulation is strongly impacted by tidal forcing, influenced by the strong variations in local bathymetry. We find in our model that only 57.4% of the total kinetic energy in all of Carmel Bay can be attributed to subtidal motion, with 17.9% attributed to M2 tidal band, and 24.7% with supertidal motion. For all of Monterey Bay, these values are 77.9%, 14.8%, and 7.3%, respectively.

The Monterey Submarine Canyon (MSC) divides Monterey Bay into nearly equal halves, enabling fairly symmetric tidal circulation in the northern and southern halves of the bay. During low tide, the depth-averaged M_2 tidal circulation flows broadly over the shelf into the Bay and toward the MSC head, with offshore (down-canyon) flow; over the flood tide, this circulation reverses with up-canyon, inshore flow in the center and offshore flow along the shelves (Carter 2010, their Figure 7). Like Monterey Bay, Carmel Bay includes a deep submarine canyon, the Carmel

Canyon, that shoals very close to shore. It is a branch of the MSC that enters Carmel Bay mostly in its southern half leaving a wider shelf in the northern half; this asymmetry results in a stronger tidal signal in the southern half of Carmel Bay. During low tide, depth-averaged tidal transport is fairly confined to the steep canyon walls, entering in the middle of the canyon, flowing southward within Carmel Bay and out along the southern edge. During flood tides, transport into the bay occurs in the shallower shelf regions of the bay along its northern and southern boundaries, with outflow in the center. The circulation reverses these patterns during high and ebb tides. Thus, canyon orientation and bay geometry render quite different ebb and flood circulation patterns within the bays.

As mentioned above, tidal motion around Point Lobos drives subtidal mean circulation that dominates the bay: an anti-cyclonic headland eddy within the southern half of Carmel Bay. We speculate that a similar headland eddy is not found in the north in part because a smooth topographic slope along the northern edge yields a smaller stretching term in the vorticity equation, limiting enhancement of relative vorticity. Time-mean headland eddies generated by tidal forcing and vorticity are a well-studied phenomenon (e.g., Pingree and Maddock 1977, 1979; Geyer and Signell 1990). In this Carmel Bay example, the headland eddy is modulated by the wind-driven circulation. During periods of northward alongshore winds, the mean flow along the broader central California coast is also poleward, increasing the northward motion around Point Lobos that occurs during one tidal phase (high tide), increasing the relative vorticity flux associated with the tidal motion, and strengthening the headland eddy in the time-mean.

In our model, we find colder mean surface temperatures in Carmel Bay than Monterey Bay during the spring/summer study periods of 2014 and 2015. In an observational study using a full year of mooring measurements from June 2006-2007, Carroll (2009) report surface temperatures outside Stillwater Cove were 2°C colder than M1 near the entrance of Monterey Bay and 3°C colder than M2 located further offshore. Carroll (2009) considered the origin of the cooler Stillwater Cove values in the context of the two closest upwelling centers: Año Nuevo to the north of Monterey Bay and Point Sur to the south of Carmel Bay (Rosenfeld et al. 1994; Traganza et al. 1981). They speculate on the latter center's impact being greater due to its proximity. In the model, upwelled water near Point Sur is transported generally further south and offshore away from Carmel Bay during upwelling-favorable alongshore winds. Northward advection mostly occurs during downwelling-favorable winds, at times when the bay temperature is relatively warmer. Our model results suggest an alternate explanation for the cooler temperature in Carmel Bay.

The Monterey Peninsula may be a lesser known headland that enhances upwelling in central California important to dynamics and resultant ecosystems within Carmel Bay. At times of sustained, strong upwelling-favorable winds, ubiquitous upwelling spans the Big Sur coast from Point Sur to the Monterey Peninsula and sometimes further north connecting to Año Nuevo. Upwelling in the lees of Año Nuevo and Point Sur often coincides based on the SST (r^2=0.74), whereas both upwelling centers have a weaker relationship with the Monterey Peninsula (r^2=0.61). Other times, the cold plumes of upwelled water remain distinct. The upwelling plume from Año Nuevo often extends partway across the mouth of

Monterey Bay, at times curling into the bay and sometimes being entrained in the offshore mesoscale field (Rosenfeld et al. 1994).This narrow plume and Monterey Bay's circulation develop an upwelling shadow zone of slightly warmer surface temperatures in the northern part of Monterey Bay (Graham and Largier 1997), but in Carmel Bay surface temperatures are cooler in the northern half of the bay relative to its southern half. Instead of a narrow plume of cold water, enhanced upwelling south of the Monterey Peninsula engulfs the coastal region, developing a strong surface temperature gradient between coastal upwelled water inshore and warmer surface water offshore. The strong temperature gradient or front frequently extends southward across Carmel Bay, whose small scale also alters the dynamics of this front relative to that of Año Nuevo, making it more similar to small scale features studied in Southern California (Dauhajre et al., 2017). We study the dynamics of this front further in Lowe et al. (2020c). Together this evidence encourages further investigation of upwelling dynamics in this region and that the Monterey Peninsula may be another important upwelling center along the central California coast.

Many other medium and small sized bays on the US west coast differ from Carmel Bay because they are semi-enclosed and mostly sheltered from offshore circulation. Bodega Bay is a medium-sized, shallow, open embayment that shares some circulation features similar to Carmel and Monterey bays. Geographically, this bay lies further to the north on the California coast and is situated between a small headland Bodega Head to its north and a large headland Point Reyes to its south. The southern end of this bay connects to Tomales Bay, whose outflow influences the circulation (Roughan et al. 2005). Observations of Bodega Bay's circulation reveal a

cyclonic flow pattern similar to Monterey Bay, but no upwelling-shadow zone (Roughan et al. 2005). Similar to Carmel Bay, there is active upwelling along the northern edge of the bay during upwelling-favorable alongshore winds, providing another example that enhanced upwelling occurs in the lees of small-headlands and may have a disproportionate effect on local marine ecosystems.

This study does not account for riverine influence on Carmel Bay's circulation. The largest river draining to this bay, the Carmel River, has intermittent flow mainly during winter to spring months. This river discharges 2.7 m^3/s during average conditions and 79.3 m^3/s during bankfull conditions (Kondolf and Curry 1984). For comparison, the horizontal transport into Carmel Bay from the mean fields shown in Figure 6a is 4,535 m^3/s, which is 1,679 times the average discharge and 57 times the bankfull discharge. This study focuses on the spring and summer seasons that will mostly experience low river discharge and thus have a limited effect on circulation.

The main focus of Carroll (2009) was nutrient transport in Carmel Bay. Similar to our calculation, their frequency band analysis of the nutrient flux into Stillwater Cove showed strong influence by tides and alongshore winds. In our observations, the majority of nutrients were delivered during upwelling-favorable winds. While intermittent upwelling dynamics generate a surge of nutrients, tides were a more consistent source. Tides enhance mixing, particularly in submarine canyons (Allen and Madron 2009), resulting in a high net nitrate flux onto the adjacent shelf region (Hickey and Banas 2008).

Another study investigated delivery of plankton to nearshore habitat in southeast Carmel Bay. The two study species were delivered to the same habitat by different mechanisms: Pseudo-nitzschia during wind-relaxations and barnacle cyprids by internal tides (Shanks et al. 2014). Although our model does not include the surf zone, the transport mechanisms delivering plankton to the surf zone can be understood in greater detail. As they suggest, the different delivery mechanisms likely arise from where the plankton originate. Offshore, Pseudo-nitzschia congregate along the upwelling front before the wind reversal event delivers them to shore. The small bay entrance limits transport from offshore and the upwelling front that develops immediately outside Carmel Bay likely delivered the large pulse of larvae. In contrast, many of the barnacle cyprids may have originated within the bay or been in the bay for a while before being transported to the nearshore habitat for settlement. Assuming available supply of larvae within the bay, tidal cycles will yield oscillatory delivery to the nearshore habitat, especially by internal tides propagating through the canyon and propelling the tidally driven bay circulation.

Both of these studies provide observational examples of how Carmel Bay's circulation supports its highy productive and species rich ecosystems. The present study attempts a comprehensive analysis of circulation patterns and local forcing, particularly flow near the surface and exchange with the open ocean. A companion paper (Lowe et al. 2020b) is directed toward understanding biological implications of the physical circulation, focusing on self-retention and connectivity of near-surface larvae from rockfish populations around the Monterey Peninsula. The concentrated marine protection within and around Carmel Bay highlight its valuable ecological

role relative to the surrounding coast, with a patchy mosaic of marine ecosystems encouraging local-scale investigation of circulation patterns and their multidisciplinary impact.

Acknowledgements

This work was supported by a grant from the National Science Foundation (Award number 1260693). The authors thank Dan Malone and Emily Saarman for their extensive field-knowledge that contributed to discussions related to this project.

REFERENCES

Allen, J. S. 1980. "Models of Wind-Driven Currents on the Continental Shelf." *Annual Review of Fluid Mechanics* 12 (1): 389–433.

Allen, S. E., and X. Durrieu de Madron. 2009. "A Review of the Role of Submarine Canyons in Deep-Ocean Exchange with the Shelf." *Ocean Science Discussions*. https://doi.org/10.5194/osd-6-1369-2009.

Allison, Gary W., Jane Lubchenco, and Mark H. Carr. 1998. "Marine Reserves Are Necessary but Not Sufficient for Marine Conservation." *Ecological Applications*. https://doi.org/10.2307/2641365.

Amante, C, and B.W. Eakins. 2009. "ETOPO1 1 Arc-Minute Global Relief Model: Procedures, Data Sources and Analysis." *NOAA Technical Memorandum NESDIS NGDC-24*. https://doi.org/10.1594/PANGAEA.769615.

Antonov, J.I., R.A. Locarini, T.P. Boyer, A.V. Mishonov, and H.E. Garcia. 2006. "World Ocean Atlas 2005, Volume 2: Salinity." *S. Levitus, Ed. NOAA Atlas NESDIS 62*. https://doi.org/10.1182/blood-2011-06-357442.

Baetscher, Diana S., Eric C. Anderson, Elizabeth A. Gilbert-Horvath, Daniel P. Malone, Emily T. Saarman, Mark H. Carr, and John Carlos Garza. 2019. "Dispersal of a Nearshore Marine Fish Connects Marine Reserves and Adjacent Fished Areas along an Open Coast." *Molecular Ecology* 28: 1611–23. https://doi.org/10.1111/mec.15044.

Breaker, L. C., and W. W. Broenkow. 1994. "The Circulation of Monterey Bay and Related Processes." *Oceanography and Marine Biology: An Annual Review. Vol. 32*.

Breaker, Laurence C., and Christopher N.K. Mooers. 1986. "Oceanic Variability off the Central California Coast." *Progress in Oceanography*. https://doi.org/10.1016/0079-6611(86)90025-X.

Carr, Mark H. 1991. "Habitat Selection and Recruitment of an Assemblage of Temperate Zone Reef Fishes." *Journal of Experimental Marine Biology and Ecology* 146: 113–37. https://doi.org/10.1016/0022-0981(91)90257-W.

Carroll, Dustin. 2009. "Carmel Bay : Oceanographic Dynamics and Nutrient Transport in a Small Embayment of the Central California Coast ." *Master's Thesis*. California State University, Monterey Bay.

Carter, G. S. 2010. "Barotropic and Baroclinic M2 Tides in the Monterey Bay Region." *Journal of Physical Oceanography*.

https://doi.org/10.1175/2010JPO4274.1.

Checkley, David M., and John A. Barth. 2009. “Patterns and Processes in the California Current System.” *Progress in Oceanography*. https://doi.org/10.1016/j.pocean.2009.07.028.

Clark, R. P., M. S. Edwards, and M. S. Foster. 2004. “Effects of Shade from Multiple Kelp Canopies on an Understory Algal Assemblage.” *Marine Ecology Progress Series* 267: 107–19. https://doi.org/10.3354/meps267107.

Dagestad, Knut Frode, Johannes Röhrs, Oyvind Breivik, and Bjørn Ådlandsvik. 2018. “OpenDrift v1.0: A Generic Framework for Trajectory Modelling.” *Geoscientific Model Development*. https://doi.org/10.5194/gmd-11-1405-2018.

Dauhajre, Daniel P., James C. McWilliams, and Yusuke Uchiyama. 2017. “Submesoscale Coherent Structures on the Continental Shelf.” *Journal of Physical Oceanography*. https://doi.org/10.1175/JPO-D-16-0270.1.

Dingler, J. R., and R. J. Anima. 1989. “Subaqueous Grain Flows at the Head of Carmel Submarine Canyon, California.” *Journal of Sedimentary Petrology*. https://doi.org/10.1306/212F8F71-2B24-11D7-8648000102C1865D.

Dingler, John R. 1981. “Stability of a Very Coarse-Grained Beach at Carmel, California.” *Marine Geology*. https://doi.org/10.1016/0025-3227(81)90052-9.

Drake, Patrick T., Christopher A. Edwards, and John A. Barth. 2011. “Dispersion and Connectivity Estimates along the U.S. West Coast from a Realistic Numerical Model.” *Journal of Marine Research*. https://doi.org/10.1357/002224011798147615.

Drake, Patrick T., Christopher A. Edwards, and Steven G. Morgan. 2015. “Relationship between Larval Settlement, Alongshore Wind Stress and Surface Temperature in a Numerical Model of the Central California Coastal Circulation.” *Marine Ecology Progress Series*. https://doi.org/10.3354/meps11393.

Drake, Patrick T., Christopher A. Edwards, Steven G. Morgan, and Edward P. Dever. 2013. “Influence of Larval Behavior on Transport and Population Connectivity in a Realistic Simulation of the California Current System.” *Journal of Marine Research*. https://doi.org/10.1357/002224013808877099.

Drake, Patrick T., Christopher A. Edwards, Steven G. Morgan, and Erin V. Satterthwaite. 2018. “Shoreward Swimming Boosts Modeled Nearshore Larval Supply and Pelagic Connectivity in a Coastal Upwelling Region.” *Journal of Marine Systems*. https://doi.org/10.1016/j.jmarsys.2018.07.004.

Egbert, Gary D., Andrew F. Bennett, and Michael G. G. Foreman. 1994. "TOPEX/POSEIDON Tides Estimated Using a Global Inverse Model." *Journal of Geophysical Research* 99 (C12): 24821. https://doi.org/10.1029/94JC01894.

Emery, W. J., and R. E. Thomson. 2001. *Data Analysis Methods in Physical Oceanography*. *Data Analysis Methods in Physical Oceanography*. https://doi.org/10.2307/1353059.

Fujimura, Atsushi G., Ad J.H.M. Reniers, Claire B. Paris, Alan L. Shanks, Jamie H. MacMahan, and Steven G. Morgan. 2017. "Numerical Simulations of Onshore Transport of Larvae and Detritus to a Steep Pocket Beach." *Marine Ecology Progress Series*. https://doi.org/10.3354/meps12331.

Geyer, W. Rockwell, and Richard Signell. 1990. "Measurements of Tidal Flow around a Headland with a Shipboard Acoustic Doppler Current Profiler." *Journal of Geophysical Research*. https://doi.org/10.1029/jc095ic03p03189.

Giddings, S. N., P. Maccready, B. M. Hickey, N. S. Banas, K. A. Davis, S. A. Siedlecki, V. L. Trainer, R. M. Kudela, N. A. Pelland, and T. P. Connolly. 2014. "Hindcasts of Potential Harmful Algal Bloom Transport Pathways on the Pacific Northwest Coast." *Journal of Geophysical Research: Oceans*. https://doi.org/10.1002/2013JC009622.

Graham, Michael H. 1997. "Factors Determining the Upper Limit of Giant Kelp, Macrocystispyrifera Agardh, along the Monterey Peninsula, Central California, USA." *Journal of Experimental Marine Biology and Ecology* 218 (1): 127–49. https://doi.org/10.1016/S0022-0981(97)00072-5.

Graham, William M., and John L. Largier. 1997. "Upwelling Shadows as Nearshore Retention Sites: The Example of Northern Monterey Bay." *Continental Shelf Research*. https://doi.org/10.1016/S0278-4343(96)00045-3.

Green, Kristen M., Ashley P. Greenley, and Richard M. Starr. 2014. "Movements of Blue Rockfish (Sebastes Mystinus) off Central California with Comparisons to Similar Species." *PLoS ONE*. https://doi.org/10.1371/journal.pone.0098976.

Green, Kristen M., and Richard M. Starr. 2011. "Movements of Small Adult Black Rockfish: Implications for the Design of MPAs." *Marine Ecology Progress Series*. https://doi.org/10.3354/meps09263.

Hallacher, Leon E., and Dale A. Roberts. 1985. "Differential Utilization of Space and Food by the Inshore Rockfishes (Scorpaenidae: Sebastes) of Carmel Bay, California." *Environmental Biology of Fishes*. https://doi.org/10.1007/BF00002762.

Hickey, Barbara M. 1998. “Coastal Oceanography of Western North America from the Tip of Baja California to Vancouver Island.” In *The Sea*, edited by Allan R. Robinson and Kenneth H. Brink, 11th ed., 345–93. John Wiley & Sons, Inc. https://books.google.com/books?hl=en&lr=&id=-uhTulqFRIgC&oi=fnd&pg=PA345&ots=17YWMPqbCw&sig=TptPd-1kvWE38CKRdz4M5NtEDXo#v=onepage&q&f=false.

Hickey, Barbara M., and Neil S. Banas. 2008. “Why Is the Northern End of the California Current System so Productive?” *Oceanography*. https://doi.org/10.5670/oceanog.2008.07.

Hodur, Richard M. 1997. “The Naval Research Laboratory’s Coupled Ocean/Atmosphere Mesoscale Prediction System (COAMPS).” *Monthly Weather Review*. https://doi.org/10.1175/1520-0493(1997)125<1414:TNRLSC>2.0.CO;2.

Huyer, Adriana. 1983. “Coastal Upwelling in the California Current System.” *Progress in Oceanography*. https://doi.org/10.1016/0079-6611(83)90010-1.

Jachec, S. M., O. B. Fringer, M. G. Gerritsen, and R. L. Street. 2006. “Numerical Simulation of Internal Tides and the Resulting Energetics within Monterey Bay and the Surrounding Area.” *Geophysical Research Letters*. https://doi.org/10.1029/2006GL026314.

Johnson, Darren W. 2006a. “Density Dependence in Marine Fish Populations Revealed at Small and Large Spatial Scales.” *Ecology* 87 (2): 319–25. https://doi.org/10.1890/04-1665.

———. 2006b. “Predation, Habitat Complexity, and Variation in Density-Dependent Mortality of Temperate Reef Fishes.” *Ecology* 87 (5): 1179–88. https://doi.org/10.1890/0012-9658(2006)87[1179:PHCAVI]2.0.CO;2.

———. 2007. “Habitat Complexity Modifies Post-Settlement Mortality and Recruitment Dynamics of a Marine Fish.” *Ecology* 88 (7): 1716–25. https://doi.org/10.1890/06-0591.1.

Kaplan, David M., John Largier, and Louis W. Botsford. 2005. “HF Radar Observations of Surface Circulation off Bodega Bay (Northern California, USA).” *Journal of Geophysical Research C: Oceans* 110 (10): 1–25. https://doi.org/10.1029/2005JC002959.

Kenner, M. C. 1992. “Population Dynamics of the Sea Urchin Strongylocentrotus Purpuratus in a Central California Kelp Forest: Recruitment, Mortality, Growth, and Diet.” *Marine Biology* 112 (1): 107–18.

https://doi.org/10.1007/BF00349734.

Kondolf, G M, and R R Curry. 1984. “The Role of Riparian Vegetation in Channel Bank Stability: Carmel River, California.” In *California Riparian Systems: Ecology, Conservation, and Management*.

Kundu, Pijush. 1976. “Ekman Veering Observed near the Ocean Bottom.” *Journal of Physical Oceanography* 6: 238–42.

Locarini, R.A., A.V. Mishonov, J.I. Antonov, T.P. Boyer, and H.E. Garcia. 2006. “World Ocean Atlas 2005, Volume 1: Temperature.” *S. Levitus, Ed. NOAA Atlas NESDIS 62*. https://doi.org/10.1182/blood-2011-06-357442.

Lubchenco, Jane, Stephen R. Palumbi, Steven D. Gaines, and Sandy Andelman. 2003. “Plugging a Hole in the Ocean: The Emerging Science of Marine Reserves.” *Ecological Applications*. https://doi.org/10.1890/1051-0761(2003)013[0003:PAHITO]2.0.CO;2.

Marchesiello, Patrick, James C. McWilliams, and Alexander Shchepetkin. 2001. “Open Boundary Conditions for Long-Term Integration of Regional Oceanic Models.” *Ocean Modelling*. https://doi.org/10.1016/S1463-5003(00)00013-5.

Morgan, Steven G., Alan L. Shanks, Jamie MacMahan, Ad J.H.M. Reniers, Chris D. Griesemer, Marley Jarvis, and Atsushi G. Fujimura. 2017. “Surf Zones Regulate Larval Supply and Zooplankton Subsidies to Nearshore Communities.” *Limnology and Oceanography*. https://doi.org/10.1002/lno.10609.

Pawlowicz, Rich, Bob Beardsley, and Steve Lentz. 2002. *Classical Tidal Harmonic Analysis with Error Analysis in MATLAB Using T_TIDE*. *Computers & Geosciences*. https://doi.org/10.1109/APS.2007.4396859.

Pingree, R. D., and Linda Maddock. 1977. “Tidal Eddies and Coastal Discharge.” *Journal of the Marine Biological Association of the United Kingdom*. https://doi.org/10.1017/S0025315400025224.

———. 1979. “The Tidal Physics of Headland Flows and Offshore Tidal Bank Formation.” *Marine Geology*. https://doi.org/10.1016/0025-3227(79)90068-9.

Reed, Daniel C., and Michael S. Foster. 1984. “The Effects of Canopy Shadings on Algal Recruitment and Growth in a Giant Kelp Forest.” *Ecology*. https://doi.org/10.2307/1938066.

Rosenfeld, Leslie K., Franklin B. Schwing, Newell Garfield, and Dan E. Tracy. 1994. “Bifurcated Flow from an Upwelling Center: A Cold Water Source for Monterey Bay.” *Continental Shelf Research*. https://doi.org/10.1016/0278-4343(94)90058-

2.

Roughan, Moninya, Amber J. Mace, John L. Largier, Steven G. Morgan, Jennifer L. Fisher, and Melissa L. Carter. 2005. “Subsurface Recirculation and Larval Retention in the Lee of a Small Headland: A Variation on the Upwelling Shadow Theme.” *Journal of Geophysical Research C: Oceans*. https://doi.org/10.1029/2005JC002898.

Shanks, Alan L., Jamie MacMahan, Steven G. Morgan, Ad J.H.M. Reniers, Marley Jarvis, Jenna Brown, Atsushi Fujimura, and Chris Griesemer. 2015. “Transport of Larvae and Detritus across the Surf Zone of a Steep Reflective Pocket Beach.” *Marine Ecology Progress Series*. https://doi.org/10.3354/meps11223.

Shanks, Alan L., Steven G. Morgan, Jamie MacMahan, Ad J.H.M. Reniers, Marley Reniers, Jenna Brown, Atsushi Fujimura, and Chris Griesemer. 2014. “Onshore Transport of Plankton by Internal Tides and Upwelling-Relaxation Events.” *Marine Ecology Progress Series*. https://doi.org/10.3354/meps10717.

Shchepetkin, Alexander F., and James C. McWilliams. 2005. “The Regional Oceanic Modeling System (ROMS): A Split-Explicit, Free-Surface, Topography-Following-Coordinate Oceanic Model.” *Ocean Modelling* 9 (4): 347–404. https://doi.org/10.1016/J.OCEMOD.2004.08.002.

Storlazzi, C. D., and M. E. Field. 2000. “Sediment Distribution and Transport along a Rocky, Embayed Coast: Monterey Peninsula and Carmel Bay, California.” *Marine Geology*. https://doi.org/10.1016/S0025-3227(00)00100-6.

Strub, P. T., J. S. Allen, A. Huyer, R. L. Smith, and R. C. Beaedsley. 1987. “Seasonal Cycles of Currents, Temperatures, Winds, and Sea Level over the Northeast Pacific Continental Shelf: 35n to 48n.” *Journal of Geophysical Research: Oceans*. https://doi.org/10.1029/JC092iC02p01507.

Terrill, E., M. Otero, L. Hazard, D. Conlee, J. Harlan, J. Kohut, P. Reuter, T. Cook, T. Harris, and K. Lindquist. 2006. “Data Management and Real-Time Distribution in the HF-Radar National Network.” *Oceans*. https://doi.org/10.1109/OCEANS.2006.306883.

Traganza, E.D. (Naval Postgraduate School), J.C. (Naval Postgraduate School) Conrad, and L.C. (Naval Postgraduate School) Breaker. 1981. “Satellite Observations of a Cyclnic Wpwelling System and Giant Plume in the California Current.” *Coastal Upwelling* 1 (March): 228–41.

Veneziani, M., C. A. Edwards, J. D. Doyle, and D. Foley. 2009. “A Central California Coastal Ocean Modeling Study: 1. Forward Model and the Influence of Realistic versus Climatological Forcing.” *Journal of Geophysical Research: Oceans*.

https://doi.org/10.1029/2008JC004774.

White, J. Wilson, Mark H. Carr, Jennifer E. Caselle, Libe Washburn, C. Brock Woodson, Stephen R. Palumbi, Peter M. Carlson, et al. 2019. “Connectivity, Dispersal, and Recruitment: Connecting Benthic Communities and the Coastal Ocean.” *Oceanography* 32 (3): 50–59. https://doi.org/10.5670/oceanog.2019.310.

Wobber, Don R. 1975. “Agonsim in Asteroids.” *The Biological Bulletin* 148 (3): 483–96.

Young, Mary, and Mark Carr. 2015a. “Assessment of Habitat Representation across a Network of Marine Protected Areas with Implications for the Spatial Design of Monitoring.” *PLoS ONE* 10 (3): 1–23. https://doi.org/10.1371/journal.pone.0116200.

Young, Mary, and Mark H. Carr. 2015b. “Application of Species Distribution Models to Explain and Predict the Distribution, Abundance and Assemblage Structure of Nearshore Temperate Reef Fishes.” *Diversity and Distributions* 21 (12): 1428–40. https://doi.org/10.1111/ddi.12378.

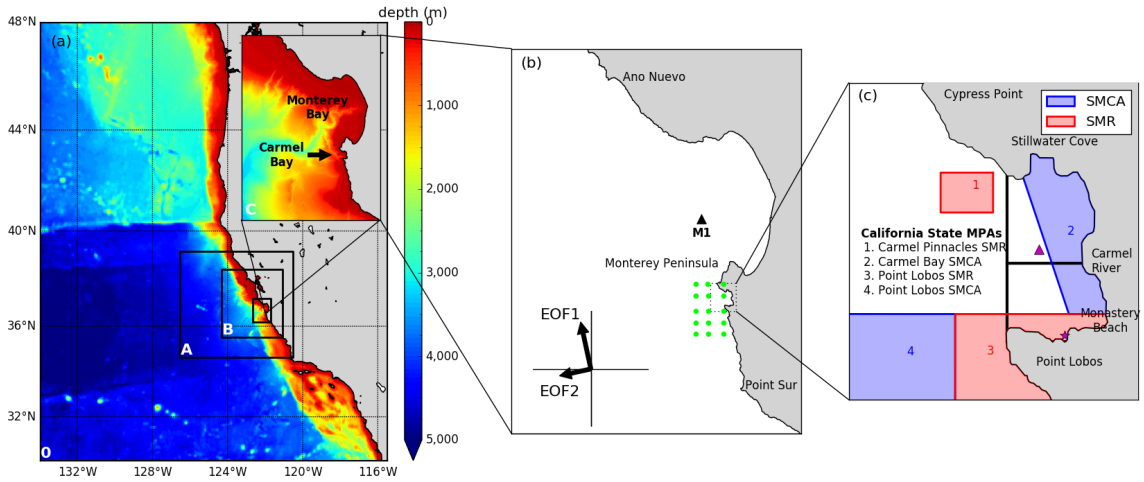

Figure 1. (a) Map of outermost domain and outlines of the finer resolution nests and inset shows the finest resolution nest domain. Color represents bathymetry. (b) C-nest domain with the COAMPS grid points in green that were used to calculate the local alongshore wind by EOF analysis and the dominant wind directions in bottom corner. (c) Region surrounding Carmel Bay and the four MPAs nearby shaded in red and blue. The Carmel Cove tidal station in Whaler's Cove is marked by the purple star and the purple triangle marks location of temperature profile in Figure 5.

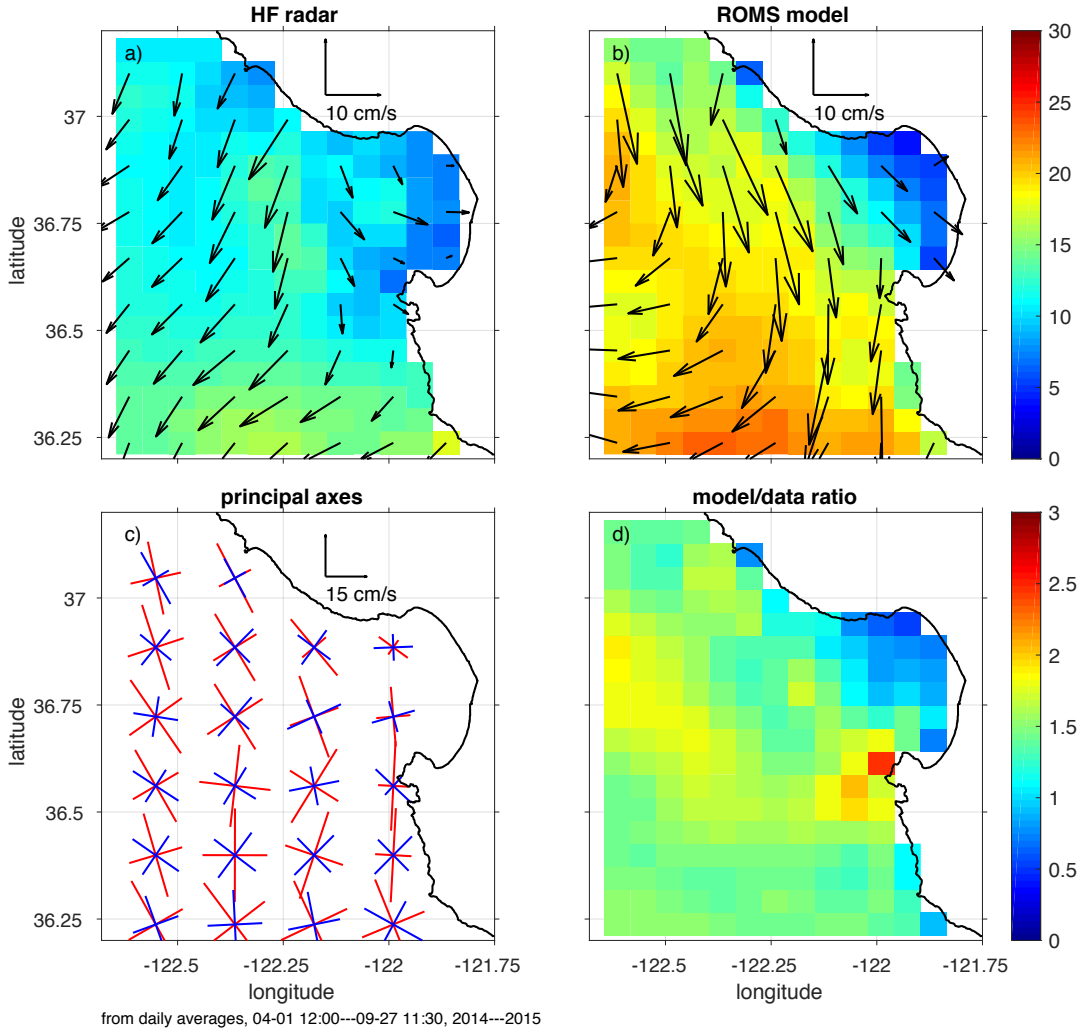

Figure 2. Time-mean velocities (arrows) and eddy speeds (color intensity) for HF radar-derived (a) and ROMS modeled (b) estimates of surface currents (cm s^{-1}). (c) Principal axes of variance for radar-derived (blue) and modeled (red) surface currents. Length of each axes from its origin gives standard deviation of current velocity. (d) Ratio of modeled to radar-derived mean eddy speed.

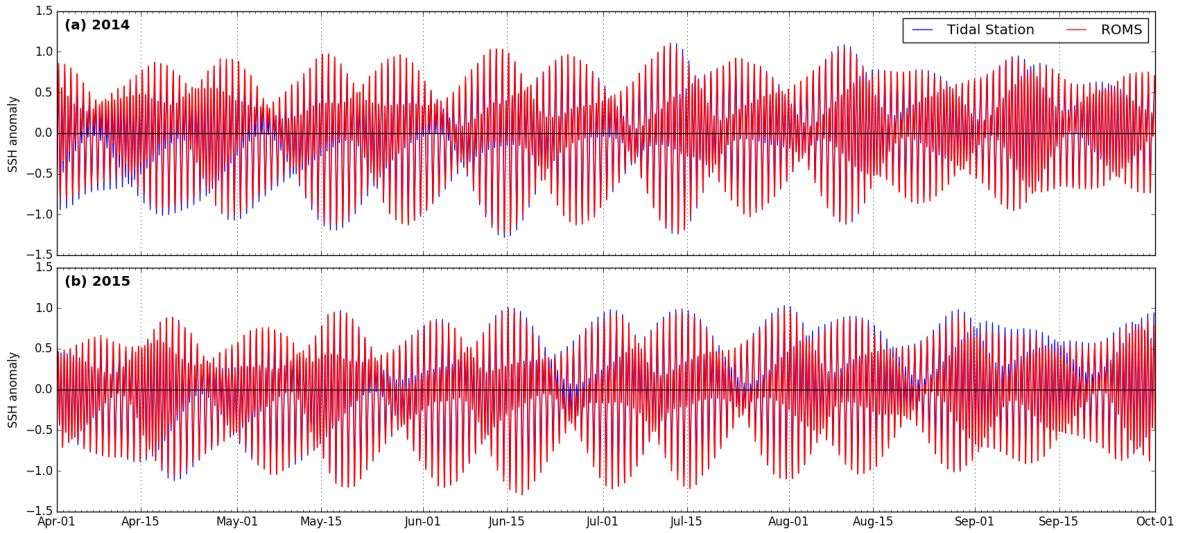

Figure 3. SSH anomaly in ROMS (red) and predicted by NOAA (blue) in 2014 (a) and 2015 (b) at Carmel Cove tidal station marked by the purple star in Figure 1. NOAA tidal prediction from https://tidesandcurrents.noaa.gov/noaatidepredictions.html?id=9413375.

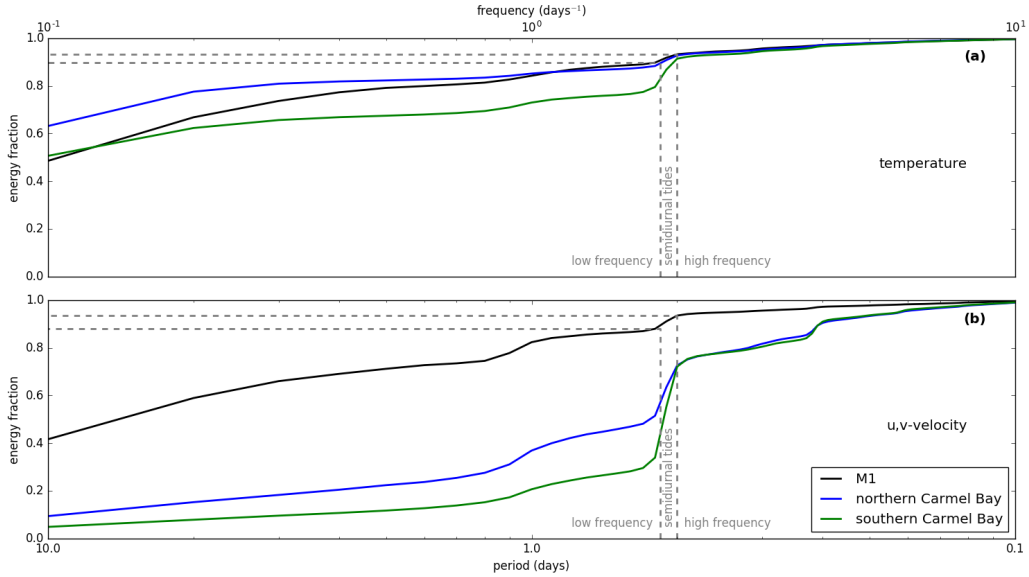

Figure 4: Power spectral density of (a) temperature and (b) complex velocities at 10 m depth, displayed as a cumulative distribution of energy. As a reference to offshore conditions, the energy spectrum at M1 is displayed in black. In northern (blue) and southern (green) Carmel Bay the energy spectrum is cumulative for all grid points.

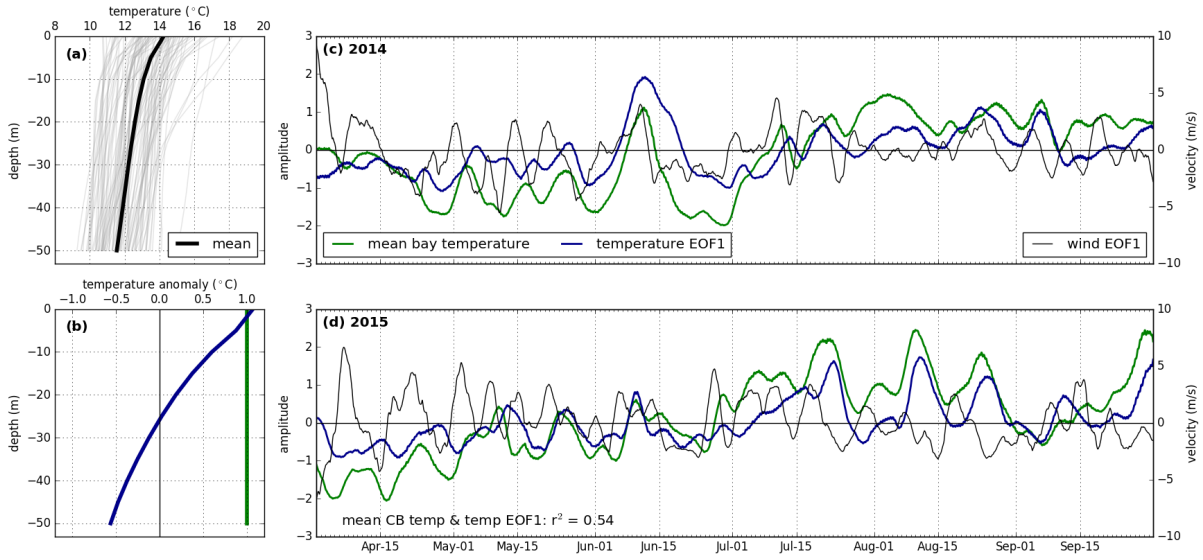

Figure 5. (a) Profiles of temperature (gray) and their mean (black) at one, representative location in central Carmel Bay shown in Figure 1c. (b) Temperature profile 'patterns' at the same representative location: vertical time-mean profile (green) and the first EOF mode (blue) of temperature variability once the time-varying bay-mean temperature has been removed. Amplitude time-series of the bay mean temperature (green) and EOF1 (blue) for 2014 (c) and 2015 (d), smoothed using a 3-day filter. Also shown are amplitude time-series for the first EOF of wind in the region, defined in methods section.

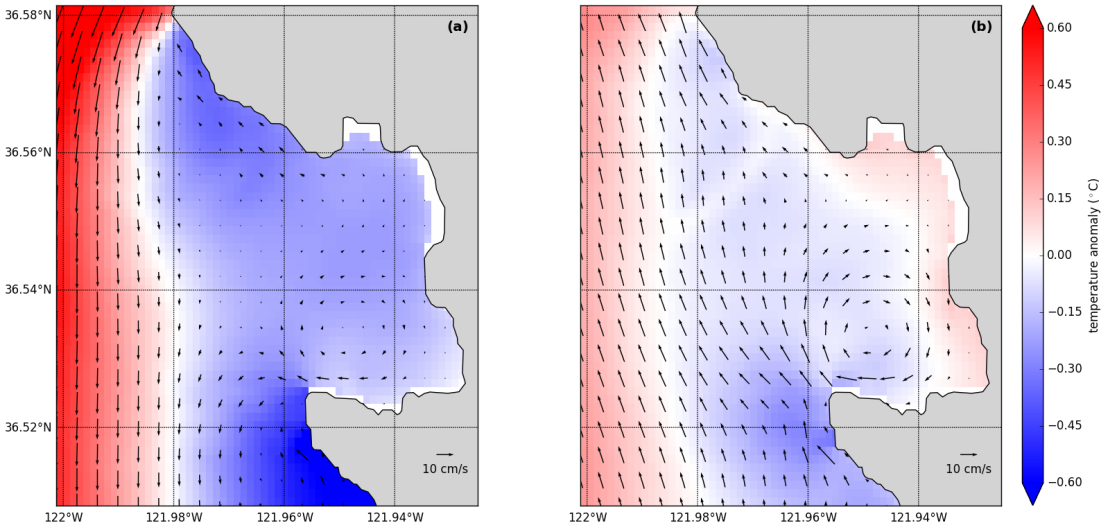

Figure 6: The mean circulation at 10 m depth during (a) upwelling- and (b) downwelling-favorable alongshore winds. Vectors show the velocity and color represents the mean spatial temperature anomaly.

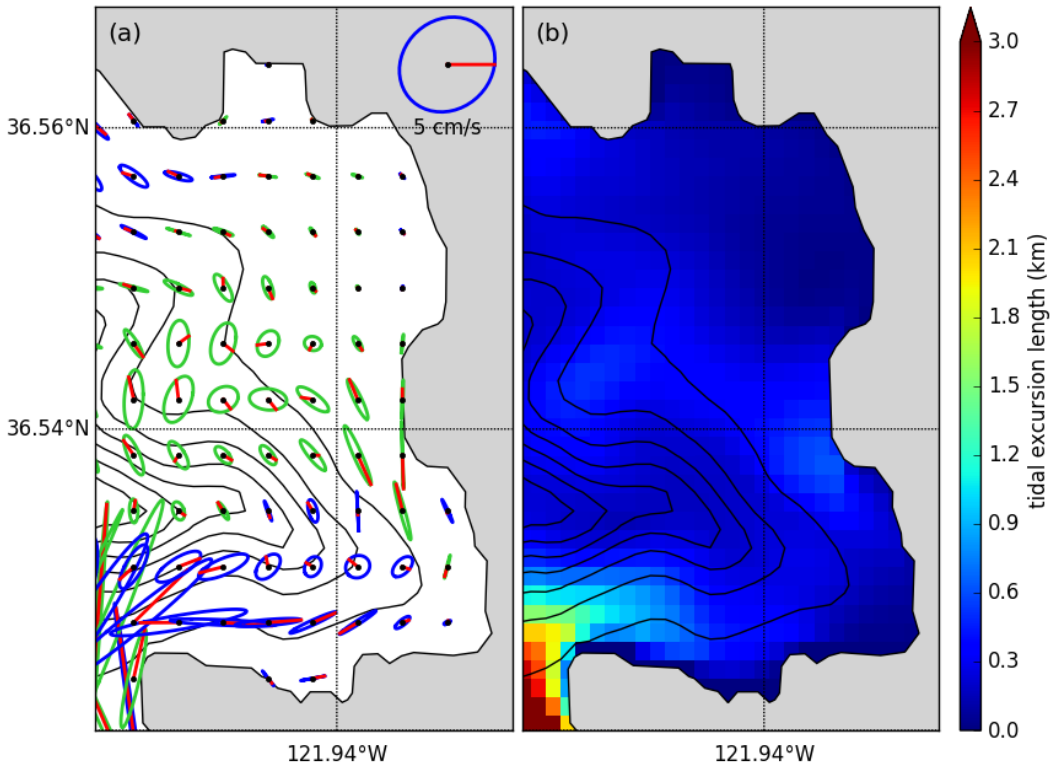

Figure 7: For the M_2 tidal constituent, (a) shows the tidal current ellipses, and (b) shows the tidal excursion length. Blue ellipses rotate anti-clockwise, green ellipses rotate clockwise, and red sticks indicate M_2 tidal velocity during high tide. Black contour lines denote bathymetry in 50 m intervals.

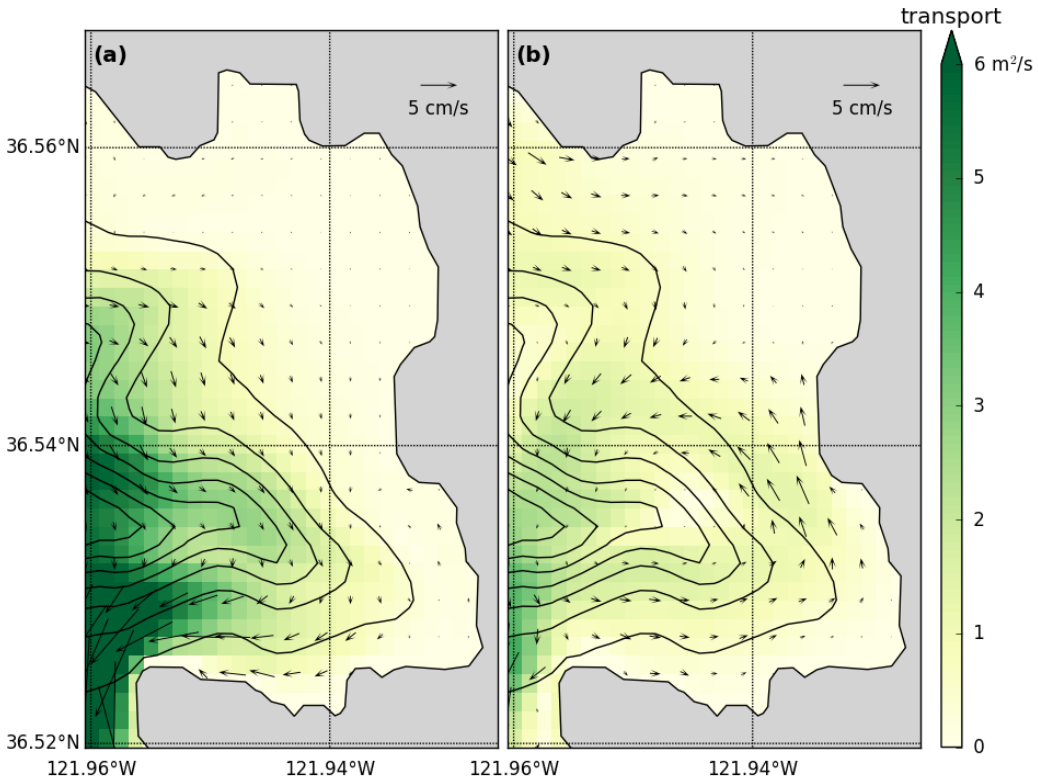

Figure 8: Shows the (a) low tide and (b) flood tide phases of the M_2 tidal constituent calculated from the depth-averaged velocity. Vectors represent the velocity and color represents the water column transport of the M_2 tidal constituent. High tide and ebb tide phases flow in the reverse direction of (a) and (b), respectively.

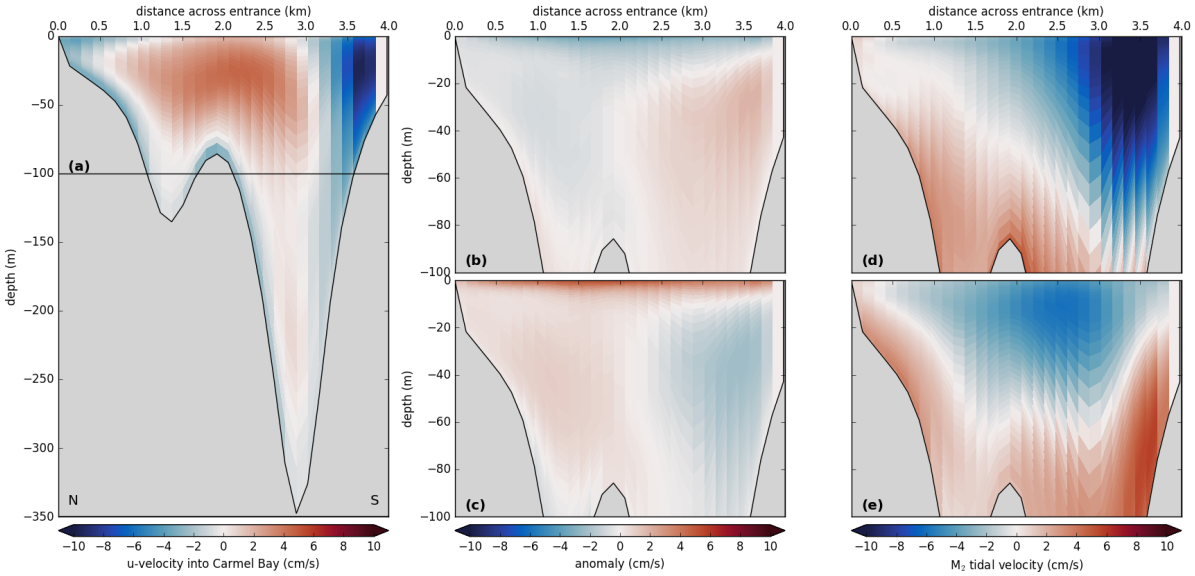

Figure 9: Depth-sections across the mouth of Carmel Bay (line in Figure 1c) show velocity in and out of the bay as (a) mean conditions from April 1 – September 30, 2014-2015, anomalies during (b) upwelling- and (c) downwelling-favorable wind conditions, and the M_2 phases (d) low tide and (e) flood tide. Exact reciprocals of (d) and (e) show the M_2 tidal velocity into the bay during high and ebb tidal phases, respectively. Note the same color scale for all subplots. The horizontal line in (a) denotes the cutoff-depth shown in the next four subplots.

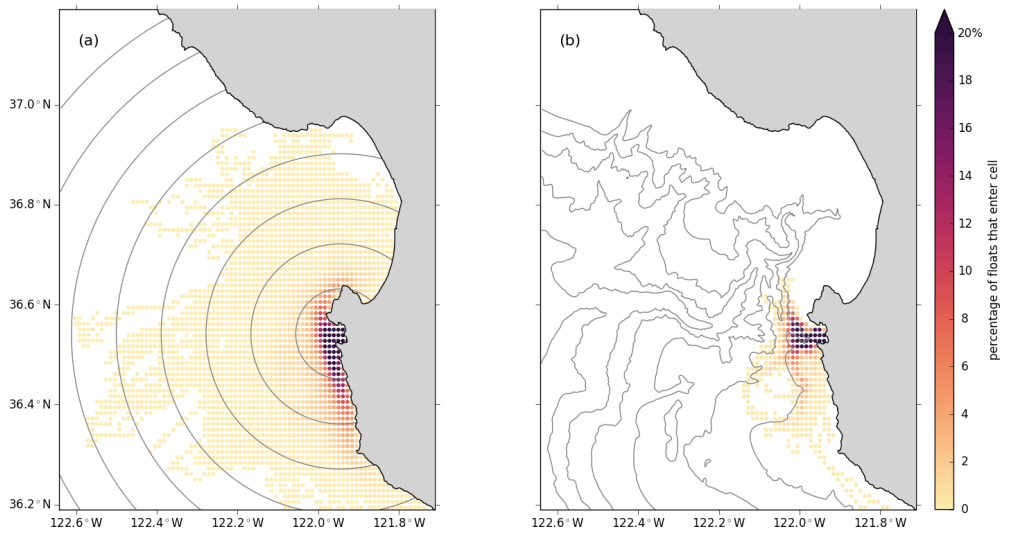

Figure 10: Maps of source water transport to Carmel Bay shown as probability of a water parcel passing through each geographic location. Source water transport is parsed by depth: (a) near the surface 0-50 m, and (b) deep water below 150 m, five days before its release location within Carmel Bay. A Godin filter is applied to source water depth trajectories to remove vertical fluctuations due to internal tides. Gray contours in (a) mark distance away from the center of Carmel Bay in 10 km intervals, and in (b) show bathymetry in 500 m depth intervals.

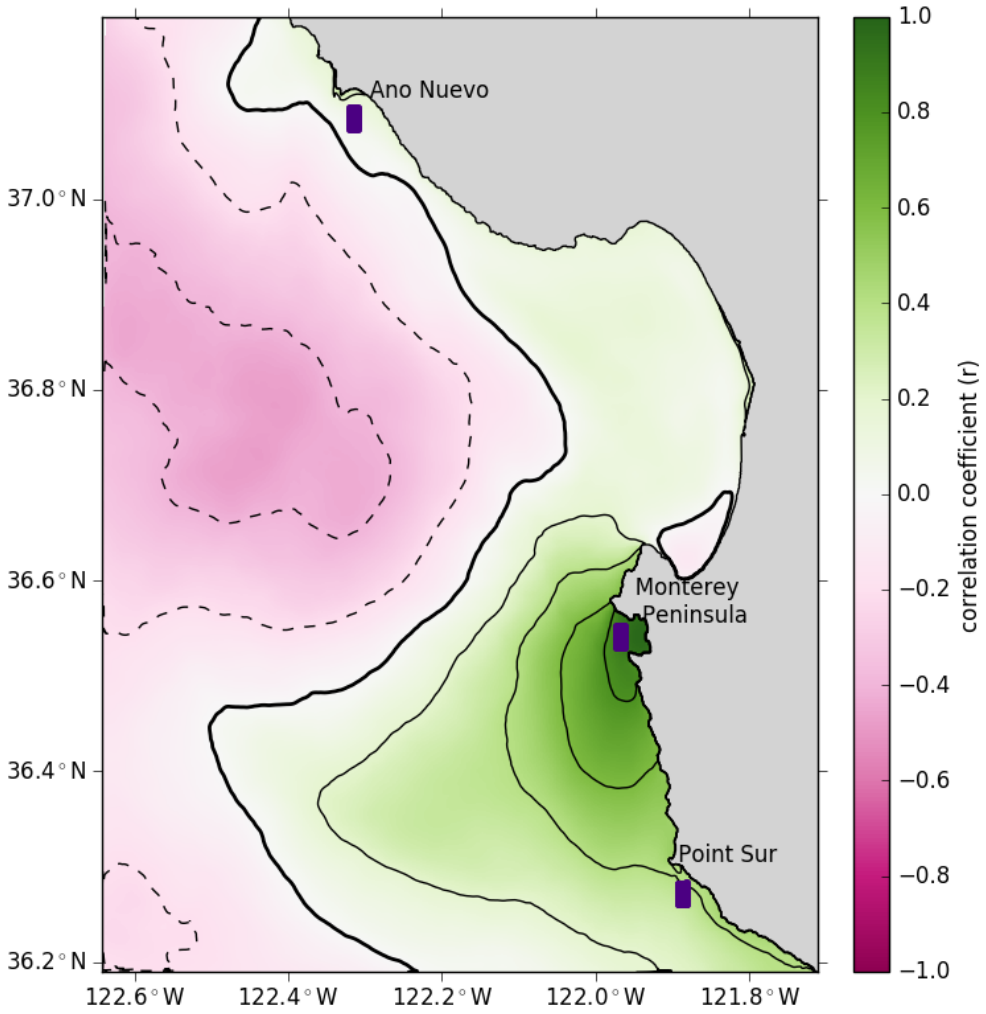

Figure 11: Map of Pearson's correlation coefficient (r) between SST anomalies at each grid point and the mean within Carmel Bay. The SST anomaly is calculated relative to the mean SST of the domain at each time-step to remove the seasonal cycle from the signal. Contour intervals of 0.2 match the color bar labels with dashed lines in areas of negative correlation. Purple areas in the lee of headlands mark where mean SST was calculated for upwelling centers.

CHAPTER THREE
A MODEL INVESTIGATION OF LARVAL TRANSPORT DURING SPRING/SUMMER UPWELLING SEASONS FOR SHALLOW-WATER ROCKFISH POPULATIONS AROUND THE MONTEREY PENINSULA

A model investigation of larval transport during spring/summer upwelling seasons for shallow-water rockfish populations around the Monterey Peninsula

Key Points:

- Particle tracking with a fine-scale regional ocean model identifies physical processes that can determine larval connectivity among coastal marine populations
- Larval retention greatly facilitates population self-replenishment: 83% of self-recruits stay within 50 km of their natal populations throughout the pelagic phase
- Alongshore wind reversals deliver near-surface larvae to Monterey Bay and Carmel Bay for recruitment

Abstract

The life cycle of many marine organisms includes a pelagic phase during which larvae are transported by ocean circulation before settling into local or distant populations. Population connectivity (i.e., patterns and rates of larval transport between populations) determines levels and spatial scales of interaction among populations and their size, dynamics and genetic exchange. We explore mechanisms of local population connectivity: self-recruitment and connectivity between populations ~10 km apart. We simulate transport of kelp rockfish (*Sebastes atrovirens*) larvae from local populations in southwest Monterey Bay and Carmel Bay which encompass numerous Marine Protected Areas (MPAs). We apply an offline nesting configuration (down to 120 m resolution) of the Regional Modeling System (ROMS) with realistic atmospheric and tidal forcing, from which Lagrangian trajectories are calculated by OpenDrift. Particles are released daily during the 2014 and 2015 spring upwelling seasons, maintained a depth of 2 m, and settle if they

reached suitable habitat within the competency period of 60-90 days. Of the particles released, less than 1% recruit locally to either region, with more settlement in southwest Monterey Bay than Carmel Bay. Local recruits spend a majority of the pelagic period within the bays, and 82% stay within 50 km from their release locations. Alongshore wind reversals and relaxations deliver larvae to the bays for recruitment. There is a weak relationship between larval transport and tides in Carmel Bay: near-surface larvae tend to enter (exit) during falling (rising) phases of the M_2 tide, with no preference for spring-neap tidal conditions. These results demonstrate that nearby populations (and thus MPAs) do not have homologous recruitment or exchange, which has important implications for MPA management.

1 Introduction

Understanding the patterns, spatial scales, and mechanisms of population connectivity (i.e., the exchange of individuals among populations) is of central importance to the ecology and evolution of any species and the communities they constitute. For the vast majority of coastal marine species, population connectivity occurs through the transport and delivery (recruitment) of propagules (animal larvae and algal spores) among populations (Cowen and Sponaugle, 2009; Kool et al. 2013). The majority of marine organisms release propagules into the water column that can eventually replenish local populations and communities or be transported hundreds of kilometers by ocean currents to replenish distant populations along the coast, thereby influencing the patterns and scales of demographic and genetic connectivity of populations. Larval dispersal and the resulting patterns of population connectivity are

also central to fisheries management by determining the distribution, abundance and rates of replenishment of fished stocks and their genetic diversity (Fogarty and Botsford, 2007), and for biodiversity conservation, including how populations and communities within marine protected areas (MPAs) contribute to both their own self replenishment and the replenishment of populations elsewhere along the coast (Carr *et al.*, 2017). During the pelagic dispersal period, a combination of physical and biological factors influences an individual larva's trajectory and ultimate survival (e.g., Morgan, 2014; Swearer et al. 2019). Only a small number of the total number of larvae released will survive to recruitment (Wiborg, 1976). Knowledge of the relative importance of the many processes that can determine propagule transport and survival is essential for advancing our understanding population connectivity and its applied significance.

Kelp rockfish (*Sebastes atrovirens*) are an abundant, ecologically and economically important shallow water species distributed along the eastern boundary of the Pacific Ocean, from central Baja, Mexico to northern California (Love *et al*., 2002). It exhibits the common bipartite life history of most marine organisms in which the distance of larval dispersal far exceeds the movement range of benthic juveniles and adults. Juveniles and adults are closely associated with giant kelp (*Macrocystis pyrifera*) (Holbrook *et al.*, 1990) Love et al. 2002), whose domain is restricted to shallow rocky substratum, bounded offshore by light limitation at the seafloor and nearshore by energetic wave action (Schiel and Foster, 2015). Adults release larvae at depths of 10-30 m during the late spring-upwelling season (Love *et*

al., 2002). Following a pelagic phase that extends up to three months (unpublished data), pelagic juveniles (20-30mm total length) settle into the surface canopy of giant kelp forests throughout the summer (Carr 1981, (Nelson, 2001). Juveniles and adults then reside within those forests throughout their lives.

During their pelagic larval phase, kelp rockfish larvae experience transport by ocean currents of the California Current System (CCS; Hickey, 1998). Coastal central California is a classic, wind-driven eastern boundary upwelling system. During spring-summer, the coastal ocean is forced by predominantly northwesterly (upwelling-favorable) winds, intermittently interrupted by periods of weak winds (wind relaxation) or southeasterly winds (downwelling-favorable) (Strub *et al.*, 1987; Strub *et al.*, 1987). Under upwelling-favorable conditions, offshore surface Ekman transport is replenished by onshore flow at depth and upwelling near the coast (Checkley and Barth, 2009). Flow reverses under downwelling-favorable winds. This broad-scale, coastwide motion is punctuated by variability on many scales owing to spatially and temporally structured forcing, flow-topography interactions, including shoreline configuration, and internally generated flow instabilities that together modify the horizontal and vertical velocities along the coast. For example, regions of intensified upwelling are often found south of coastal promontories (Rodrigues and Lorenzzetti, 2001; Castelao and Barth, 2006). The result is a very dynamic environment with mesoscale eddies, transient fronts, filaments, and other submesoscale features that influence the rate and trajectories of dispersal. Following the pelagic phase, kelp rockfish larvae may recruit to local populations if they find themselves in suitable habitat, shallow (nearshore) kelp-rich environments. The

degree to which rates and patterns of larval dispersal, delivery and recruitment are governed by large-scale, wind-driven motion versus local, variable fluid motions remains an open question.

Numerical modeling has become a powerful tool to investigate the effect of oceanographic processes and species traits (e.g., larval duration, behavior) on larval transport through studies of individual and ensembles of trajectories representing virtual larvae transported by modeled ocean currents (Paris *et al.*, 2005; Narváez *et al.*, 2012; Rochette *et al.*, 2012; Röhrs *et al.*, 2014). On the central California coast, modeled larval trajectories have been used to investigate the role of large-scale wind forcing on larval settlement. For example, in a 1.5 km resolution model of Monterey Bay on the central California coast, Pfeiffer-Herbert *et al.*, (2007) showed for a species of barnacle (*Balanus glandula*) that circulation patterns during wind relaxations led to more settlement than during upwelling-favorable winds. In a study using a broad, CCS-wide model at 3 km resolution, Drake *et al*., (2015) found that modeled settlement of larvae were coherent with wind stress on time scales longer than the pelagic duration for a variety of larval behaviors. In contrast, an idealized 4 km resolution study by Mitarai *et al*., (2008) and Siegel *et al.*, (2008) argued that settlement in a coastal upwelling system is not predictable, and unrelated to the wind stress, owing to the variability of mesoscale eddies that stochastically transport larvae toward or away from shore.

While these studies are illuminating, they suffer from resolutions that represent the larger scale wind patterns and resulting coastal circulations but are not well suited to investigate smaller-scale environments that may be dominated by

additional variability generated by local bathymetric and shoreline configurations as well as internal circulation processes (McWilliams, 2016; Dauhajre *et al*., 2017). Along the California coast, a network of Marine Protected Areas (MPAs) was created to protect fished populations, increase larval production, and foster coast-wide replenishment of species populations and communities (Botsford *et al.*, 2014). Many of these MPAs targeted kelp forest ecosystems with numerous species (including kelp rockfish) that rely on larval delivery for population replenishment. Within the greater Monterey Bay area, 17 such MPAs were established (https://wildlife.ca.gov/Conservation/Marine/MPAs/Network/Central-California). The MPAs in this region extend only a few kilometers in length (Figure 1b; mean area= 22km^2; Saarman and Carr, 2013 and many of the MPAs are adjacent to one another or only 10s of kilometers apart. How well these MPAs function as an interacting network connected by larval dispersal as opposed to a set of independent protected populations remains an outstanding question. To what extent do the larvae produced by populations within an MPA contribute to its own self-replenishment, nearby MPAs, or the fished populations outside of MPAs? To evaluate larval dispersal at these small spatial scales requires higher resolution ocean models than those previously used to study larval transport along the coast of California. The small spatial scale required to address these questions in this region render previous model studies of larval transport are inadequate to investigate MPA-specific domains and necessitate new model investigations at considerably higher spatial resolution.

This study investigates the transport of kelp rockfish larvae along the central California coast using a high resolution numerical model. It is focused specifically on

an ecologically-rich region of particular interest, Monterey and Carmel bays, which contain numerous MPAs. We examine larval export from a source population and the dynamics that retain or return larvae to the region, enabling self-recruitment and connectivity between MPAs within the two embayments. The goals of this study are three-fold: (1) to approximate the relative proportions of larvae that replenish their natal populations (self-recruitment) and supply nearby suitable habitat regions through the combined effects of large and small scale oceanographic processes, (2) to identify common pathways and modes of transport leading to self-recruitment and connectivity around the Monterey Peninsula, and (3) relate larval delivery to the physical forcing conditions.

2 Materials and Methods

2.1 Ocean circulation model

This study uses the same ocean circulation model configuration described in Part I (Lowe et al., 2020a) and is introduced here briefly. This application of the Regional Ocean Modeling System (ROMS) (Shchepetkin and McWilliams, 2005) uses offline, one-way nesting to resolve the nearshore circulation along the central California coast. This model includes atmospheric forcing derived from Coupled Ocean/Atmosphere Mesoscale Prediction System (COAMPS) (Hodur, 1997) and tidal forcing using 9 tidal constituents drawn from TPXO8-Atlas (Egbert *et al*., 1994). The model configuration consists of four telescoping grids with horizontal resolutions, each increasing by a factor of 3 and ranging from 1/30^{o} to 1/810^{o}. The outermost

domain spans a majority of the California Current System, from Washington State to Mexico.

For the study described here, only the two highest resolution nests (1/270^{o} and 1/810^{o}) were used, hereafter referred to as the b- and c-nests (Figure 1). The b-nest spans the central California coast from Point Reyes to just north of Morro Bay and extends offshore 155 km at roughly 350 m horizontal grid resolution. The c-nest covers a smaller domain from Pescadero to Point Sur and offshore 46 km at roughly 120 m horizontal resolution. These two innermost grids were run from January through September of 2014 and 2015. Because our focus is dispersal during the spring and summer upwelling seasons, calculations use model output from April through September each year.

2.2 Particle tracking

Lagrangian particle trajectories were calculated using the python-based, open source model OpenDrift, developed by the Norwegian Meteorological Institute (Dagestad *et al.*, 2018). The OpenDrift model framework was designed to be flexible, enabling a variety of transport applications. It has been used to investigate transport of Northeast Arctic cod eggs (Röhrs *et al.*, 2014), oil droplets in the Deepwater Horizon Oil Spill (Hole *et al.*, 2018), and benthic marine litter in the North Sea (Gutow *et al.*, 2018). We used OpenDrift to calculate the transport of kelp rockfish larvae off the central California coast. OpenDrift is capable of seamless particle trajectory integration across multiple nested grids, which was particularly useful in our application using the b- and c-nests. Our implementation of OpenDrift calculated

trajectories from hourly stored Eulerian fields using a second-order Runge-Kutta method.

Particle parameters were based on expectations for *S. atrovirens* larvae. In nature, adult rockfish are found in regions of kelp coverage. Suitable habitat for kelp rockfish was based on observed *M. pyrifera* distributions and defined here as regions within and near the MPAs with model depths between 5 m and 40 m. Specifically, we encompassed Pacific Grove Marine Gardens SMCA, Lover's Point SMR, and Edward F. Ricketts SMCA in southwest Monterey Bay and Carmel Bay SMCA and the part of Point Lobos SMR within Carmel Bay (Figure 1b and 1c). Particles were released from locations corresponding to density coordinates of the ROMS grid. In total, 222 and 205 release locations were considered as suitable habitat within southwest Monterey Bay (swMB) and Carmel Bay (CB), respectively (Figure 1b and 1c).

At parturition, a female rockfish releases *100,000-200,000* viviparous larvae (Romero, 1988; Dick, 2009) from bottom and mid-depths, yet kelp rockfish juveniles are predominantly collected in the kelp canopy near the surface (Carr, 1991; Nelson, 2001; Love *et al.*, 2002). Larvae of *S. atrovirens* (or similar nearshore rockfish species) have not demonstrated vertical swimming behavior; instead, larvae are thought to shift their position in the water column rapidly through positive buoyancy after release. Tank experiments revealed *S. atrovirens* larvae are capable of instantaneous horizontal swimming speeds of ~0.5 cm/s at parturition, slightly increasing until flexion at 6-8 weeks since release, then develop strong swimming abilities, reaching speeds comparable to currents at settlement (Kashef *et al.*, 2014).

These are instantaneous speeds, so it still remains unknown if these larvae swim persistently for their behavior to influence transport and delivery. Since these larvae reach the competency period soon after flexion and persistent swimming is unknown, horizontal swimming was not included in our simulations. In our primary analysis, we released larvae at 2 m depth, and their transport resulted from interpolated horizontal currents at this depth. We also considered sensitivity to these choices, analyzing additional trajectories from particles transported by 2-dimensional ocean currents released at 10, 20, and 30 m depths, and particles transported by 3-dimensional ocean currents and released at 2 m depth.

In nature, kelp and similar nearshore rockfish larvae are released in the spring and develop into juveniles over a pelagic period ranging from 2-3 months (Gilbert, 2000; Watson and Robertson, 2004; Fisher *et al.*, 2007). In our study, we released particles April-June and tracked particle trajectories for a total of 90 days following release. Settlement was allowed to occur if larvae encountered suitable habitat within the study regions (i.e., the release locations) during a modeled competency window of 60-90 days since release. A total of 77,714 particles were released and analyzed (Table 1).

3 Results

3.1 Trajectory analysis for southwest Monterey Bay and Carmel Bay regions

Over the course of several months, virtual larvae experience a range of velocity conditions that disperse them throughout the domain. The potential extent of dispersal can be seen in Figure 2, which presents an example set of larval trajectories

from each release region. Grey lines represent non-recruits, those larvae that did not return to an allowable settlement habitat (either southwest Monterey Bay (swMB) or Carmel Bay (CB)) during their larval duration. Colored lines indicate particles that successfully settled, with self-recruits colored purple and navy from swMB and CB, respectively. Larvae that were released from one region and recruited to the other region are referred to as connected recruits; southward recruits were transported from swMB to CB and are colored pink, and northward recruits, transported in the reverse direction from CB to swMB are shown in turquoise. This color scheme will be maintained throughout this paper.

Particles released from both release locations experienced primarily three modes of transport: (1) southwestward movement away from the Monterey Peninsula study region, (2) cyclonic transport within Monterey Bay, and (3) random offshore transport in varied directions. Generally, a larger fraction of particles originating in CB than swMB experience mode 1, whereas a larger fraction released from swMB than from CB had a greater likelihood of experiencing mode 2. Mode 3 results from stochastic transport associated with variable ocean conditions throughout the domain and is dominated by non-recruits.

The transport patterns just described are also visible in percentage maps that provide probabilities of a float being present at locations throughout the domain during the spring/summer period (April through August) calculated on a grid of 9x9 c-nest grid cell aggregates (Figure 3). The vast majority of particles released did not recruit to either region (Figure 3a,d). Of 40,404 larvae released from swMB, 40,288 did not return to either swMB or CB during their competency period, constituting

99.7% of floats; a total of 37,310 particles were released from CB and 37,211 (99.8%) were lost to these two regions. From both release regions, particles dispersed throughout the entire domain, though mostly with exceedingly low probabilities (less than 1%). Probabilities of non-recruiting particles released in swMB being found within MB were higher (above 5%) than in offshore regions, partly resulting from entrainment within Monterey Bay's characteristic cyclonic circulation (Broenkow and Smethie, 1978). Monterey Bay was a less common, but still non-negligible, destination for CB non-recruitment releases. Highest probabilities of non-recruits released from either swMB or CB were to their southwest: within 5 km of the coast around the Monterey Peninsula from swMB and simply to the southwest from CB. These probabilities reflect the dominant southward and offshore transport of the surface flow during spring/summer upwelling conditions. The black lines in Figures 3a,d which present the (smoothed) mode of the zonal probability distribution for each latitude south of latitude 36.58°N.

A total of 100 particles (0.25%) self-recruited to swMB and 32 (0.09%) to CB. Self-recruits to both regions exhibited highest probabilities within a few km of each suitable habitat region. The swMB self-recruits were transported primarily within Monterey Bay with scattered transport northward, southward, and offshore. The self-recruits to CB show relatively high probability of transport to the south and diagonally offshore and some transport northward into Monterey Bay.

From swMB, 16 floats (0.04%) recruited southward to CB, and from CB 57 particles (0.2%) recruited northward to swMB. The percentage maps show highest values along an oceanographically shortest route around the Monterey Peninsula for

connectivity in both directions. Northward recruits exit Carmel Bay and the majority move immediately northward around the peninsula, while some travel southward off the Big Sur coast before flow reverses and carries them northward. Once inside Monterey Bay, a majority of the Northward recruits are transported within Monterey Bay's cyclonic circulation before reaching competency and finding suitable habitat in swMB. The handful of Southward recruit trajectories present the same transport patterns but in reverse order.

The time larvae spend in MB and CB before becoming competent to recruit (60 days after release) further defines the pathways for recruitment (Figure 4). More than 50% of all non-recruits from both regions spent less than 4 days within either MB or CB. Vastly different from non-recruits, self-recruits to both populations spent almost the entire pelagic period within either bay. Half of CB and swMB self-recruits spent more than 60 and 48 days, respectively, within either bay. Connected recruits naturally spent more time outside of the bays than the self-recruits, but still spent more time within the bays than elsewhere offshore. More than half of the connected recruits in each direction spent well over half of the PLD within the bays. Notably, a handful of recruits to Monterey Bay (self-recruits and northward recruits) spent very little time within either bay. Although the number of larvae that spend a large amount of time offshore and later recruit locally is trifling compared to the number of non-recruits, they constitute a small fraction of the total recruits to swMB. There is no

equivalent mode of sustained offshore transport before recruitment to Carmel Bay in our model results.

Differences in trajectories between recruits and non-recruits are further highlighted when examining the maximum distance from release over the lesser of the pelagic larval duration (PLD) or time to settlement (Figure 5). Here distances are calculated as geographic distance from release location throughout the trajectory and not following circuitous trajectories. Non-recruits experienced a wide range in maximum distance, with 81% and 94% of floats traveling over 100 km from the swMB and CB source regions, respectively. The difference in these percentages can be interpreted similarly to the percentage maps. Many particles released in swMB experienced transport within Monterey Bay and the surrounding region offshore, but not necessarily back to the settlement habitat, thus limiting their maximum distance traveled to 40 km or less for 15.2% of non-recruits. There is no similar pathway for non-recruiting particles released in CB; most were transported to the southwest and out of the domain altogether. In contrast, the majority of recruits remained quite close to natal regions. Only 6.3% and 10.5% of connected recruits travelling southward and northward, respectively, exceeded a maximum distance of 60 km from their starting locations. Connected-recruits both directions and swMB self-recruits all showed peaks near 40 km, indicating that the majority of these recruits were limited by Monterey Bay's northern boundary. There is also a secondary peak of maximum distance away near 10 km, showing that a sizeable portion of southward recruits went solely around the Monterey Peninsula and some swMB self-recruits stayed very close

to the suitable habitat region throughout the PLD. Self-recruits to Carmel Bay were highly constrained with 50% of them travelling 4.4 km or less from their release locations. The larger median distance away for recruits to swMB compared to CB again reflects the transport of a large number of floats throughout Monterey Bay and the ability to enter the suitable habitat region in southwest Monterey Bay.

Although the majority of recruits stay near Monterey and Carmel bays, a portion of recruits traveled further before they were transported back to the region in time to settle. The geographical extent of recruit trajectories is shown by Figure 6. In a few cases, recruits to swMB traveled just north of Point Año Nuevo whereas northern Monterey Bay was the northern extent of trajectories by recruits to CB. More recruits traveled south of Point Sur, up to 55 km offshore from the Big Sur Coast. In general, recruits to swMB (Figure 6b,c) traveled greater distances along the coast and offshore than recruits to CB (Figure 6a,d).

3.2 Influence of alongshore winds and tidal conditions on nearshore transport

The statistical differences in trajectories between non-recruits and recruits emerge rapidly following release. Figure 7 shows the mean distance from release for non-recruits, connected recruits, and self-recruits, as well as their 5% to 95% distributions for different times since release. These distances can be considered relative to the minimum and maximum distances between swMB and CB suitable habitat regions (6.7 and 13.6 km, respectively). For particles released in swMB, non-recruits rapidly separate from recruits, with their mean distance from release exceeding 13.6 km after 2 days and continually increasing subsequently.

Comparatively, the mean dispersal distance of swMB self-recruits reaches 13.6 km after 8 days. Southward recruits initially follow non-recruits by rapidly moving away from their release locations, but after 1.5 days their mean dispersal distance fluctuates between 5.9 and 13.6 km from release throughout the pelagic period with a brief spike above 20 km around 40 days since release. Particles released in CB disperse slightly slower than those released in swMB. Non-recruits from CB pass the mean distance of 13.6 km from release after 3.5 days, whereas northward recruits reach this mean distance 10 days following release. Recruits released in CB diverge from non-recruits after 2 days. Southward and northward recruits settle with mean distances of 10.2 and 10.1 km from their release locations, respectively. Self-recruits to swMB and CB settle with mean distances of 1.9 and 2.2 km from release, respectively.

The particle trajectories may be considered in the context of local wind conditions. Alongshore winds represent a dominant forcing mechanism along the California coast, particularly at weather-band frequencies of a few days and longer (Allen, 1980; Checkley and Barth, 2009). To examine how the circulation changes under different wind conditions, we used empirical orthogonal functions (EOFs) of the surface wind field, averaged over a subdomain in the immediate vicinity of Carmel Bay (Figure 1b). The leading mode points -12.4 degrees from true north and characterizes the alongshore wind component over this portion of the coast. We focused on subtidal frequencies and removed the high frequency variability through a wind-intermittency index following Giddings et al. (2014) with a 0.5 day exponentially-weighted running mean of the EOF1 amplitude, hereafter called the alongshore wind. In this region and during the study period, this alongshore wind has

very small mean values (approximately 0 m/s each year) and exhibits large-amplitude oscillations, with northerly winds (defined by EOF1<0) occurring roughly 53% of the time, interrupted with intermittent, reversal events (EOF1>0). Wind relaxation refers to intermediate conditions, when the alongshore winds are weak (EOF1 between 0 and -2 m/s).

The alongshore wind strongly impacts recruitment around the Monterey Peninsula. We find that 69.3% and 65.4% of non-recruits exit Carmel and Monterey bays, respectively, when EOF1 is less than zero. In contrast, recruits are delivered to Carmel Bay and Monterey Bay primarily during wind reversal events (Figure 8). To isolate the impact of wind reversals on delivery from the possible tidal influences, this analysis includes only self-recruits that were outside CB or MB for at least one day (13 of 32 CB self-recruits and 89 of 100 swMB self-recruits) and connected-recruits first entrance into the recruitment bay. Recruits to Carmel Bay primarily enter when the winds are reversed (i.e., southerly): 84.6% CB self-recruits and 68.8% of southward recruits. This mechanistic relationship exists also for MB, though less strongly: 77.2% of northward recruits enter during wind reversal conditions, and 65.2% of MB self-recruits re-enter during wind relaxation or reversal conditions. The 5^{th} to 95^{th} percentile range of EOF1 for recruits entering the bays are skewed positive: -2.1 to +6.0 m/s (CB self-recruits), -0.5 to +8.1 m/s (southward recruits), -2.3 to +4.0 m/s (swMB self-recruits), and -1.8 to +6.4 m/s (northward recruits). Comparing these percentile ranges to the alongshore wind conditions throughout the study period (with

5th to 95th percentiles of -3.4 and +4.2 m/s), clearly supports that recruits are being delivered to the bays when the northerly alongshore winds relax and reverse.

In addition to the alongshore wind influence, we considered if tidal motion contributed to settlement. As discussed in Lowe et al. (2020a), this region experiences mixed, semidiurnal tides, dominated by the M2 tidal constituent, and particle paths nearshore exhibit small-scale tidal deviations. To quantify the effect of tidal motion on recruitment, we calculated the particle flux across the mouth of Carmel Bay as a function of tidal phase and range. This analysis used the SSH from the ROMS grid point closest to Carmel Cove Tidal Station. The python version of T-TIDE (Pawlowicz *et al.*, 2002) was used to extract the signal of the M_2 tidal constituent. We did not find any clear qualitative relationship with other tidal constituents' phases and particle flux into and out of CB. The tidal range was calculated as the running difference between the maximum and minimum SSH using a 30-hour window. This set of calculations includes every time a particle exits or enters Carmel Bay to investigate the effect of tides on recruitment.

Here, we will briefly describe the tidal circulation and its relationship to particle transport in and out of Carmel Bay. During low tide, the M_2 surface tide is mostly outward and strongest in southern Carmel Bay. During flood tide in Carmel Bay, near surface waters are primarily outward and deeper water especially in the canyon flows inward and dominates the signal. These patterns reverse during high and ebb tidal phases. See Lowe et al. (2020a) for greater detail on the tidal circulation. Figure 9 shows particle statistics for the M_2 phase in 10^o divisions.

Particle flow in and out of Carmel Bay occurs during all phases of the M_2 tide, albeit asymmetrically. A weak majority of non-recruits exit Carmel Bay during rising tidal conditions (58.9%) and enter during falling tidal conditions (56.2%). Similarly, the southward recruits have the strongest majority (74.0%) that enter during rising tidal conditions. Northward recruits (33.3%) exit Carmel Bay during flood to high M_2 tide conditions. Self-recruits tend to exit and enter Carmel Bay during opposite phases of the tide: 35.0% exit during ebb to low M_2 tide conditions, and 34.4% enter during flood to high tide conditions. These matching statistics indicate that self-recruits exit and return over a tidal cycle.

During spring tidal conditions, there is greater exchange between Carmel Bay and offshore. However, non-recruits and local-recruits did not show a preference for spring or neap tidal conditions. For reference, 53.4% of non-recruits exit and re-enter Carmel Bay when the tidal range is greater than the median (1.6 m). Showing preference for spring tidal conditions, 70.4% of southward recruits enter Carmel Bay when the tidal range is greater than the median. The minimal differentiation between non-recruits, self-recruits, and northward recruits indicate spring tidal conditions do not directly increase recruitment. As a lower frequency process, the spring-neap tidal cycle oscillates over a 2-week period. Statistical preference for spring tidal conditions by southward recruits may result from transport by higher frequency processes (alongshore winds and M_2 tides described above) and recruit proximity to Carmel

Bay. This analysis indicates that spring tidal conditions did not enhance local recruitment to and from Carmel Bay.

3.3 Sensitivity Analysis

We acknowledge that the depth(s) of *S. atrovirens* larvae throughout the pelagic phase remains unknown. Therefore, we conducted all the above analysis with floats at constant depths of 10, 20, and 30 m (Table 1). We also analyzed floats released at a depth of 2 m and transported by the 3-dimensional circulation, but do not include this case in our description because the results appear to be a combination of the constant depth cases and require more rigorous analysis including depth throughout the trajectory to adequately describe and relate to oceanographic processes. The 10 m case had the most local recruits: 7x more local recruits than the base case at 2 m. The 20 m case also had more local recruits, whereas the 30 m case had fewer but comparable numbers to the base case.

There were three major differences between the base case at 2 m and floats that maintained deeper depths throughout their trajectories: (1) shift in the most common type of local recruitment, (2) inter-annual shift in local recruitment, and (3) dispersal trajectories. When the floats were run at constant depths of 10, 20, and 30 m, there were far more recruits released in CB than swMB, with the majority of local recruits being CB self-recruits. This result was very different from the base case that had the most local recruits to swMB, and the majority were swMB self-recruits. The near-surface base case had more recruits in 2015 than 2014, whereas the deeper floats had more local recruitment in 2014 than 2015. This interannual shift with depth is likely due to interannual variability in the alongshore winds and related upwelling

dynamics along the coast. A different relationship emerges between alongshore winds and recruitment to Carmel Bay than was found for near-surface floats. At 10, 20, and 30 m, the majority of recruits to CB arrive during upwelling-favorable wind conditions, opposite timing of near-surface arrival. The relationship between alongshore winds and recruitment to Monterey Bay is less clear. The majority of recruits to swMB arrived during wind reversal conditions at depths of 2 and 10 m and upwelling-favorable conditions at 20 m. There were also notable differences in float trajectories with depth. At 10 m, local recruits were transported offshore far more often before returning to recruit locally around the peninsula; additionally, a few local recruits (in all 4 categories) were entrained in an eddy along the Big Sur coast before returning northward to recruit. At 20 m, many local recruits released in CB were transported southward or southwestward to approximately midway down the Big Sur coast, before returning to the peninsula to recruit. In both these cases, local recruits traveled greater distances away before recruitment than floats at 2 m. Additionally, there was far more cross-shore transport, whereas transport was mostly in the alongshore direction near the surface at 2 m. In stark contrast, at 30 m the CB self-recruits stay almost exclusively against the coast from the tip of the Monterey Peninsula to Point Sur, and northward recruits hug the coast in a very direct route of transport around the Monterey Peninsula, with two exceptions in both cases. These differences in timing and trajectories of floats transported at depths near the surface to 30 m, add to a mechanistic understanding of the relationship between alongshore wind and dispersal along the central California coast.

4 Discussion

In this study, we used a high-resolution ocean model to calculate near-surface Lagrangian particle trajectories to investigate larval transport and connectivity of nearshore organisms within a limited region of the coastal ocean off central California. Specifically, we focused on two regions of larval release of kelp rockfish that spawn during late spring and summer from MPAs in southwest Monterey Bay (swMB) and Carmel Bay (CB) and whose larvae experience a 2 months-long PLD before settlement. Of all larvae released in this study, less than 1% recruit locally (either region), with more recruitment to swMB than CB. The local recruits spent a majority of the pelagic period within Monterey and Carmel bays, and 82% of all recruits stayed within 50 km from their release location. We provide strong evidence that alongshore wind relaxation and reversal events deliver larvae into the bays for recruitment. We find a weak but noteworthy relationship between larval transport and the tides in Carmel Bay: larvae tend to enter (exit) during ebb (flood) phases of the M2 tidal cycle, with no preference for spring versus neap tidal conditions.

There is an ongoing discussion about whether larval transport and the resultant population connectivity is stochastic (Woodin, 1991; Domingues *et al.*, 2011; Smale *et al.*, 2011; Williams and Hastings, 2013) or predictable (Smith and Suthers, 2000; Aburto-Oropeze *et al.*, 2007; Ogburn *et al.*, 2012). The episodic nature of larval settlement has been attributed to the organism's life history and variable mesoscale circulation that stochastically delivers larvae to shore (Mitarai *et al*., 2008; Siegel *et al.*, 2008). Both of these studies use an idealized coastal model with homogenous forcing throughout the domain that yields heterogeneous settlement

patterns for various scenarios. Since these settlement patterns are statistically similar, the authors conclude that settlement is inherently a stochastic process. In contrast, empirical and modeling studies have linked larval settlement to upwelling dynamics (Farrell *et al.*, 1991; Roughgarden *et al.*, 1991; Wing *et al.*, 1995; Wing *et al.*, 1995; Dudas *et al.*, 2009), winds (Cuif *et al.*, 2014; Bonicelli *et al.*, 2014), submesoscale processes (Bjorkstedt *et al.*, 2002; Sponaugle *et al.*, 2005), and tides (Criales *et al.*, 2015). Off the central CA coast just south of our study location, an empirical study considered the relationship between oceanographic data and larval recruitment of rockfish (Wilson *et al.*, 2008). They found a relationship between rockfish recruitment and coastal upwelling conditions on a seasonal cycle. Species whose adults aggregate in the water column, spawn in winter to early spring, and have pelagic larval durations of 3-4 months (BYO complex) recruit during upwelling-favorable conditions, whereas species whose adults are more benthic, kelp-associated, spawn in early to late spring, and have shorter pelagic larval durations of 2-3 months (KCGB complex), which includes our study species *S. atrovirens*, recruited during downwelling-favorable conditions. More recently, a modeling study on the central CA coast concluded that alongshore wind stress drives larval settlement on timescales of days to a year and that wind stress averaged over the PLD provides a useful metric to predict settlement (Drake *et al.*, 2015). While several studies connect larval settlement to wind relaxation and reversal events (Wing *et al.*, 1995; Morgan *et al.*, 2000), the results from this study emphasize the importance of reversals with 70.9% of recruits being delivered to Monterey and Carmel bays when the alongshore winds are reversed and an additional 16.6% of recruits delivered when the winds are

relaxed. Thus, delivery to the coast (especially to Carmel Bay) prior to recruitment occurs in our study primarily during downwelling-favorable wind conditions. It is important to note that delivery for recruitment does not occur on every wind reversal event because ready-to-recruit larvae (within or near competency) were not always available near Monterey or Carmel bays when such a wind event occurred. A study with a broader spatial scope (for example with more suitable habitat regions releasing larvae and seeding the coastal ocean with more larvae) may bolster this relationship.

Over the course of the pelagic period, an individual larva may experience a variety of oceanographic conditions. The CCS exhibits cross-shore changes with offshore circulation dominated by mesoscale eddies and larger-scale motion and the near-coastal zone in which wind-driven forcing drives complicated transient motion through upwelling, tides, and flow-topography interactions. Energy is evenly divided between tidal motion and wind-driven circulation within Carmel Bay (Lowe et al., 2020a). Therefore, individual larvae may experience vastly different oceanographic conditions from one another as a function of cross-shore positioning at any given time. The majority of local recruits spend their pelagic period primarily within Monterey and Carmel bays and were transported by a combination of bay, tidal, and wind-driven circulation. Larvae that stay on the innermost portion of the continental shelf experience slower alongshore velocities and increased cross-shore mixing, which amount to increased variance in the dispersal of propagules and a dramatic increase in local replenishment to a region (Nickols *et al.*, 2012). Most often, non-recruits were quickly expelled from both bays into the primarily wind-driven, strong circulation off the coast. A portion of local recruits were transported by the offshore

circulation for brief and longer periods of time. The variability in the stronger, offshore circulation retained these larvae in the region, which later enabled them to recruit (mostly to swMB).

Combining self-recruits and connected-recruits by destination yielded 3 times more recruits to swMB than CB. It is important to note that in our experiment, release/settlement regions in swMB and CB have roughly equal areas (3.4 and 3.1 km^2, respectively) with 4% more floats released from swMB than CB. Thus, the three-fold increase in probability of recruitment to swMB than CB is a substantial difference not accounted for by area. The mouth of Monterey Bay is 36 km wide compared to 3 km in Carmel Bay. Therefore, Monterey Bay experiences greater exchange with the open ocean than Carmel Bay, increasing the potential for capture of occasionally distant particles, and increasing the probability of recruitment to suitable habitat in swMB. Often during upwelling events, a jet flows southward across the mouth of Monterey Bay and bifurcates with some flow into Monterey Bay, creating cyclonic circulation within the bay and anticyclonic circulation outside of the bay (Rosenfeld *et al.*, 1994). A similar circulation pattern can also develop during wind relaxation events (Shulman *et al.*, 2010). More often during relaxation events, the strong alongshore flow slows and reverses, moving northwestward along the mouth of Monterey Bay with flow into and out of the southern and northern ends of the bay, respectively. The offshore anticyclonic circulation retains some larvae in the region and captures larvae that have ventured further away and returned, allowing these larvae to later recruit within Monterey Bay. Shulman et al. (2007) offer models of fluxes into southern Monterey Bay during wind relaxation and Manzer et al. (2019)

and studied how such relaxation events also contribute to phytoplankton abundance in southern Monterey Bay; the implications of these studies are consistent with our own results. Varied fluxes at the entrance to Monterey Bay lead to less dependence on wind relaxation/reversal events for larval delivery than to Carmel Bay.

In Carmel Bay, larval delivery occurred almost exclusively during wind reversal events, and the M_2 tidal circulation carries larvae in and out over a tidal cycle. The predominant physical forcing varies spatially and influences larval dispersal in other eastern boundary upwelling systems as well. An empirical study in Chile provided evidence that settlement of crab larvae was controlled by winds in the outer estuary and the spring/neap tidal cycle in the inner estuary (Pardo *et al.*, 2012). A probative study in the Benguella Upwelling System related onshore larval transport to a sequential combination of downwelling-favorable wind conditions and local-scale tidal and wave processes (Pfaff *et al.*, 2015). In our study, we do not identify a sequential necessity, but infer the order of transport mechanisms based on the propagule's cross-shore position throughout its trajectory.

It is well-known that marine larval dispersal spans multiple spatial and temporal scales. Our nested model configuration was specifically designed to simulate small-scale circulation and allow for particles to be transported great distances during the pelagic period and potentially recruit. This modeling experiment captures recruitment to the Monterey Peninsula that remained local throughout the entire PLD and a few examples of larvae that were transported longer distances but managed to return and recruit locally. A subset of self-recruits to swMB and CB

never leave the bay where they were released. To evaluate self-recruitment, especially to CB, one must resolve the local circulation within the bay to allow for this subset of the overall population that never makes it out. While our model configuration allows for the larger-scale influences on transport, it does not resolve the very fine-scale dynamics that may be important for settlement in the kelp forest for *S. atrovirens* or surf zone dynamics important for species that enter the intertidal zone. In Carmel Bay, four pulses of *Pseudo-nitzschia* entered a nearshore observation region during periods of warm SST due to upwelling-relaxation events, whereas shoreward transport of barnacle larvae was driven by internal tides, particularly the spring-neap cycles (Shanks *et al.*, 2014). Our analysis of *S. atrovirens* recruitment to Carmel Bay includes strong evidence of delivery during wind reversal events, but no preference for spring-neap tidal cycles. Carmel Bay's tidal circulation is strongly shaped by Carmel Canyon (Lowe et al. 2020a), therefore larval transport at deeper depths and nearshore settlement processes may be driven by internal tides and relate to spring-neap cycles, but this modeling study does not account for such motion. Modeling studies of particle transport in the surf zones in Monterey Bay and Carmel Bay show onshore transport of positively buoyant larvae during wind-driven surface currents, then waves and small eddies retain particles in the surf zone, and turbulence induces sinking of particles for recruitment (Fujimura *et al.*, 2014; Shanks *et al.*, 2015). For studies of species that recruit to the intertidal zone, we suggest compromising the

expansive geographic extent of our study for a smaller domain that still allows some stochastic offshore transport with finer resolution of the nearshore zone.

In part, this modeling study was motivated by a larger effort to understand how MPAs in this region function as a network. To sustain a population, marine organisms rely on a combination of self-replenishment, local connectivity, and important occasional and inconsistent receipt of larvae from distant sources that contribute to genetic diversity (Cowen *et al.*, 2003). Asymmetry in dispersal is an important consideration for MPA design in regions of directional larval transport like the CCS (Roughgarden *et al.*, 1988; Possingham and Roughgarden, 1990; Gaines *et al.*, 2003). Shanks *et al.*, 2003 suggest that individual reserves within the CCS should be approximately 4-6 km wide to enable ample self-recruitment and spaced 10-20 km apart for connectivity between nearby reserves. The suitable habitat regions in this study meet the smallest specifications of this criteria, serving as an example of self-recruitment and exchange between both regions, and suggest the MPAs around the Monterey Peninsula function effectively. We reiterate the importance of asymmetric dispersal considerations into the design of MPA networks because connectivity was not equivalent between suitable habitat regions 10 km apart. Around the Monterey Peninsula, asymmetry was in an unexpected direction for near-surface dispersal: there was more northward connectivity than southward due to a transient front in the region that temporarily impeded access for larval exchange between populations (Lowe and Edwards 2020 *in prep*). Local recruits mostly stayed close to the Monterey Peninsula with a few sporadic trajectories further away that were re-captured by circulation features within and around Monterey Bay and related to upwelling/downwelling

dynamics. We presume these circulation features will also capture propagules from distant populations and likely deliver larvae to these populations. Understanding the circulation processes and accounting for species differences in larval duration and behavior in a region offers a more-wholistic perspective of recruitment to and from an MPA for many species.

This modeling study was conducted in parallel to Baetscher *et al.* (2019), which collected genetic samples from adult and juvenile *S. atrovirens* around the Monterey Peninsula. Of the 6,091 adult and juvenile fishes sampled, genetic parentage analysis identified 8 parent-offspring pairs and 25 full-sibling pairs. This analysis revealed connectivity in multiple directions: 1 self-recruit to southwest Monterey Bay, 3 self-recruits to Carmel Bay, 3 southward recruits from southwest Monterey Bay to Carmel Bay, and 1 northward recruit from Carmel Bay settling in southwest Monterey Bay. As with the empirical results, we calculate a very small proportion of recruitment (to both populations) relative to the number of particles released in the model. We also find that recruitment exists in multiple directions, with some recruits returning to their natal population in both CB and swMB and some supplying the other suitable habitat region. Given the extraordinarily small numbers of parent-offspring pairs in the field analysis, we do not attempt a more sophisticated comparison of the genetic results with our simulations.

There remains uncertainty about the biological parameters pertaining to the pelagic period for *S. atrovirens* and other nearshore rockfish larvae. In particular, larval depth in the water column plays a major role in the direction of transport

(Petersen *et al.*, 2010; Morgan *et al.*, 2018). The initial and final depths of *S. atrovirens* larvae are well known, but how these larvae vertically migrate from depth to the kelp canopy, remains unknown. In this study, we assume larvae are positively buoyant, meaning upon release they immediately move to the surface and spend their whole PLD at this depth. The sensitivity analysis revealed better interannual agreement between the model and observations for passive transport at 10 m compared to 2 m depths. This suggests larvae likely spend a portion of their pelagic phase at depth, but probably within 20m of the surface, before rising near the surface for recruitment. Additionally, larvae of *S. atrovirens* develop their swimming capabilities during the pelagic phase (Kashef *et al.*, 2014). Adding a horizontal swimming behavior will increase settlement (Morgan, 2014, Drake et al. 2018). Our ROMS model configuration excludes physical factors that have been shown to influence dispersal. The coastal boundary layer slows flow and thereby transport away from a source region (Nickols *et al.*, 2012). For particles transported near the surface, as in this study, Stokes drift from waves applies a quasi-consistent onshore force, likely keeping larvae closer to the coast (Monismith and Fong, 2004; Röhrs *et al.*, 2014). Both of these circulation elements retain larvae near the coast increasing the likelihood of settlement. For this study, we assumed passive, near-surface dispersal because our focus is on the relationship between oceanographic conditions and recruitment. Based on the shortcomings in our model, the relative proportions of self-recruits, vs. connected-recruits may change. We feel confident that circulation features and larval delivery mechanisms are applicable to *S. atrovirens* and other species in the region whose larval stage is spent near the surface.

5 Conclusions

Dispersal of larvae during the pelagic phase is a major determinant of the distribution, dynamics, structure, and genetic diversity of marine populations. During this phase, larvae may travel up to hundreds of kilometers and then settle in local or distant populations. The paradigm has shifted from purely 'open' marine populations created by an offshore larval pool and long-distance dispersal to more consistent connectivity between more local communities yielding a greater role for self-recruitment (Cowen *et al.*, 2000; Levin, 2006). Because of this and the spatial distribution of MPAs in the study region, the focus of this study is exclusively on local connectivity. We release propagules representative of kelp rockfish (*S. atrovirens*) larvae from populations in southwest Monterey Bay (swMB) and Carmel Bay (CB), which are moved passively by the 2-dimensional ocean currents. Propagules are able to settle if they enter suitable habitat within either region during the competency window of 60-90 days since release. Of the 77,714 particles released around the Monterey Peninsula, less than 1% recruit locally, with 3x more recruits settling in swMB than CB. Local recruits spend the majority of their pelagic phase very close to the suitable habitat regions around the Monterey Peninsula, staying mostly within the bays with brief excursions further away. The majority of particles outside either bay longer than a day enter Monterey and Carmel bays during wind reversal or relaxation events. Our results emphasize the importance of wind reversal events in delivering larvae to both bays for recruitment.

We further explored larval transport in and out of Carmel Bay. The sensitivity analysis revealed a clear picture of the relationship between upwelling dynamics and depth-dependent transport into Carmel Bay: larvae within the surface-mixed layer (10 m or shallower) enter during downwelling-favorable winds, whereas larvae beneath the surface-mixed layer (at 20 and 30 m depths) enter Carmel Bay during upwelling-favorable wind conditions. This understanding of larval transport into Carmel Bay is applicable to many species.

Our results may be summarized by two take-away messages with implications for MPA management. First, marine populations do not have homologous recruitment nor exchange of individuals, even when populations are geographically separated by only a few kilometers. Second, larger-scale oceanographic processes significantly impact larval transport, but close attention must also be paid to location-specific, coastal processes that ultimately determine recruitment. Therefore, to evaluate connectivity between MPAs requires high resolution on the *scale of ca. 100 m* that resolve complex, nearshore dynamics with large domains that allow larvae to travel potentially long distances before returning for recruitment. Further investigation of the smaller-scale processes that transport larvae briefly during the PLD may explain asymmetric connectivity between populations and yield a better understanding of larval transport off the central California coast. The next step in this research is to make this modeling process more efficient and potentially automated to encourage future connectivity studies at this scale. Then, conducting connectivity studies between several MPAs in this region may contribute to MPA management and further understand the degree of interdependency between MPAs.

Acknowledgements

This work was supported by a grant from the National Science Foundation (Award number 1260693). The authors thank Dan Malone, Emily Saarman, and Patrick Drake for their knowledge of the seafloor and kelp maps and insight that contributed to this project.

REFERENCES

Aburto-Oropeze, Octavio, Enric Sala, Gustavo Paredes, Abraham Mendoza, and Enric Ballesteros. 2007. "Predictability of Reef Fish Recruitment." *Ecology*.

Allen, J. S. 1980. "Models of Wind-Driven Currents on the Continental Shelf." *Annual Review of Fluid Mechanics* 12 (1): 389–433.

Baetscher, Diana S., Eric C. Anderson, Elizabeth A. Gilbert-Horvath, Daniel P. Malone, Emily T. Saarman, Mark H. Carr, and John Carlos Garza. 2019. "Dispersal of a Nearshore Marine Fish Connects Marine Reserves and Adjacent Fished Areas along an Open Coast." *Molecular Ecology* 28: 1611–23. https://doi.org/10.1111/mec.15044.

Bjorkstedt, Eric P., Leslie K. Rosenfeld, Brian A. Grantham, Yehoshua Shkedy, and Joan Roughgarden. 2002. "Distributions of Larval Rockfishes Sebastes Spp. across Nearshore Fronts in a Coastal Upwelling Region." *Marine Ecology Progress Series*. https://doi.org/10.3354/meps242215.

Bonicelli, Jessica, Fabian J. Tapia, and Sergio A. Navarrete. 2014. "Wind-Driven Diurnal Temperature Variability across a Small Bay and the Spatial Pattern of Intertidal Barnacle Settlement." *Journal of Experimental Marine Biology and Ecology*. https://doi.org/10.1016/j.jembe.2014.09.003.

Botsford, Louis W., J. Wilson White, Mark H. Carr, and Jennifer E. Caselle. 2014. "Marine Protected Area Networks in California, USA." In *Advances in Marine Biology*. https://doi.org/10.1016/B978-0-12-800214-8.00006-2.

Broenkow, William W., and William M. Smethie. 1978. "Surface Circulation and Replacement of Water in Monterey Bay." *Estuarine and Coastal Marine Science*. https://doi.org/10.1016/0302-3524(78)90033-6.

Carr, Mark H. 1991. "Habitat Selection and Recruitment of an Assemblage of Temperate Zone Reef Fishes." *Journal of Experimental Marine Biology and Ecology* 146: 113–37. https://doi.org/10.1016/0022-0981(91)90257-W.

Carr, Mark H., Sarah P. Robinson, Charles Wahle, Gary Davis, Stephen Kroll, Samantha Murray, Ervin Joe Schumacker, and Margaret Williams. 2017. "The Central Importance of Ecological Spatial Connectivity to Effective Coastal Marine Protected Areas and to Meeting the Challenges of Climate Change in the Marine Environment." *Aquatic Conservation: Marine and Freshwater Ecosystems* 27 (S1): 6–29. https://doi.org/10.1002/aqc.2800.

Castelao, Renato M., and John A. Barth. 2006. "Upwelling around Cabo Frio, Brazil: The Importance of Wind Stress Curl." *Geophysical Research Letters*.

https://doi.org/10.1029/2005GL025182.

Checkley, David M., and John A. Barth. 2009. “Patterns and Processes in the California Current System.” *Progress in Oceanography*. https://doi.org/10.1016/j.pocean.2009.07.028.

Cowen, Robert K., Kamazima M.M. Lwiza, Su Sponaugle, Claire B. Paris, and Donald B. Olson. 2000. “Connectivity of Marine Populations: Open or Closed?” *Science*. https://doi.org/10.1126/science.287.5454.857.

Cowen, Robert K., Claire B. Paris, Donald B. Olson, and John L. Fortuna. 2003. “The Role of Long Distance Dispersal Versus Local Retention in Replenishing Marine Populations.” *Gulf and Caribbean Research*. https://doi.org/10.18785/gcr.1402.10.

Cowen, Robert K., and Su Sponaugle. 2009. “Larval Dispersal and Marine Population Connectivity.” *Annual Review of Marine Science*. https://doi.org/10.1146/annurev.marine.010908.163757.

Criales, Maria M., Laurent M. Cherubin, and Joan A. Browder. 2015. “Modeling Larval Transport and Settlement of Pink Shrimp in South Florida: Dynamics of Behavior and Tides.” *Marine and Coastal Fisheries*. https://doi.org/10.1080/19425120.2014.1001541.

Cuif, Marion, David Michael Kaplan, Jér Ôme Lefèvre, Vincent Martin Faure, Matthieu Caillaud, Philippe Verley, Laurent Vigliola, and Christophe Lett. 2014. “Wind-Induced Variability in Larval Retention in a Coral Reef System: A Biophysical Modelling Study in the South-West Lagoon of New Caledonia.” *Progress in Oceanography*. https://doi.org/10.1016/j.pocean.2013.12.006.

Dagestad, Knut Frode, Johannes Röhrs, Oyvind Breivik, and Bjørn Ådlandsvik. 2018. “OpenDrift v1.0: A Generic Framework for Trajectory Modelling.” *Geoscientific Model Development*. https://doi.org/10.5194/gmd-11-1405-2018.

Dauhajre, Daniel P., James C. McWilliams, and Yusuke Uchiyama. 2017. “Submesoscale Coherent Structures on the Continental Shelf.” *Journal of Physical Oceanography*. https://doi.org/10.1175/JPO-D-16-0270.1.

Dick, Edward Joseph. 2009. “Modeling the Reproductive Potential of Rockfishes (Sebastes Spp.).” University of California, Santa Cruz.

Domingues, Carla P., Maria João Almeida, Jesus Dubert, Rita Nolasco, Nuno Cordeiro, Silke Waap, Ana Sequeira, Sofia Tavares, and Henrique Queiroga. 2011. “Supply of Crab Larvae to an Estuary in the Eastern Atlantic Upwelling System Exhibits Predictable and Haphazard Variation at Different Temporal

Scales." *Marine Ecology Progress Series*. https://doi.org/10.3354/meps08992.

Drake, Patrick T., and Christopher A. Edwards. 2010. "A Linear Diffusivity Model of Near-Surface, Cross-Shore Particle Dispersion from a Numerical Simulation of Central California's Coastal Ocean." *Journal of Marine Research*. https://doi.org/10.1357/002224009790741094.

Drake, Patrick T., Christopher A. Edwards, and Steven G. Morgan. 2015. "Relationship between Larval Settlement, Alongshore Wind Stress and Surface Temperature in a Numerical Model of the Central California Coastal Circulation." *Marine Ecology Progress Series*. https://doi.org/10.3354/meps11393.

Dudas, Sarah E., Brian A. Grantham, Anthony R. Kirincich, Bruce A. Menge, Jane Lubchenco, and John A. Barth. 2009. "Current Reversals as Determinants of Intertidal Recruitment on the Central Oregon Coast." In *ICES Journal of Marine Science*. https://doi.org/10.1093/icesjms/fsn179.

Egbert, Gary D., Andrew F. Bennett, and Michael G. G. Foreman. 1994. "TOPEX/POSEIDON Tides Estimated Using a Global Inverse Model." *Journal of Geophysical Research* 99 (C12): 24821. https://doi.org/10.1029/94JC01894.

Farrell, Terence M., David Bracher, and Jonathan Roughgarden. 1991. "Cross-shelf Transport Causes Recruitment to Intertidal Populations in Central California." *Limnology and Oceanography*. https://doi.org/10.4319/lo.1991.36.2.0279.

Fisher, Rebecca, Susan M. Sogard, and Steven A. Berkeley. 2007. "Trade-Offs between Size and Energy Reserves Reflect Alternative Strategies for Optimizing Larval Survival Potential in Rockfish." *Marine Ecology Progress Series*. https://doi.org/10.3354/meps06927.

Fogarty, Michael J., and Louis W. Botsford. 2007. "Population Connectivity and Spatial Management of Marine Fisheries." *Oceanography* 20 (3): 112–23. https://doi.org/10.5670/oceanog.2007.34.

Fujimura, Atsushi G., Ad J H M Reniers, Claire B. Paris, Alan L. Shanks, Jamie H. MacMahan, and Steven G. Morgan. 2014. "Numerical Simulations of Larval Transport into a Rip-Channeled Surf Zone." *Limnology and Oceanography*. https://doi.org/10.4319/lo.2014.59.4.1434.

Gaines, Steven D., Brian Gaylord, and John L. Largier. 2003. "Avoiding Current Oversights in Marine Reserve Design." *Ecological Applications*.

Giddings, S. N., P. Maccready, B. M. Hickey, N. S. Banas, K. A. Davis, S. A. Siedlecki, V. L. Trainer, R. M. Kudela, N. A. Pelland, and T. P. Connolly. 2014.

"Hindcasts of Potential Harmful Algal Bloom Transport Pathways on the Pacific Northwest Coast." *Journal of Geophysical Research: Oceans*. https://doi.org/10.1002/2013JC009622.

Gilbert, Elizabeth A. 2000. "Molecular Genetic Analysis of Temporal Recruitment Pulses in Juvenile Kelp Rockfish." San Francisco State University.

Gutow, Lars, Marcel Ricker, Jan M. Holstein, Jennifer Dannheim, Emil V. Stanev, and Jörg-Olaf Wolff. 2018. "Distribution and Trajectories of Floating and Benthic Marine Macrolitter in the South-Eastern North Sea." *Marine Pollution Bulletin* 131 (June): 763–72. https://doi.org/10.1016/J.MARPOLBUL.2018.05.003.

Hickey, Barbara M. 1998. "Coastal Oceanography of Western North America from the Tip of Baja California to Vancouver Island." In *The Sea*, edited by Allan R. Robinson and Kenneth H. Brink, 11th ed., 345–93. John Wiley & Sons, Inc. https://books.google.com/books?hl=en&lr=&id=-uhTulqFRIgC&oi=fnd&pg=PA345&ots=17YWMPqbCw&sig=TptPd-1kvWE38CKRdz4M5NtEDXo#v=onepage&q&f=false.

Hodur, Richard M. 1997. "The Naval Research Laboratory's Coupled Ocean/Atmosphere Mesoscale Prediction System (COAMPS)." *Monthly Weather Review*. https://doi.org/10.1175/1520-0493(1997)125<1414:TNRLSC>2.0.CO;2.

Holbrook, S. J., M. H. Carr, R. J. Schmitt, and J. A. Coyer. 1990. "Effect of Giant Kelp on Local Abundance of Reef Fishes: The Importance of Ontogenetic Resource Requirements." *Bulletin of Marine Science*. https://doi.org/10.1038/344238a0.

Hole, Lars R, Knut-Frode Dagestad, Johannes Röhrs, Cecilie Wettre, Vassiliki H Kourafalou, Ioannis Androulidakis, Matthieu Le Hénaff, Heesook Kang, and Oscar Garcia-Pineda. 2018. "Revisiting the DeepWater Horizon Spill: High Resolution Model Simulations of Effects of Oil Droplet Size Distribution and River Fronts." *Ocean Science Discussions*. https://doi.org/10.5194/os-2018-130.

Kashef, Neosha S., Susan M. Sogard, Rebecca Fisher, and John L. Largier. 2014. "Ontogeny of Critical Swimming Speeds for Larval and Pelagic Juvenile Rockfishes (Sebastes Spp., Family Scorpaenidae)." *Marine Ecology Progress Series*. https://doi.org/10.3354/meps10669.

Kool, Johnathan T., Atte Moilanen, and Eric A. Treml. 2013. "Population Connectivity: Recent Advances and New Perspectives." *Landscape Ecology*. https://doi.org/10.1007/s10980-012-9819-z.

Levin, Lisa A. 2006. “Recent Progress in Understanding Larval Dispersal: New Directions and Digressions.” In *Integrative and Comparative Biology*, 282–97. https://doi.org/10.1093/icb/icj024.

Love, Milton S., Mary Yoklavich, and Lyman K. Thorsteinson. 2002. *The Rockfishes of the Northeast Pacific*. *University of California Press*. https://doi.org/10.1007/s13398-014-0173-7.2.

McWilliams, James C. 2016. “Submesoscale Currents in the Ocean.” *Proceedings of the Royal Society A: Mathematical, Physical and Engineering Sciences*. https://doi.org/10.1098/rspa.2016.0117.

Mitarai, S., D. A. Siegel, and K. B. Winters. 2008. “A Numerical Study of Stochastic Larval Settlement in the California Current System.” *Journal of Marine Systems*. https://doi.org/10.1016/j.jmarsys.2006.02.017.

Monismith, Stephen G., and Derek A. Fong. 2004. “A Note on the Potential Transport of Scalars and Organisms by Surface Waves.” *Limnology and Oceanography*. https://doi.org/10.4319/lo.2004.49.4.1214.

Morgan, Lance E., Stephen R. Wing, Louis W. Botsford, Carolyn J. Lundquist, and Jennifer M. Diehl. 2000. “Spatial Variability in Red Sea Urchin (Strongylocentrotus Franciscanus) Recruitment in Northern California.” *Fisheries Oceanography*. https://doi.org/10.1046/j.1365-2419.2000.00124.x.

Morgan, Steven G. 2014. “Behaviorally Mediated Larval Transport in Upwelling Systems.” *Advances in Oceanography*. https://doi.org/10.1155/2014/364214.

Morgan, Steven G., Seth H. Miller, Matt J. Robart, and John L. Largier. 2018. “Nearshore Larval Retention and Cross-Shelf Migration of Benthic Crustaceans at an Upwelling Center.” *Frontiers in Marine Science*. https://doi.org/10.3389/fmars.2018.00161.

Narváez, Diego A., John M. Klinck, Eric N. Powell, Eileen E. Hofmann, John Wilkin, and Dale B. Haidvogel. 2012. “Modeling the Dispersal of Eastern Oyster (Crassostrea Virginica) Larvae in Delaware Bay.” *Journal of Marine Research*. https://doi.org/10.1357/002224012802851940.

Nelson, Peter A. 2001. “Behavioral Ecology of Young-of-the-Year Kelp Rockfish, Sebastes Atrovirens Jordan and Gilbert (Pisces: Scorpaenidae).” *Journal of Experimental Marine Biology and Ecology*. https://doi.org/10.1016/S0022-0981(00)00305-1.

Nickols, K. J., B. Gaylord, and J. L. Largier. 2012. “The Coastal Boundary Layer: Predictable Current Structure Decreases Alongshore Transport and Alters Scales

of Dispersal." *Marine Ecology Progress Series*. https://doi.org/10.3354/meps09875.

Ogburn, Matthew B., Megan Hall, and Richard B. Forward. 2012. "Blue Crab (Callinectes Sapidus) Larval Settlement in North Carolina: Environmental Forcing, Recruit-Stock Relationships, and Numerical Modeling." *Fisheries Oceanography*. https://doi.org/10.1111/j.1365-2419.2011.00606.x.

Pardo, Luis Miguel, Carlos Simón Cardyn, and J. Garcés-Vargas. 2012. "Spatial Variation in the Environmental Control of Crab Larval Settlement in a Micro-Tidal Austral Estuary." *Helgoland Marine Research*. https://doi.org/10.1007/s10152-011-0267-y.

Paris, Claire B., Robert K. Cowen, Rodolfo Claro, and Kenyon C. Lindeman. 2005. "Larval Transport Pathways from Cuban Snapper (Lutjanidae) Spawning Aggregations Based on Biophysical Modeling." *Marine Ecology Progress Series*. https://doi.org/10.3354/meps296093.

Pawlowicz, Rich, Bob Beardsley, and Steve Lentz. 2002. *Classical Tidal Harmonic Analysis with Error Analysis in MATLAB Using T_TIDE*. *Computers & Geosciences*. https://doi.org/10.1109/APS.2007.4396859.

Petersen, Christine H., Patrick T. Drake, Christopher A. Edwards, and Stephen Ralston. 2010. "A Numerical Study of Inferred Rockfish (Sebastes Spp.) Larval Dispersal along the Central California Coast." *Fisheries Oceanography*. https://doi.org/10.1111/j.1365-2419.2009.00526.x.

Pfaff, Maya C., George M. Branch, Jennifer L. Fisher, Vera Hoffmann, Allan G. Ellis, and John L. Largier. 2015. "Delivery of Marine Larvae to Shore Requires Multiple Sequential Transport Mechanisms." *Ecology*.

Pfeiffer-Herbert, Anna S., Margaret A. McManus, Peter T. Raimondi, Yi Chao, and Fei Chai. 2007. "Dispersal of Barnacle Larvae along the Central California Coast: A Modeling Study." *Limnology and Oceanography*. https://doi.org/10.4319/lo.2007.52.4.1559.

Possingham, H. P., and J. Roughgarden. 1990. "Spatial Population Dynamics of a Marine Organism with a Complex Life Cycle." *Ecology*. https://doi.org/10.2307/1937366.

Rochette, Sebastien, Martin Huret, Etienne Rivot, and Olivier Le Pape. 2012. "Coupling Hydrodynamic and Individual-Based Models to Simulate Long-Term Larval Supply to Coastal Nursery Areas." *Fisheries Oceanography*. https://doi.org/10.1111/j.1365-2419.2012.00621.x.

Rodrigues, Regina R., and João A. Lorenzzetti. 2001. “A Numerical Study of the Effects of Bottom Topography and Coastline Geometry on the Southeast Brazilian Coastal Upwelling.” *Continental Shelf Research*. https://doi.org/10.1016/S0278-4343(00)00094-7.

Röhrs, Johannes, Kai Håkon Christensen, Frode Vikebø, Svein Sundby, Øyvind Saetra, and Göran Broström. 2014. “Wave-Induced Transport and Vertical Mixing of Pelagic Eggs and Larvae.” *Limnology and Oceanography*. https://doi.org/10.4319/lo.2014.59.4.1213.

Romero, M. 1988. “Life History of the Kelp Rockfish, Sebastes Atrovirens (Scorpaenidae).” San Francisco State University.

Rosenfeld, Leslie K., Franklin B. Schwing, Newell Garfield, and Dan E. Tracy. 1994. “Bifurcated Flow from an Upwelling Center: A Cold Water Source for Monterey Bay.” *Continental Shelf Research*. https://doi.org/10.1016/0278-4343(94)90058-2.

Roughgarden, J., J. T. Pennington, D. Stoner, S. Alexander, and K. Miller. 1991. “Collisions of Upwelling Fronts with the Intertidal Zone: The Cause of Recruitment Pulses in Barnacle Populations of Central California.” *Acta Oecologica*.

Roughgarden, Jonathan, Steven Gaines, and Hugh Possingham. 1988. “Recruitment Dynamics in Complex Life Cycles.” *Science*. https://doi.org/10.1126/science.11538249.

Saarman, Emily T., and Mark H. Carr. 2013. “The California Marine Life Protection Act: A Balance of Top down and Bottom up Governance in MPA Planning.” *Marine Policy*.

Schiel, D. R., and M. S. Foster. 2015. *The Biology and Ecology of Giant Kelp Forests*. *University of California Press*. Oakland, CA, USA.

Shanks, Alan L., Brian A. Grantham, and Mark H. Carr. 2003. “Propagule Dispersal Distance and the Size and Spacing of Marine Reserves.” *Ecological Applications*.

Shanks, Alan L., Jamie MacMahan, Steven G. Morgan, Ad J.H.M. Reniers, Marley Jarvis, Jenna Brown, Atsushi Fujimura, and Chris Griesemer. 2015. “Transport of Larvae and Detritus across the Surf Zone of a Steep Reflective Pocket Beach.” *Marine Ecology Progress Series*. https://doi.org/10.3354/meps11223.

Shanks, Alan L., Steven G. Morgan, Jamie MacMahan, Ad J.H.M. Reniers, Marley Reniers, Jenna Brown, Atsushi Fujimura, and Chris Griesemer. 2014. “Onshore

Transport of Plankton by Internal Tides and Upwelling-Relaxation Events." *Marine Ecology Progress Series*. https://doi.org/10.3354/meps10717.

Shchepetkin, Alexander F., and James C. McWilliams. 2005. "The Regional Oceanic Modeling System (ROMS): A Split-Explicit, Free-Surface, Topography-Following-Coordinate Oceanic Model." *Ocean Modelling* 9 (4): 347–404. https://doi.org/10.1016/J.OCEMOD.2004.08.002.

Shulman, Igor, Stephanie Anderson, Clark Rowley, Sergio Derada, James Doyle, and Steven Ramp. 2010. "Comparisons of Upwelling and Relaxation Events in the Monterey Bay Area." *Journal of Geophysical Research: Oceans*. https://doi.org/10.1029/2009JC005483.

Siegel, D. A., S. Mitarai, C. J. Costello, S. D. Gaines, B. E. Kendall, R. R. Warner, and K. B. Winters. 2008. "The Stochastic Nature of Larval Connectivity among Nearshore Marine Populations." *Proceedings of the National Academy of Sciences*. https://doi.org/10.1073/pnas.0802544105.

Smale, Dan A., Thomas Wernberg, and Thomas Vance. 2011. "Community Development on Subtidal Temperate Reefs: The Influences of Wave Energy and the Stochastic Recruitment of a Dominant Kelp." *Marine Biology*. https://doi.org/10.1007/s00227-011-1689-4.

Smith, K. A., and I. M. Suthers. 2000. "Consistent Timing of Juvenile Fish Recruitment to Seagrass Beds within Two Sydney Estuaries." *Marine and Freshwater Research*. https://doi.org/10.1071/MF99142.

Sponaugle, Su, Thomas Lee, Vassiliki Kourafalou, and Deanna Pinkard. 2005. "Florida Current Frontal Eddies and the Settlement of Coral Reef Fishes." *Limnology and Oceanography*. https://doi.org/10.4319/lo.2005.50.4.1033.

Strub, P. T., J. S. Allen, A. Huyer, R. L. Smith, and R. C. Beaedsley. 1987. "Seasonal Cycles of Currents, Temperatures, Winds, and Sea Level over the Northeast Pacific Continental Shelf: 35n to 48n." *Journal of Geophysical Research: Oceans*. https://doi.org/10.1029/JC092iC02p01507.

Strub, P. Ted, J. S. Allen, A. Huyer, and R. L. Smith. 1987. "Large-Scale Structure of the Spring Transition in the Coastal Ocean off Western North America." *Journal of Geophysical Research: Oceans*. https://doi.org/10.1029/JC092iC02p01527.

Swearer, Stephan E., Eric A. Treml, and Jeffrey S. Shima. 2019. "A Review of Biophysical Models of Marine Larval Dispersal." *Oceanography and Marine Biology* 57: 325–56.

Watson, William, and Larry L. Robertson. 2004. "Development of Kelp Rockfish,

Sebastes Atrovirens (Jordan and Gilbert 1880), and Brown Rockfish, S. Auriculatus (Girard 1854), from Birth to Pelagic Juvenile Stage, with Notes on Early Larval Development of Black-and-Yellow Rockfish, S. Chrysomelas (Jorda."

Wiborg, Kr Fr. 1976. "Larval Mortality in Marine Fishes and the Critical Period Concept." *ICES Journal of Marine Science*. https://doi.org/10.1093/icesjms/37.1.111.

Williams, Paul David, and Alan Hastings. 2013. "Stochastic Dispersal and Population Persistence in Marine Organisms." *American Naturalist*. https://doi.org/10.1086/671059.

Wilson, J. R., B. R. Broitman, J. E. Caselle, and D. E. Wendt. 2008. "Recruitment of Coastal Fishes and Oceanographic Variability in Central California." *Estuarine, Coastal and Shelf Science*. https://doi.org/10.1016/j.ecss.2008.05.001.

Wing, S. R., L. W. Botsford, J. L. Largier, and L. E. Morgan. 1995. "Spatial Structure of Relaxation Events and Crab Settlement in the Northern California Upwelling System." *Marine Ecology Progress Series*. https://doi.org/10.3354/meps128199.

Wing, Stephen R., John L. Largier, Louis W. Botsford, and James F. Quinn. 1995. "Settlement and Transport of Benthic Invertebrates in an Intermittent Upwelling Region." *Limnology and Oceanography*. https://doi.org/10.4319/lo.1995.40.2.0316.

Woodin, Sarah Ann. 1991. "Recruitment of Infauna: Positive or Negative Cues?" *Integrative and Comparative Biology*. https://doi.org/10.1093/icb/31.6.797.

Table 1: Reports the numbers of particles released in each region and parses them by their recruitment status. swMB is southewest Monterey Bay, CB is Carmel Bay. These numbers reflect only the particles released at a depth of 2 m and whose trajectories were calculated using the horizontal circulation at that depth. These particle trajectories were used for the main body of analysis.

release region	year	particles released	non-recruits		connected-recruits		self-recruits	
swMB	2014	20,202	20,177	99.88%	0	0.00%	25	0.12%
	2015	20,202	20,111	99.55%	16	0.08%	75	0.37%
CB	2014	18,655	18,634	99.89%	21	0.11%	0	0.00%
	2015	18,655	18,587	99.64%	36	0.19%	32	0.17%
swMB	2014-2015	40,404	40,288	99.71%	16	0.04%	100	0.25%
CB	2014-2015	37,310	37,221	99.76%	57	0.15%	32	0.09%

Table 2: Reports the results from the sensitivity analysis defined in the left column. Since the definition of suitable habitat for S. atrovirens remains the same, fewer particles are released from deeper depths, therefore the percentages should be used to compare to Table 1 (base case: 2m, 2D).

release depth	release region	year	non-recruits		connected-recruits		self-recruits	
10m, 2D	swMB	2014	19,854	98.28%	259	1.28%	89	0.44%
		2015	20,156	99.77%	38	0.19%	8	0.04%
	CB	2014	13,024	73.77%	276	1.56%	4,354	24.66%
		2015	17,192	97.38%	96	0.54%	366	2.07%
	swMB	2014-2015	40,010	99.02%	297	0.74%	97	0.24%
	CB	2014-2015	30,216	85.58%	372	1.05%	4,720	13.37%
20m, 2D	swMB	2014	15,738	99.97%	0	0.00%	4	0.03%
		2015	15,743	100.00%	0	0.00%	0	0.00%
	CB	2014	9,252	82.66%	357	3.19%	1,584	14.15%
		2015	11,149	99.61%	21	0.19%	23	0.21%
	swMB	2014-2015	31,481	99.98%	0	0.00%	4	0.01%
	CB	2014-2015	20,401	91.13%	378	1.69%	1,607	7.18%
30m, 2D	swMB	2014	6,914	99.97%	2	0.03%	0	0.00%
		2015	6,916	100.00%	0	0.00%	0	0.00%
	CB	2014	3,943	86.66%	38	0.84%	569	12.51%
		2015	4,479	98.44%	19	0.42%	52	1.14%
	swMB	2014-2015	13,830	99.99%	2	0.01%	0	0.00%
	CB	2014-2015	8,422	92.55%	57	0.63%	621	6.82%

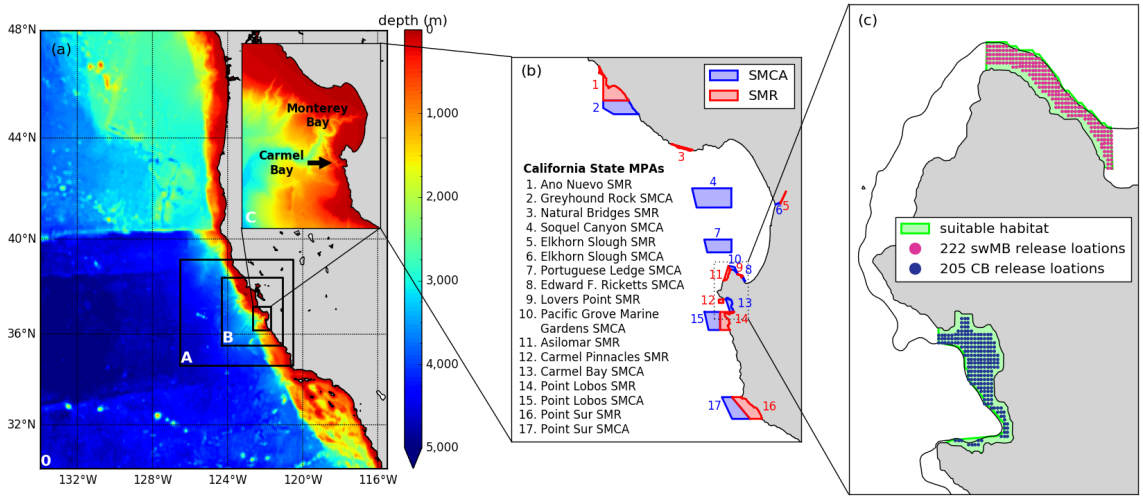

Figure 1: (a) Four model domains (labeled in the bottom left corner) used in the present study with bathymetry. Inset shows the domain of the C-nest (highest resolution grid). (b) Outlines and labels the domains of California State Marine Protected Areas (MPAs), with State Marine Conservation Areas (SMCA) in blue and State Marine Reserves (SMR) in red. (c) higher resolution of the Monterey Peninsula with outlines in green of the suitable habitat regions for S. atrovirens recruitment used in this study with the offshore extent defined by the 40 m bottom depth (black contour). Pink and blue dots mark the release locations in swMB and CB, respectively.

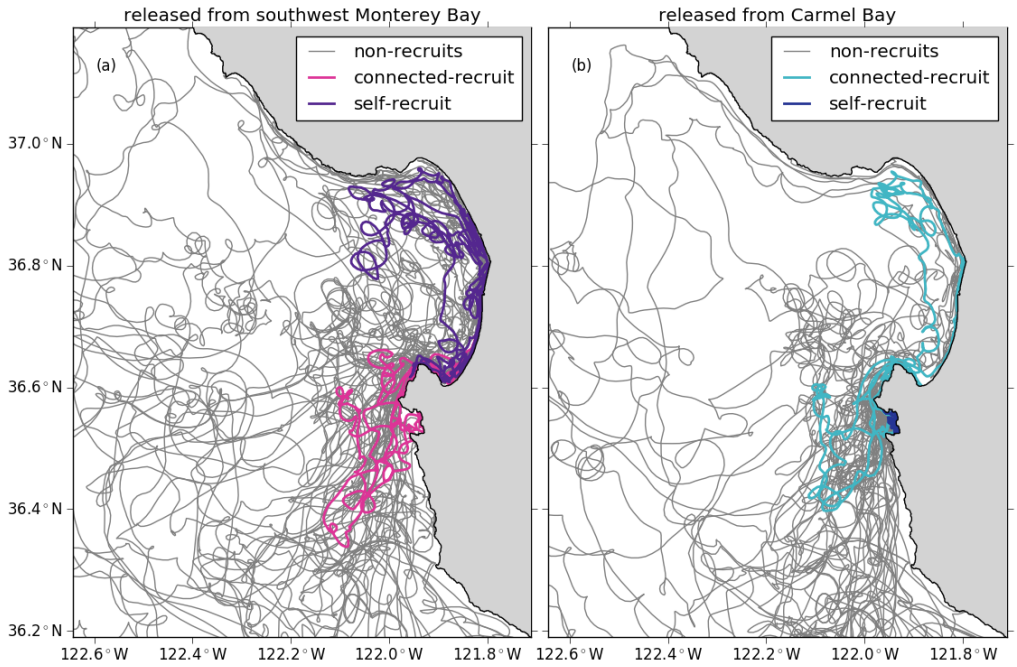

Figure 2: Shows a random sample of trajectories of particles released from swMB (a) and CB (b) on the c-nest domain. Each subplot includes 50 trajectories of non-recruits in gray, 2 connected-recruits (southward recruits (pink); northward recruits (turquoise)), and 2 self-recruits to swMB (purple) and CB (n

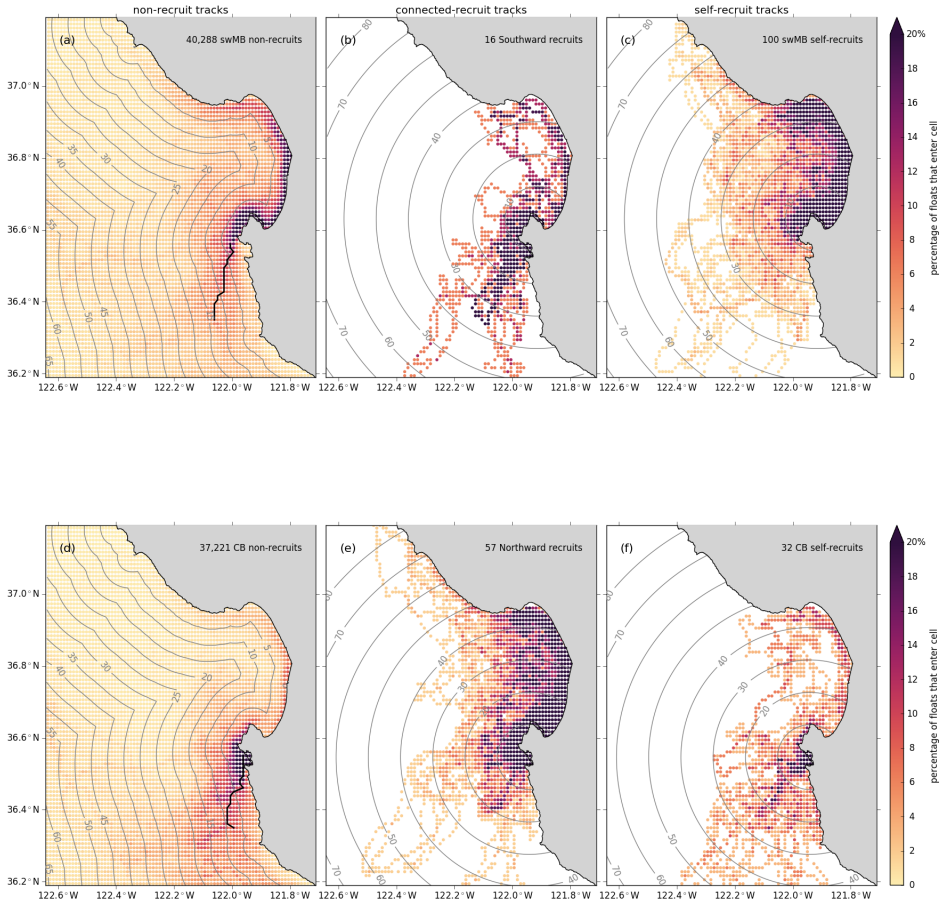

Figure 3: Probability of a particle being present at a location during the simulation period, calculated on a grid of 9x9 c-nest grid cell aggregates corresponding to approximately 1 km^2. Top row: swMB released (a) non-recruits, (b) southward recruits, and (c) self-recruits. Bottom row: CB released (d) non-recruits, (e) northward recruits, and (f) self-recruits. Gray contours indicate distance from the coast (a,d) and from release region (b,c,e,f). Black lines show the meridionally smoothed longitude of the mode-obtained zonal distributions of non-recruits south of 36.58°N (a,d). The number of floats contributing to each percentage map is given. Color-scale was capped at 20%.

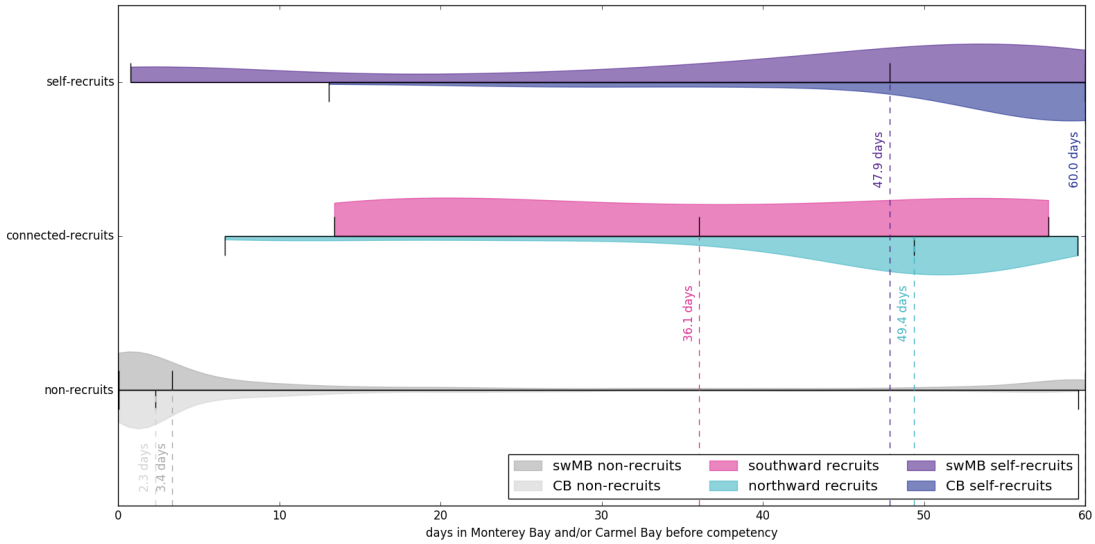

Figure 4: Violin plots of the time spent by non-recruits, connected-recruits, and self-recruits in both Monterey and Carmel Bay before becoming competent to recruit at 60 days old. Violin plots show the probability density distribution with markers denoting the extrema (minimum and maximum) and labeled dashed lines indicate the median for each float-type.

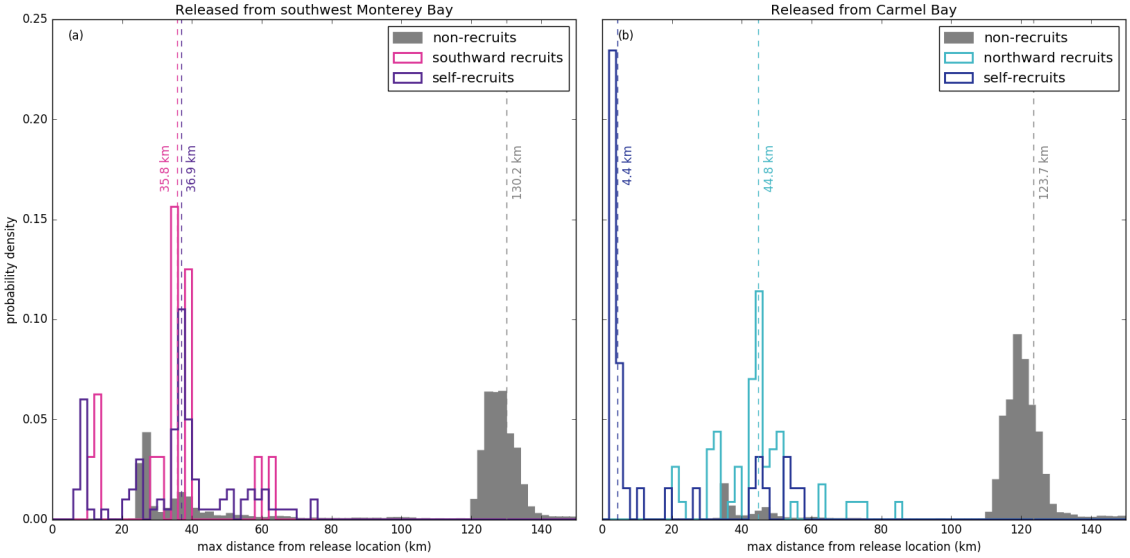

Figure 5: Probability density plots of the maximum (geographical) distance a float travelled from its release location in swMB (a) and CB (b). Gray bars represent the maximum distance non-recruits travelled before exiting the b-nest domain or until 90 days since release. The dashed lines represent the median distance from release location for each recruitment type.

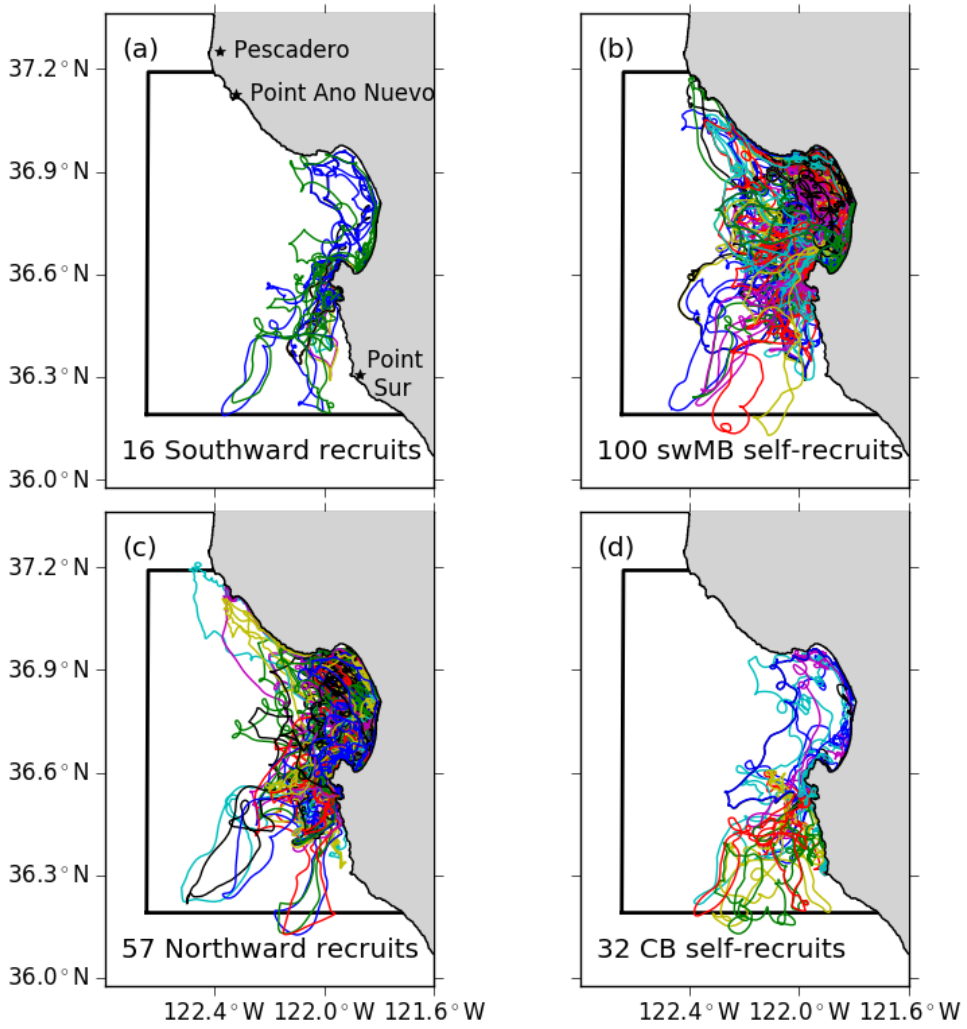

Figure 6: Successful recruits for 2m depth larvae: (a) southward recruits and (b) self-recruits released from swMB; (c) northward recruits and (d) self-recruits released from CB. The c-nest domain is outlined in black, and each colored line represents the trajectory of an individual recruit.

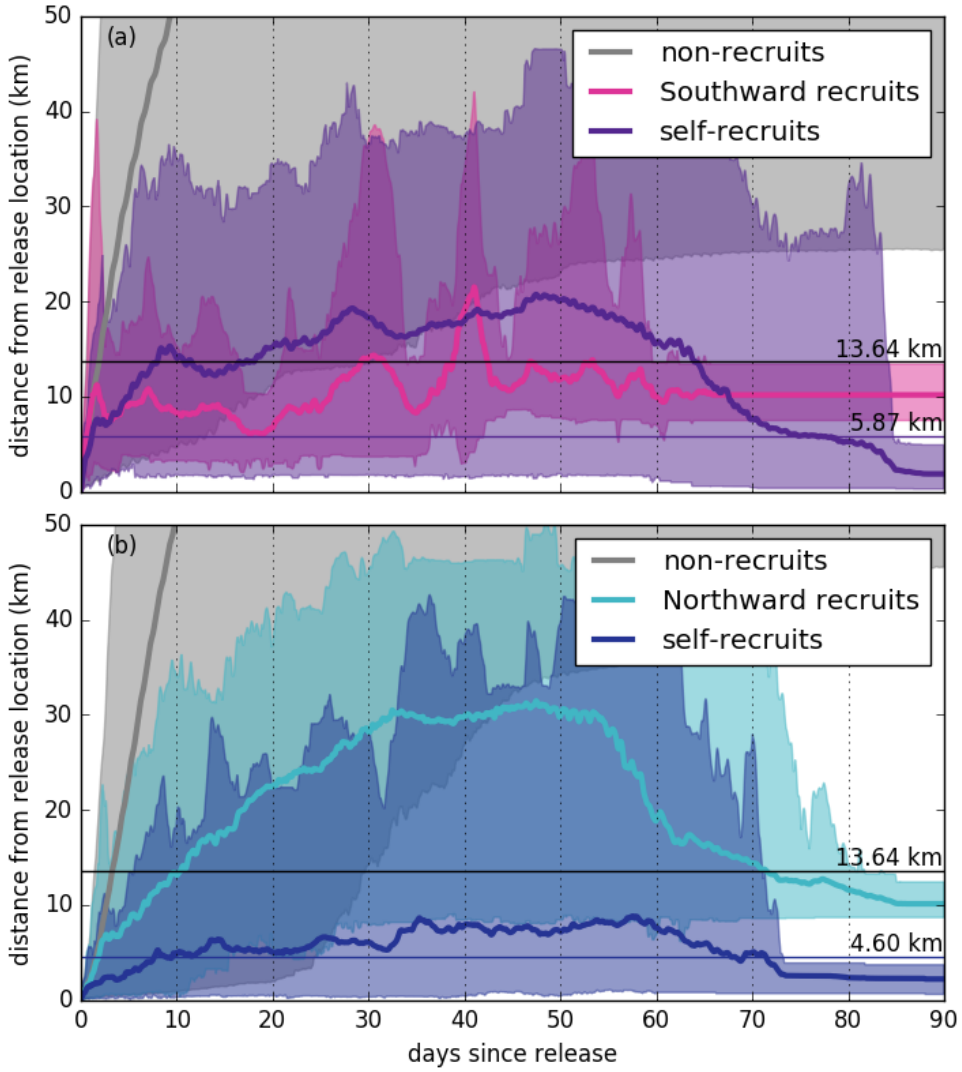

Figure 7: Time-series of the distance away from release location from release to the end of their larval duration for particles released in swMB (a) and CB (b). Colored lines and the corresponding shaded regions represent the mean and 5th to 95th percentiles for each recruitment category. Horizontal lines represent the maximum distance within suitable habitat regions in swMB (5.87 km) and CB (4.60 km), and between the regions (13.64 km).

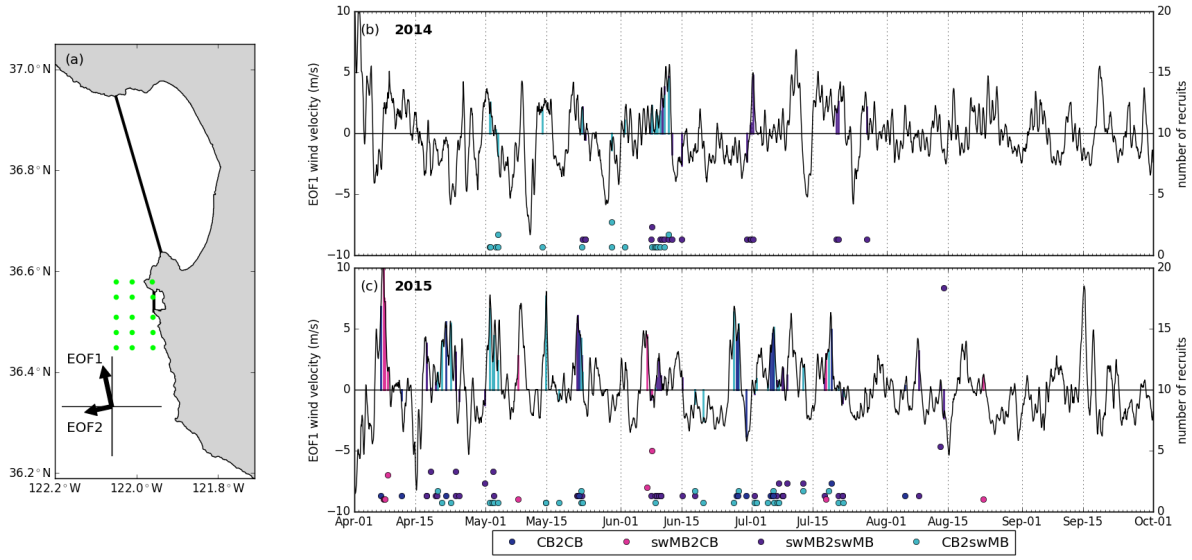

Figure 8: Map (a) marks the subset of COAMPS grid points (green dots) around Carmel Bay used to calculate the wind EOF for this analysis. Black lines across the mouths of Monterey Bay and Carmel Bay were used to determine when recruits entered each bay. Time-series of the EOF1 wind velocity in 2014 (b) and 2015 (c) in black. Colored lines on these time-series mark when recruits arrive to Monterey Bay or Carmel Bay for recruitment, and corresponding colored dots represent the number of recruits that entered the recruitment bay at that time.

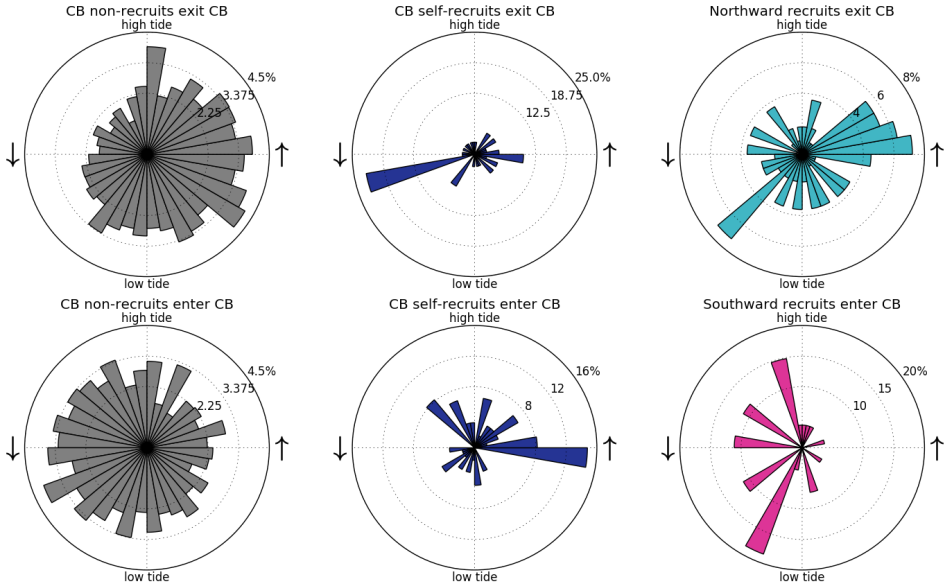

Figure 9: Polar plots showing the M_2 tidal phase when particles exit (top row) and enter (bottom row) Carmel Bay. Each bar represents the percentage of recruits that exit/enter Carmel Bay within that 10° window of the M_2 phase. Note the differences in scale between subplots.

CHAPTER FOUR
CHARACTERIZATION OF SUBMESOSCALE FRONTS OFF THE MONTEREY PENINSULA BY STRAIN AND LAGRANGIAN TRANSPORT

Characterization of Submesoscale Fronts off the Monterey Peninsula by Strain and Lagrangian Transport

Key Points:

- Categorizing fronts by the strain percentage differentiates two types of fronts resulting in different Lagrangian transport patterns
- Fronts dominated by normal strain generally accumulate material along the front and retain it in the region, potentially leading to enhanced local recruitment
- Fronts dominated by shear strain concentrate material along the front and export it away from the region, but slower velocities inshore may retain material

Abstract:

Submesoscale fronts in the coastal ocean are highly dynamic transport features, largely viewed as accumulation centers for nutrients, larvae, and foraging species. This study investigates the Lagrangian transport near fronts off the southern edge of the Monterey Peninsula on the central California coast using a high-resolution (120 m resolution) configuration of the Regional Ocean Modeling System (ROMS). Fronts are characterized by their squared strain percentage. Fronts dominated by normal strain tend to accumulate material along the front and retain that material in the immediate region. Fronts dominated by shear strain concentrate material along the front but generally export material from the immediate region. A comparable metric, the Okubo-Weiss parameter commonly used for eddy detection, distinguishes approximately linear fronts dominated by normal strain and is less effective for strain dominated features. These differences in Lagrangian transport have potential implications for larval recruitment and population connectivity.

1 Introduction

Fronts have long been recognized as important biophysical structures in the ocean. On the largest scale, the North Pacific transition zone chlorophyll front marks the transition between the subtropical and polar gyres and is a common path for migrations (Polovina et al. 2001). On much smaller scales, fronts are hotspots for biological activity with important implications for nutrients and animal larvae (Lévy et al. 2012; Lévy, Franks, and Smith 2018). Submesoscale fronts are largely viewed as accumulation centers of plankton (e.g., phytoplankton, zooplankton, animal larvae, etc.) (Wolanski and Hamner 1988). Recurrent and longer-lasting fronts attract larger, foraging marine animals (Snyder et al. 2017; Sims and Quayle 1998; Russell et al. 1999; Siegelman et al. 2019). A longstanding paradigm in coastal zones describes upwelling fronts pooling larvae offshore and, upon cessation of wind-forcing, delivering them to the coast for recruitment (Roughgarden et al. 1991; Shanks et al. 2000). Observations document high concentrations of nutrients and larvae near fronts (Bjorkstedt et al. 2002; Russell et al. 1999). Compelling empirical evidence links areas with high probabilities of fronts with high recruitment in adjacent coastal habitats (Woodson et al. 2012).

Fronts and filaments delineate the interface between waters having different properties, often visible in large lateral buoyancy gradients, strong cyclonic vorticity, strong convergence and downwelling (McWilliams 2016). Submesoscale fronts and filaments in coastal environments are rapidly evolving, ephemeral features about 0.1-10 km in length and lasting hours to days with a Rossby radius O(1). When releasing particles throughout a coastal zone with numerous submesoscale fronts, Dauhajre et

al. (2017) note that particle patches morph into shapes coincident with the fronts because convergence draws particles together and then these particles are moved along these features.

There is a disconnect between the physical understanding of fronts as dynamical transport features (Dauhajre et al. 2017; Gula et al. 2014; Romero et al. 2016; Harrison et al. 2013) and the ecological perception of fronts as catching mechanisms that enhance nearby larval recruitment (e.g., Shanks et al. 2000; Woodson et al. 2012; Ryan et al. 2014). This study intends to bridge this gap. We investigate Lagrangian transport along fronts, with a specific focus on implications for near-surface larvae. We characterize these fronts by strain and demonstrate a continuum of fronts between two extreme types: those that retain material in the region and those that export material from the region.

In this paper, we examine fronts near the southern edge of the Monterey Peninsula along the central coast of California, immediately south of Monterey Bay. High frequency radar observations show high probability of fronts in this area (Woodson et al. 2012), just outside of Carmel Bay which houses a species-rich environment (e.g., Reed and Foster 1984; Graham 1997; Wobber 1975; Kenner 1992; Clark et al. 2004; Hallacher and Roberts 1985; Carr 1991; Johnson 2006a,b; Johnson 2007; Green and Starr 2011; Green et al. 2014). The model simulation reproduces a recurrent front near the southern edge of the Monterey Peninsula and provides ample resolution and domain extent to investigate associated Lagrangian transport.

2 Methods

This research uses the same Regional Ocean Modeling System (ROMS) application described in greater detail in Lowe et al. (2020 a,b), and we therefore describe here briefly. The forcing for this model is derived from COAMPS atmospheric fields (Hodur 1997) and TPXO8-Atlas tidal constituents (Egbert et al. 1994). A telescoping series of four grids resolves the ocean circulation off the US west coast at 1/30° resolution, zooming by factors of 3 to the Carmel Bay region at 1/810° (~120 m) horizontal resolution (Figure 1a, b). This study uses only the highest resolution nest, hereafter called the c-nest, which covers the central California coast from Pescadero (just north of Año Nuevo) to Point Sur and extends offshore about 46 km. The nested model configuration was run for the years 2014 and 2015. We focus here on the spring-summer period from April 1 to September 30 when larvae of the nearshore rockfish complex are known to be within the water column (Anderson 1983; Carr 1991; Ammann 2004; Caselle et al., 2010).

In this study, fronts are defined by adjacent grid points whose local sea surface temperature (SST) gradient exceeds 2°C/km, and we limit our focus to those near the southern edge of the Monterey Peninsula (Figure 1c). We calculate the front length as the linear distance between extreme meridional and zonal front points (i.e., not curvilinear frontal length). Front presence is recognized only when its length exceeds 1 km. Fronts off the Monterey Peninsula take on a variety of shapes; some are nearly linear, others sinuous or sharply bent, and some include branches off the main axis. When calculating circulation fields (e.g., strain or relative vorticity) along

the face of the front, we calculate the diagnostic field at each grid point and then average only frontal points.

As has been found in other studies, strain is elevated relative to the surrounding region. Horizontal strain (S) is defined by two terms: normal strain (S_n) and shear strain (S_s).

$$\boldsymbol{S} = \sqrt{\boldsymbol{S_n}^2 + \boldsymbol{S_s}^2}$$

$$\boldsymbol{S} = \sqrt{\left(\frac{\boldsymbol{du}}{\boldsymbol{dx}} - \frac{\boldsymbol{dv}}{\boldsymbol{dy}}\right)^2 + \left(\frac{\boldsymbol{dv}}{\boldsymbol{dx}} + \frac{\boldsymbol{du}}{\boldsymbol{dy}}\right)^2}$$

Here, u and v refer to the velocities in the zonal (x) and meridional (y) directions. To investigate the diversity of fronts observed, we calculate the proportion of shear strain squared to the total strain squared along a front and refer to this metric, multiplied by 100, as the strain squared percentage. A strain squared percentage much greater than 50% indicates a front strongly dominated by shear strain; when the strain percentage is much less than 50%, the front is dominated by normal strain. Strain squared percentages near 50% share near equal contributions of normal and shear strain. In some cases, a section of a front may be dominated by shear strain while another segment is dominated by normal strain, but here we focus on a front's average spatial value during a time-snapshot.

For this study we analyze near-surface, horizontal Lagrangian transport in a generic sense. Lagrangian trajectories are calculated using OpenDrift (Dagestad et al. 2018) from hourly stored Eulerian velocities using a fourth-order Runge-Kutta

method. Particles are depth-keeping and only move horizontally by the model circulation estimated at 2 m depth.

We acknowledge that our analysis includes simplifications of these complex, dynamic features. Namely, mean metrics along a front and bulk particle statistics smooth variations within the front and the resultant Lagrangain transport; some fronts include sections that behave oppositely from one another (e.g., drawing particles into one section of the front, and expelling them in another) whose effects are smoothed by averaged statistics. Fronts are three dimensional features, but we do not address the vertical dimension: fronts are calculated only from the SST gradient, and we consider only horizontal Lagrangian transport. Additionally, our algorithm may cut a front short if there is a gap of adjacent grid points that do not meet or exceed the temperature gradient threshold. For consistency, we chose to use a constant threshold rather than a dynamic threshold that adjusts for seasonality in ocean temperature and stratification.

3 Results

3.1 Eulerian circulation during two example fronts

Overall, 3,664 fronts with mean front lengths greater than 1 km were identified in the 12 months (two 6-month periods) studied with strain squared percentages that ranged from 1.2 to 99.7% (Figure 2). Approximately 60.3% of fronts had a strain squared percentages exceeding 50%, with 39.7% less than that value. Although many fronts shared contributions by both shear and normal strain, 40.7% of fronts fall into relative extreme categories, with strain squared percentages less than 40%, dominated by normal strain, or greater than 80%, dominated by shear strain. On

average, fronts dominated by shear strain tend to be longer (t-test value=3.4, pval<0.01) than fronts characterized by normal strain. Of the 3,664 instances of fronts outside Carmel Bay, only 265 were found to retain their relative dominance of normal vs. shear strain for 12 hours or longer. Fronts that were sustained for longer than 48 hours were rare. In this study, we focus on these long and sustained subsets of all fronts as they illustrate end-member behavior within the diversity of fronts and are typically associated with distinctive circulations.

Two examples highlight these differences. The fronts on July 5, 2015 and June 22, 2014 are representative of fronts dominated by normal and shear strain, respectively. First, we describe their instantaneous Eulerian velocities (Figure 3).

The front on July 5, 2015 at 18:00 PST, which we hereafter refer to as NF1 (normal front 1; Figure 3b) was 8.3 km long and spanned the coast from central Carmel Bay (~1 km from the coast) to about 6 km south of the bay (~2.5 km from the coast) with a branch oriented southeast connecting to Point Lobos (Figure 3 a,b,c). Strong onshore velocities transported warm (~18°C) offshore water mass toward the coast, converging with cooler (~16°C) water inshore that was generally moving away from the coast. Strong onshore and offshore convergence at the front generated strong normal strain and a mean strain percentage of 30.3%. This front's complex shape results from a rapidly evolving circulation. Therefore, circulation before and after the time chosen in merits description.

Ten hours before the snapshot of NF1 at 18:00 PST, remnants of a strong upwelling front were 2-3 km offshore and outside of our front capture zone. In many places along the Monterey Peninsula and further south the velocities inshore of that

gradient were oriented away from the coast, moving the gradient offshore. Simultaneously, velocities along the offshore edge were oriented northward and northeastward around the peninsula and southward/southeastward south of Carmel Bay. Onshore velocities grew stronger, bringing warm waters closer to the coast. Ten hours after NF1 at 18:00 PST, strong southwestward velocities off the southern edge of the Monterey Peninsula collide with the warmer offshore water mass whose velocities were moving southward outside of Carmel Bay. Throughout the 24 hours centered on July 5, 2015 at 18:00 PST, the highly dynamic environment maintained strong convergence along the front. Fluctuations in the front's position resulted from interplay between opposing velocities; at times some sections move in opposite directions morphing the interface into a variety of shapes and breaking the front into sections. This normal-strain dominated example demonstrates a front that develops from two water masses converging in the direction perpendicular to the front and whose dynamic interplay may generate complex frontal shapes.

During the second example on June 22, 2014 at 13:00 PST, hereafter called SF1 (shear front 1), southward and slightly southwest velocities engulf the outer edge of the Monterey Peninsula and offshore relative to the front (Figure 3 d,e,f). Alongshore winds drive the circulation and generate upwelling of cold, deep water in the lee of the peninsula. The SST front is oriented southwestward and approximately linear (15.9 km long), marking the division between the cold upwelling plume and warmer offshore waters. The circulation inshore of the front is much slower and, in some sections, drives a strong convergence at the front, as in this case. However, the normal strain generated along the inshore frontal edge is overwhelmed by the shear

strain produced, primarily on the offshore edge. In some cases, both inshore and offshore waters move in approximately the same direction, but offshore velocities are larger, generating high relative vorticity and shear strain along the front. This front has a strain squared percentage of 83.4%, and predominantly shear strain continued to dominate this front for the following 12 hours. Unlike the highly dynamic environment of the previous example, the circulation pattern throughout this example is relatively steady with only slight shifts in position and strength of velocity and the SST gradient. Shear strain dominated fronts tend to be linear like this example.

3.2 Lagrangian transport before and after two example fronts

One paradigm of larval transport in coastal environments describes larvae accumulating along a front, thus being retained in the region and leading to enhanced local recruitment (Woodson et al. 2012). Here, we explore this relationship by analyzing the Lagrangian transport to and from the fronts for our two near-endmember examples (Figure 4).

Particles were released on a regular grid throughout a large portion of the c-nest domain shown in Figure 1b. Hourly releases up to 12 hours before the front reveal origination locations for particles that accumulated along each front at the specified time. Figure 4a and 4c show the Lagrangian trajectories of particles whose final positions were within 200 m of the front at the specified hour. Transport from the front was more straightforward, with particles released along the front and tracked for the following 12 hours; these trajectories are shown in Figure 4b and 4d.

In Figure 4a, particles accumulated along NF1 from both the offshore and inshore water masses due to strong, convergent velocities. This front accumulated particles from up to 4.9 km away 12 hours before the front. The majority of particles came from offshore, carried along or near the front as the warm offshore water mass moved towards the coast. Inshore, some particles were drawn to the front from a variety of directions. Particles released along this front moved cross-shore with the motion of the front itself. As the front started to break apart and the gradient lessen, particles in the southern half of the front were transported slightly southward. Particles along the northern half of the front were transport slightly northward and then many were pushed towards Carmel Bay's southern coast. Particles released along the front traveled a mean distance of 3.8 km and up to 6.9 km over 12 hours, but the mean change in latitude was only 2.4 km to the north over that time frame. The strong frontal convergence associated with the surrounding circulation accumulated particles and retained them in the nearby region.

In contrast, SF1 is characterized by considerable alongfront motion and thus the movement of particles through the region: nearly the same number of particles were swept into the front as those released along it, and then particles were exported from the immediate vicinity. Differing from the previous example, this front did not retain particles nearby. Twelve hours before the front, particles from the north up to 4.9 km away were moved southward by the strong alongshore circulation. A few particles from the inshore water mass were also drawn into the front along the Monterey Peninsula. The particles released along the front were rapidly transported southward with slight shifts towards and away from shore as the circulation evolved.

These particles traveled up to 16.0 km over 12 hours with a net mean distance of 11.2 km, mostly moving alongshore. The mean flow along this front, and the strong shear, rapidly moved particles along the front itself and out of the immediate area.

Both of these fronts concentrate material, but only one retains material nearby in the region; the other exports material away from the region. We focus the remaining analysis on Lagrangain transport after the front.

3.3 Statistics of alongshore transport from many fronts

In the rapidly evolving submesoscale circulation, a front's strain squared percentage can vary significantly over several hours. Here, we analyze fronts that last six hours or longer with a mean length greater than 3 km, about the scale of the Carmel Bay mouth. For fronts dominated by normal strain, their strain squared percentage throughout their duration must be less than 50%. In our model output, these criteria yielded 11 independent fronts dominated by normal strain for six hours or longer. Equivalent criteria for fronts dominated by shear strain (strain squared percentage greater than 50% throughout their six hour duration) returned 67 independent fronts. For comparison, only the 11 strongest strain percentage fronts in each category were included in the analysis. Particles were released along the fronts during the initial timestep and transported for six hours. The change in latitude over six hours was calculated for each particle. Figure 5 shows mean change in latitude for all particles released during each front. We record change in latitude instead of net distance to separate zonal differences from net movement along the coast. For larvae, latitudinal distance travelled quantifies the likelihood of local recruitment (i.e., to a

suitable habitat in the immediate vicinity of their release) versus more remote recruitment, to a more distant habitat.

The two types of fronts drive different patterns of Lagrangian transport. Fronts dominated by normal strain typically retain particles in the nearby region. Fronts dominated by shear strain often export particles further southward. This analysis calculates a mean latitudinal distance of 0.13 km over six hours for particles released along normal strain dominated fronts. Comparatively, fronts dominated by shear strain yield a mean latitudinal transport of 2.64 km southward over the same time interval. The difference in latitudinal transport of these two fronts is statistically significant (t-test: 2.53, $p \leq 0.03$). Figure 5 reveals that the main difference between front types and alongshore transport is robust.

The two example fronts discussed above with reference to Figure 4 are outlined in black and thus represent the longest front from each subset. To be clear, Figure 4 shows Lagrangian trajectories over 12 hours, whereas Figure 5 calculates the mean latitudinal distance over 6 hours. When fronts sustain dominance by normal or shear strain over a longer time period, these differences in Lagrangian transport amplify.

3.4 Comparison to the Okubo-Weiss Parameter

The Okubo-Weiss (OW) parameter (W) is another widely-used metric to identify coherent features in a flow field (Okubo 1970; Weiss 1991). It calculates the difference between strain and relative vorticity ($\omega = v_x - u_y$) and is defined:

$$W = {s_n}^2 + {s_s}^2 - \omega^2$$

This metric is often used to map the boundaries of eddies which are dominated by relative vorticity and thus negative values in their center, transitioning rapidly to strain dominated and thus positive values near their edges before decaying to low magnitudes more distantly. We find that the OW parameter is illuminating with respect to these submesoscale fronts.

Using all instances when fronts off the Monterey Peninsula are longer than 3 km, we extract the upper and lower quartile based on the mean strain squared percentage. The lower quartile values range from 1.7 to 43.4% and represent fronts dominated by normal strain. The upper quartile (shear strain dominated fronts) range from 73.6 to 98.2%. The relationship between these subsets of fronts and the OW parameter is shown as a cumulative distribution function (Figure 6). Fronts characterized by normal strain tend to have a large OW parameter (median = 5.6 hr^{-2}), whereas fronts characterized by shear strain have a much smaller OW parameter (median = 1.1 hr^{-2}). Fronts dominated by shear strain typically also have high relative vorticity. Indeed, for a purely linear front, $s_s^2 = \omega^2$, thus W is defined solely by the normal strain. In the approximately linear coastal fronts analyzed here, the shear strain and relative vorticity terms nearly cancel (r=0.91), producing a low OW parameter, particularly when shear strain dominates. In contrast, fronts resulting from normal strain have higher OW values. If the OW parameter was used for detection, it would recognize fewer than half the fronts off the southern edge of the Monterey Peninsula.

4 Discussion

Coastal fronts typically are centers for convergence, strong relative vorticity, and high strain compared to the surrounding region. Submesoscale features analyzed here at the mouth of Carmel Bay along the central California coast can be characterized by their strain squared percentages which express the fraction of total squared strain resulting from shear (as opposed to normal) strain. At the edges of the spectrum of this percentage are two types of fronts. A low strain percentage indicates the front results primarily from normal strain and is highly convergent; a high strain percentage means circulation along the front is dominated by shear strain deformation. Shear strain linear fronts also have strong relative vorticity.

Our classification of fronts dominated by normal and shear strain aligns with the accumulation and barrier models described in Woodson et al. (2012) and transport of fish eggs and larvae observed near coastal fronts (Nakata 1989). Fronts dominated by normal strain accumulate larvae on the front and retain these larvae in the immediate region. This type of front may draw larvae from both inshore and offshore, as was the case in the NF1 example on July 5, 2015, or from only one direction. Fronts dominated by shear strain most closely resemble the barrier model. These fronts act as a barrier to transport from offshore, quickly moving material along the front and further alongshore, away from local coastal habitat. Inshore of the front, velocities are much reduced. When the shear extends across the front, inshore circulation nearly aligns with the front and, though slower, it shuttles material away from the region, similar to offshore material. Other times, when the slower inshore circulation is nearly perpendicular to the front, material may converge near the

inshore frontal edge and be retained locally. Thus, shear strain dominated fronts act as a barrier to material from offshore, channeling it away from the immediate region.

These differences in Lagrangian transport patterns near the fronts have important implications for population connectivity derived from larval dispersal between separated coastal populations. If we assume that larvae offshore from the front primarily come from distant populations, normal strain dominated fronts may increase local connectivity with distant regions by drawing larvae from offshore and retaining them in the region, whereas shear strain dominated fronts shield the nearby coast from distant settlers. The concentrated export of larvae along the shear strain dominated front may sporadically lead to recruitment further down the coast. If we assume the majority of larvae inshore of the fronts were released locally, both normal and shear strain dominated fronts may enhance self-recruitment of populations in that region. Normal strain fronts accumulate material along the front, whereas shear strain dominated fronts will mostly retain the material in the region by acting as a preventive barrier to offshore transport. Because the submesoscale circulation is highly dynamic, this assumption of the relative proportion of larval origination based on position relative to the front may not hold true.

In this region off the Monterey Peninsula fronts longer than 1 km and dominated by shear strain occur 1.5 times more often than those characterized by normal strain (Figure 2). For fronts longer than 3 km (the length of the opening to Carmel Bay), this rate increases to shear dominated fronts being 2.0 times more frequent. If these probabilities typify other coastal areas with recurrent fronts, fewer than half of the fronts are characterized by normal strain associated with increased

retention of larvae from local and distant sources. Instead, the majority of fronts result from shear strain that rapidily export material from the region along their offshore edge and act as a barrier to offshore transport. Since regions with high probabilities of fronts commonly have high chlorophyll concentrations and larval recruitment (Woodson et al. 2012), the frequency of shear strain dominated fronts emphasizes their role in concentrating plankton inshore (Shanks and McCulloch 2003; McCulloch and Shanks 2003).

As a biophysical process, larval recruitment depends on biological parameters (e.g., pelagic larval duration, settlement window, swimming ability, etc.) in additional to the physical processes described here. Although larval recruitment only occurs if larvae are at the correct development stage and find suitable habitat, our research shows that the different kinds of fronts may either increase or decrease the likelihood of local recruitment by either retaining particles in the region or exporting them from the region, respectively.

Submesoscale fronts are complex, ephemeral features rapidly evolving in shape, length, and structure. Even though a front may overall be dominated by normal or shear strain, there may be sections of the front that behave differently, contributing to variability in Lagrangian transport. Additionally, fronts often transition from being dominated by shear to normal strain or vice versa over time-scales of hours. Thus, a front may initially export material from a region but later retain material in the region, or the reverse pattern. regardless, knowledge of the relative frequencies of the different forms of fronts (i.e., normal vs shear strain) along a coastline can provide insight into how local processes act to determine spatial and temporal probabilities of

larval retention and delivery and the consequences of these rates for populations of marine organisms. Our categorization of fronts by their strain squared percentage demonstrates the difference in Lagrangian transport between approximate end members on the spectrum of fronts.

Acknowledgements

This work was supported by a grant from the National Science Foundation (Award number 1260693).

REFERENCES

Ammann, Arnold J. 2004. "SMURFs: Standard Monitoring Units for the Recruitment of Temperate Reef Fishes." *Journal of Experimental Marine Biology and Ecology*. https://doi.org/10.1016/j.jembe.2003.08.014.

Anderson, T. W. (California State University). 1983. "Identification and Development of Nearshore Juvenile Rockfishes (Genus Sebastes) in Central California Kelp Forests." California State University, Fresno.

Bjorkstedt, Eric P., Leslie K. Rosenfeld, Brian A. Grantham, Yehoshua Shkedy, and Joan Roughgarden. 2002. "Distributions of Larval Rockfishes Sebastes Spp. across Nearshore Fronts in a Coastal Upwelling Region." *Marine Ecology Progress Series*. https://doi.org/10.3354/meps242215.

Carr, Mark H. 1991. "Habitat Selection and Recruitment of an Assemblage of Temperate Zone Reef Fishes." *Journal of Experimental Marine Biology and Ecology* 146: 113–37. https://doi.org/10.1016/0022-0981(91)90257-W.

Caselle, Jennifer E., Jono R. Wilson, Mark H. Carr, Dan P. Malone, and Dean E. Wendt. 2010. "Can We Predict Interannual and Regional Variation in Delivery of Pelagic Juveniles to Nearshore Populations of Rockfishes (Genus Sebastes) Using Simple Proxies of Ocean Conditions?" http://calcofi.org/~calcofi/publications/calcofireports/v51/Vol51_Casselle_pg91-105.pdf.

Clark, R. P., M. S. Edwards, and M. S. Foster. 2004. "Effects of Shade from Multiple Kelp Canopies on an Understory Algal Assemblage." *Marine Ecology Progress Series* 267: 107–19. https://doi.org/10.3354/meps267107.

Dagestad, Knut Frode, Johannes Röhrs, Oyvind Breivik, and Bjørn Ådlandsvik. 2018. "OpenDrift v1.0: A Generic Framework for Trajectory Modelling." *Geoscientific Model Development*. https://doi.org/10.5194/gmd-11-1405-2018.

Dauhajre, Daniel P., James C. McWilliams, and Yusuke Uchiyama. 2017. "Submesoscale Coherent Structures on the Continental Shelf." *Journal of Physical Oceanography*. https://doi.org/10.1175/JPO-D-16-0270.1.

Egbert, Gary D., Andrew F. Bennett, and Michael G. G. Foreman. 1994. "TOPEX/POSEIDON Tides Estimated Using a Global Inverse Model." *Journal of Geophysical Research* 99 (C12): 24821. https://doi.org/10.1029/94JC01894.

Graham, Michael H. 1997. "Factors Determining the Upper Limit of Giant Kelp, Macrocystispyrifera Agardh, along the Monterey Peninsula, Central California, USA." *Journal of Experimental Marine Biology and Ecology* 218 (1): 127–49. https://doi.org/10.1016/S0022-0981(97)00072-5.

Green, Kristen M., Ashley P. Greenley, and Richard M. Starr. 2014. “Movements of Blue Rockfish (Sebastes Mystinus) off Central California with Comparisons to Similar Species.” *PLoS ONE*. https://doi.org/10.1371/journal.pone.0098976.

Green, Kristen M., and Richard M. Starr. 2011. “Movements of Small Adult Black Rockfish: Implications for the Design of MPAs.” *Marine Ecology Progress Series*. https://doi.org/10.3354/meps09263.

Gula, Jonathan, Jeroen J. Molemaker, and James C. Mcwilliams. 2014. “Submesoscale Cold Filaments in the Gulf Stream.” *Journal of Physical Oceanography*. https://doi.org/10.1175/JPO-D-14-0029.1.

Hallacher, Leon E., and Dale A. Roberts. 1985. “Differential Utilization of Space and Food by the Inshore Rockfishes (Scorpaenidae: Sebastes) of Carmel Bay, California.” *Environmental Biology of Fishes*. https://doi.org/10.1007/BF00002762.

Harrison, Cheryl S., David A. Siegel, and Satoshi Mitarai. 2013. “Filamentation and Eddy-Eddy Interactions in Marine Larval Accumulation and Transport.” *Marine Ecology Progress Series*. https://doi.org/10.3354/meps10061.

Hodur, Richard M. 1997. “The Naval Research Laboratory’s Coupled Ocean/Atmosphere Mesoscale Prediction System (COAMPS).” *Monthly Weather Review*. https://doi.org/10.1175/1520-0493(1997)125<1414:TNRLSC>2.0.CO;2.

Johnson, Darren W. 2006a. “Density Dependence in Marine Fish Populations Revealed at Small and Large Spatial Scales.” *Ecology* 87 (2): 319–25. https://doi.org/10.1890/04-1665.

———. 2006b. “Predation, Habitat Complexity, and Variation in Density-Dependent Mortality of Temperate Reef Fishes.” *Ecology* 87 (5): 1179–88. https://doi.org/10.1890/0012-9658(2006)87[1179:PHCAVI]2.0.CO;2.

———. 2007. “Habitat Complexity Modifies Post-Settlement Mortality and Recruitment Dynamics of a Marine Fish.” *Ecology* 88 (7): 1716–25. https://doi.org/10.1890/06-0591.1.

Kenner, M. C. 1992. “Population Dynamics of the Sea Urchin Strongylocentrotus Purpuratus in a Central California Kelp Forest: Recruitment, Mortality, Growth, and Diet.” *Marine Biology* 112 (1): 107–18. https://doi.org/10.1007/BF00349734.

Lévy, Marina, Raffaele Ferrari, Peter J.S. Franks, Adrian P. Martin, and Pascal

Rivière. 2012. “Bringing Physics to Life at the Submesoscale.” *Geophysical Research Letters*. https://doi.org/10.1029/2012GL052756.

Lévy, Marina, Peter J.S. Franks, and K. Shafer Smith. 2018. “The Role of Submesoscale Currents in Structuring Marine Ecosystems.” *Nature Communications*. https://doi.org/10.1038/s41467-018-07059-3.

McCulloch, Anita, and Alan L. Shanks. 2003. “Topographically Generated Fronts, Very Nearshore Oceanography and the Distribution and Settlement of Mussel Larvae and Barnacle Cyprids.” *Journal of Plankton Research* 25 (11): 1427–39. https://doi.org/10.1093/plankt/fbg098.

McWilliams, James C. 2016. “Submesoscale Currents in the Ocean.” *Proceedings of the Royal Society A: Mathematical, Physical and Engineering Sciences*. https://doi.org/10.1098/rspa.2016.0117.

Nakata, Hideaki. 1989. “Transport and Distribution of Fish Eggs and Larvae in the Vicinity of Coastal Fronts.” *Rapports et Proces-Verbaux Des Réunions. Conseil International Pour l’Éxploration de La Mer* 191: 153–59. http://www.ices.dk/sites/pub/Publication Reports/Marine Science Symposia/Phase 2/Rapport et Proces-Verbaux des Reunions - Volume 191 - 1989 - Partie 23 de 161.pdf.

Okubo, Akira. 1970. “Horizontal Dispersion of Floatable Particles in the Vicinity of Velocity Singularities Such as Convergences.” *Deep-Sea Research and Oceanographic Abstracts*. https://doi.org/10.1016/0011-7471(70)90059-8.

Polovina, Jeffrey J., Evan Howell, Donald R. Kobayashi, and Michael P. Seki. 2001. “The Transition Zone Chlorophyll Front, a Dynamic Global Feature Defining Migration and Forage Habitat for Marine Resources.” *Progress in Oceanography*. https://doi.org/10.1016/S0079-6611(01)00036-2.

Reed, Daniel C., and Michael S. Foster. 1984. “The Effects of Canopy Shadings on Algal Recruitment and Growth in a Giant Kelp Forest.” *Ecology*. https://doi.org/10.2307/1938066.

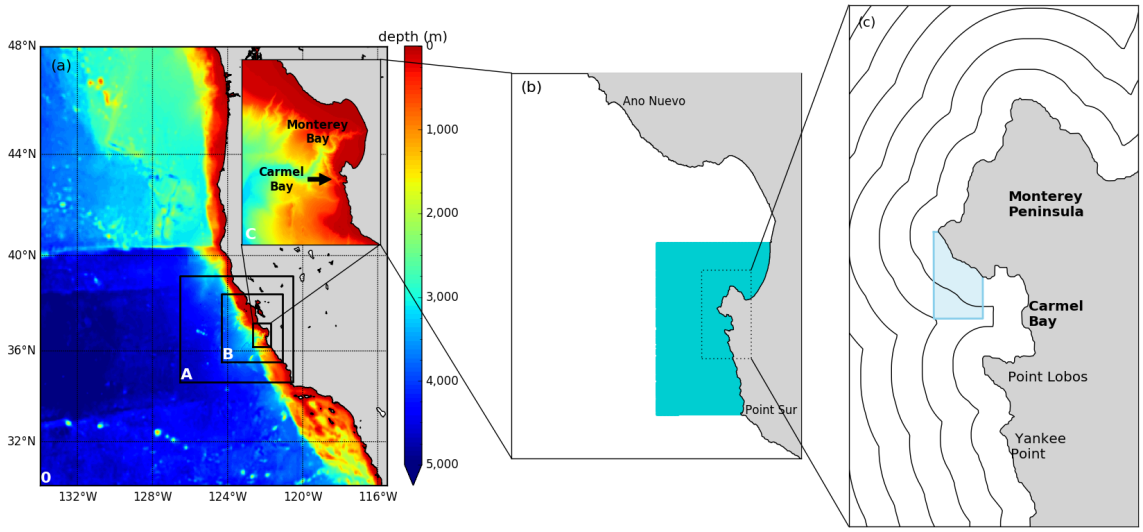

Figure 1. (a) Map of outermost domain and outlines of the finer resolution nests and inset shows the finest resolution nest domain. Color represents bathymetry. (b) C-nest domain and the region (in blue) where particles were released to calculate a front's spatial footprint from which it draws material. (c) Region surrounding the Monterey Peninsula showing area where algorithm searches for fronts in blue and black contours of distance from coast in 1 km intervals.

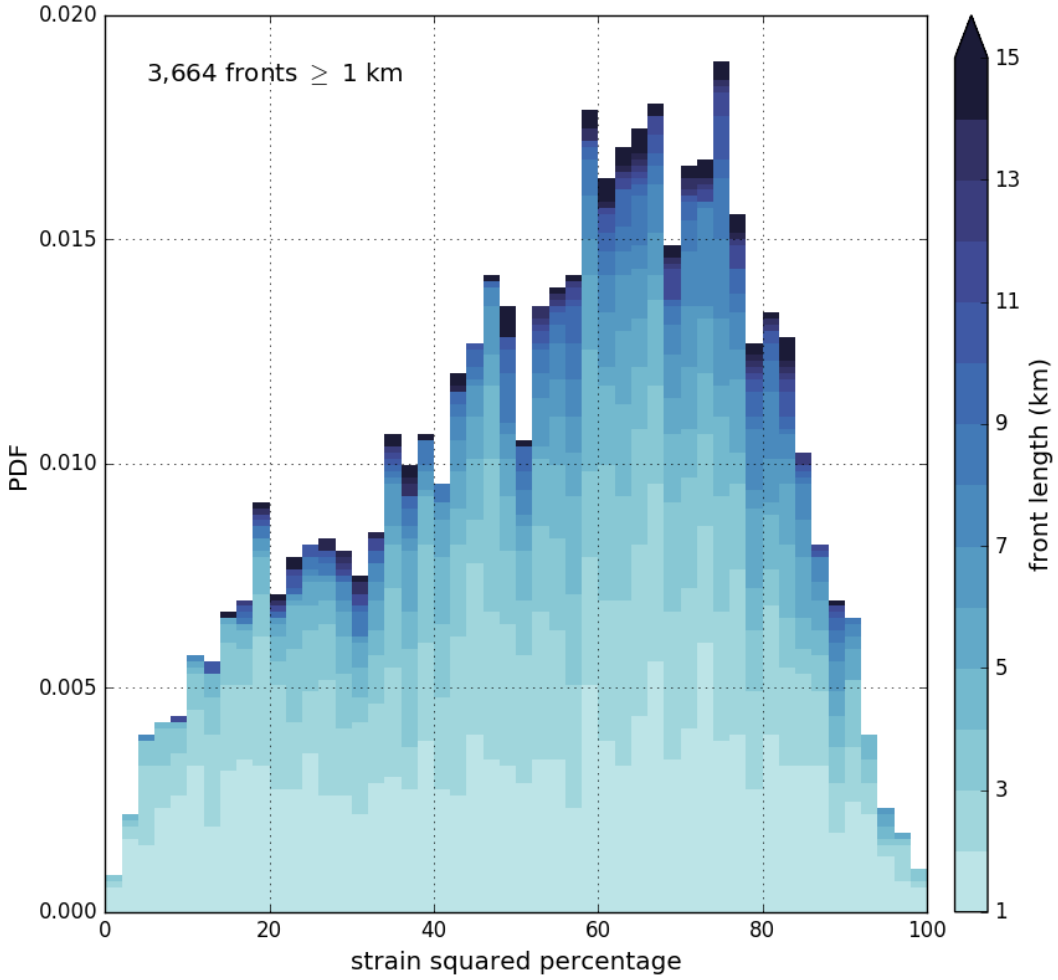

Figure 2. Probability distribution of strain squared percentage of fronts longer than 1 km outside of Carmel Bay. Colormap shows length of fronts.

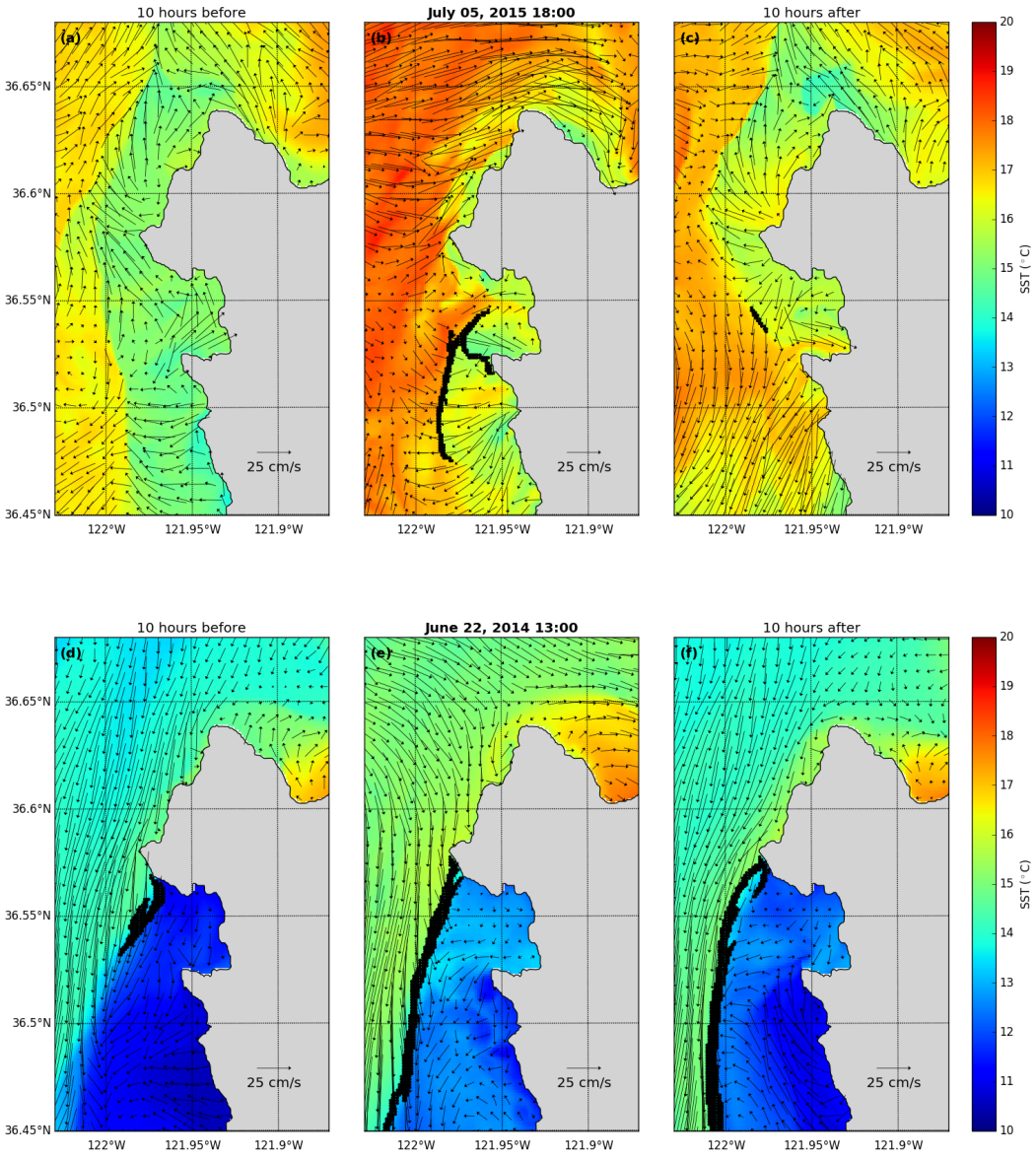

Figure 3. Maps of instantaneous Eulerian circulation during fronts characterized by normal strain (a-c) and shear strain (d-f) centered on two examples on July 5, 2015 18:00 PST (b) and June 22, 2014 13:00 PST (e), each flanked by the circulation 10 hours before (a,d) and after (c,f). Colormap shows SST, black points mark the front's location, and velocity vectors show instantaneous direction of velocity.

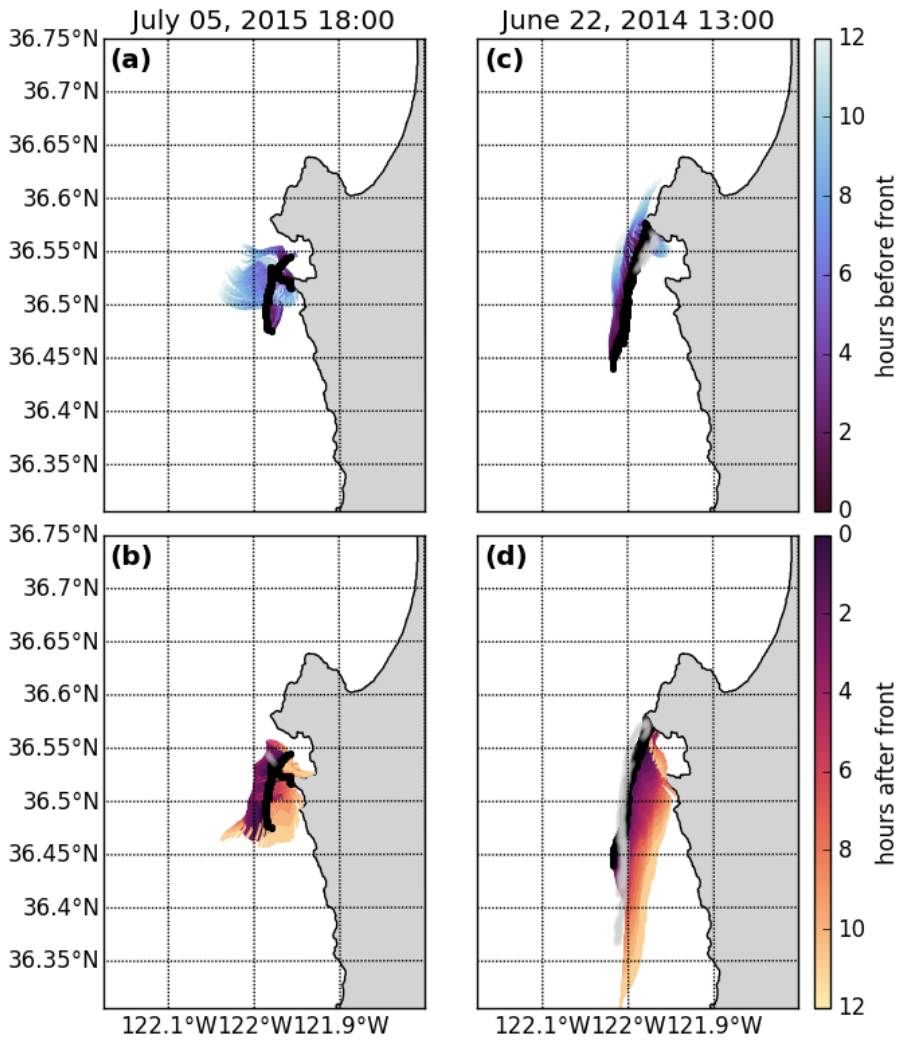

Figure 4. Maps of Lagrangian particle trajectories directly associated with the front: (a,c) particle trajectories showing location up to 12 hours before the front, and (b,d) particle trajectories of particles released along the front. Color of Lagrangian trajectory indicates the age of the particle in hours before it reaches the front or hours after the front. As in Figure 2b and 2e, black dots mark the frontal points, and now light gray dots mark the front's position 10 hours before (a,c) and after (b,d) the example time.

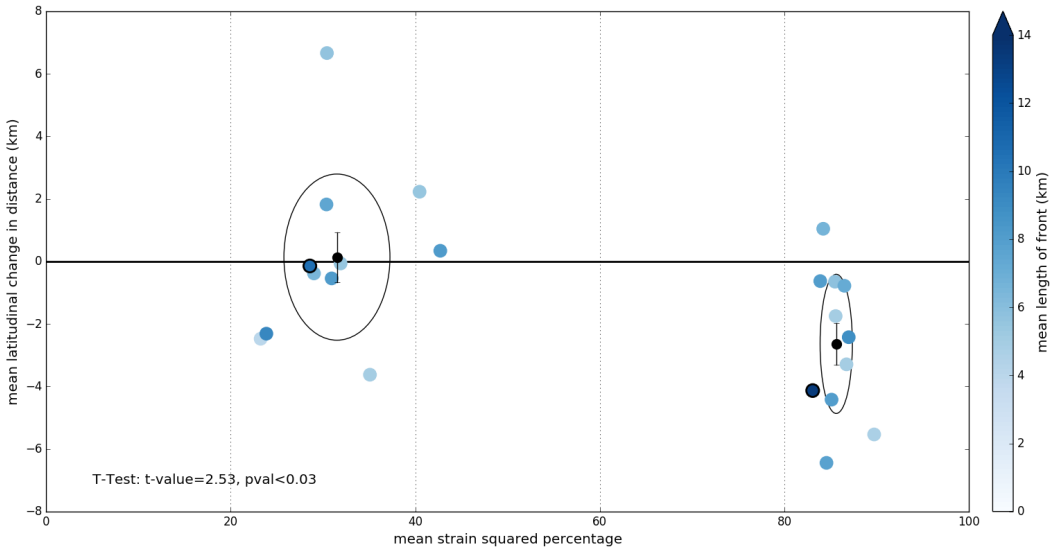

Figure 5. Two front types categorized by their mean strain squared percentage: fronts dominated by normal strain (left) and shear strain (right). Each dot represents a front and includes its mean conditions over the six hour duration: color represents mean length of front, x-position represents mean strain percentage, and y-position indicates mean latitudinal distance travelled over six hours by particles released along each front. Centered in each cluster, the black dot represents mean conditions for each type of front. Error bars show standard deviation of the mean; the surrounding black ellipses show standard deviation of the population. A t-test yields a t-value of 2.53 signficiant to the 97% level. The two front examples from Figures 3,4 are circled in black.

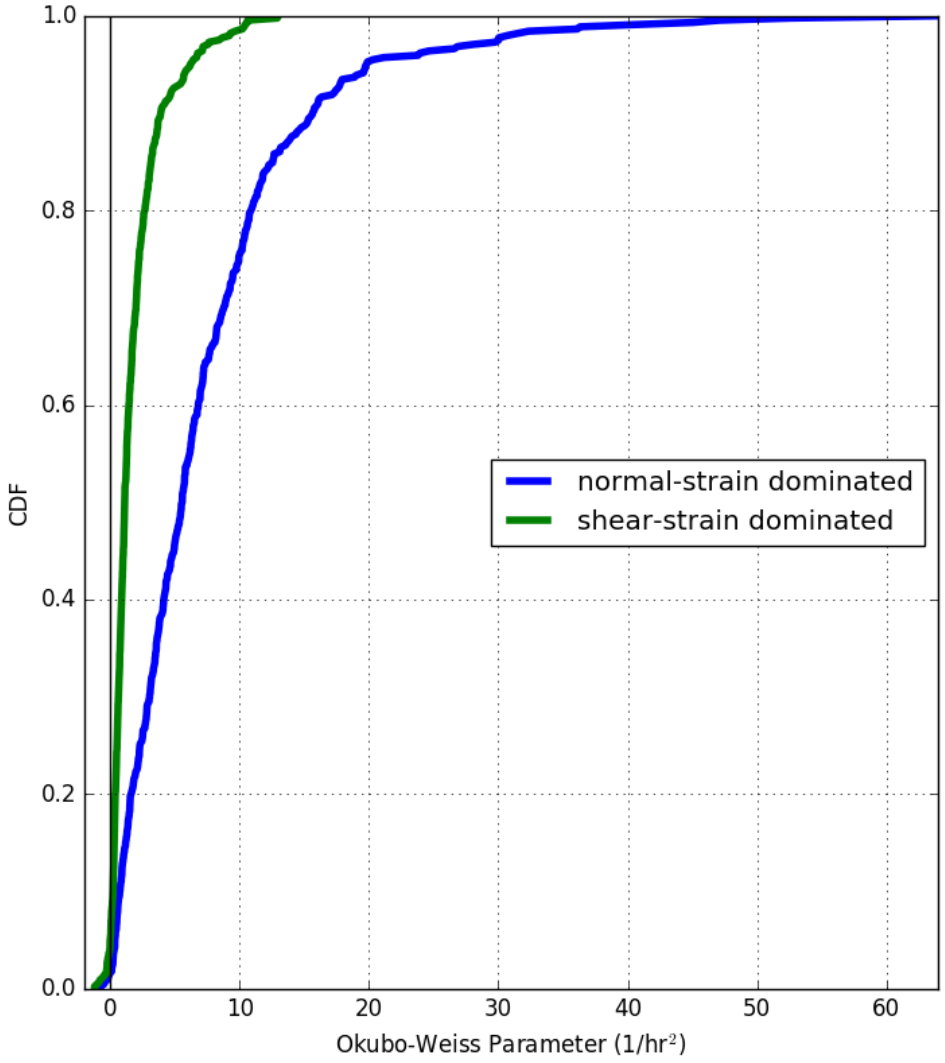

Figure 6. Cumulative distributions of the Okubo-Weiss parameter calculated along fronts. Fronts are categorizeds per mean strain percentage calculated along the face of the front: (1) dominated by normal strain (blue), and (2) dominated by shear strain (green).

CHAPTER FIVE
CONCLUSIONS

Larval transport processes driving population connectivity are inherently challenging to study. These processes straddle large spatial and temporal scales: propagules are transported by velocities changing on fine scales (e.g., near the coast, and vertically) and potentially travel 100s of kilometers over their pelagic larval duration lasting up to a few months. This dissertation presents a modeling method that includes both a large spatial domain and fine-scale coastal processes that influence larval transport. The next steps are to make this modeling processes more efficient and readily useable, which will encourage further evaluation of population connectivity between more MPAs and potential usage for decisions by MPA management.

In Chapter 2, I described a thorough study of Carmel Bay's circulation. An uncommon feature of this embayment's circulation was the development of a headland eddy over the canyon. Similar to headland eddies in other locations, this feature develops in the tidal residual circulation due to a vorticity flux into Carmel Bay by tidal motion past Point Lobos and the subsequent stretching of vortex tubes over the deep canyon. This feature was enhanced or reduced by northward and southward wind stress, respectively, due to the additional wind-driven vorticity flux near the headland. Another notable feature of the circulation was upwelling in the lee of the Monterey Peninsula that acts independently from the two nearest recognized upwelling centers near Point Sur to the south and Año Nuevo to the north. This local source of upwelling fuels the nearby ecosystems, enabling the marine communities within and around Carmel Bay to thrive. Building on the results from this study, we

encourage further investigation of upwelling in the lee of the Monterey Peninsula and southward along the Big Sur coast to the upwelling center off Point Sur.

In Chapter 3, I discussed consistent pathways of near-surface larval transport between southwest Monterey Bay and Carmel Bay. The parameters chosen for this study were based on kelp rockfish (*Sebastes atrovirens*) larvae, but the results are applicable to many other species with similar life histories and whose larvae are transported near the surface. Although the majority (99%) of larvae released in this study did not recruit to either suitable habitat region, we focus exclusively on the transport and connectivity of settlers to both habitat regions. The critical finding from this study was that exchange between larval sources separated by only a few kilometers was not equal. In fact, there were more northward recruits than southward recruits due to the dynamics around the Monterey Peninsula. This connection is in opposition to generally southward and offshore mean circulation of the California Current during the upwelling season. Unequal exchange between regions provides insight to how MPA systems function and has important implications for their management. Because 2014 and 2015 were rather anomalous years in the California Current System, extending this study temporally will strengthen the analysis. Building on this study, I suggest adding additional MPAs within and around Monterey Bay to investigate the levels of connectivity between these regions. One extension of this research is to compare dispersal of particles given parameters reflective of different fishes (e.g., KCGB complex and the BYO complex, two groups of nearshore rockfishes differentiated by shallow and deeper habitat preference and life histories). This results from this type of study will provide further detail of the

similarities and differences in dispersal patterns of larvae with different vertical trajectories and timing of the pelagic period for MPA management.

A larger next step is to add waves to the model. In southern Carmel Bay, wave focusing by the Carmel Canyon leads to a highly erosional sediment regime (Storlazzi and Wingfield 2005); the coarse sand (pebbles) and steep slope attest to the high energy pounding Monastery Beach near the canyon head. The inclusion of waves in a further investigation of the circulation within Carmel Bay may yield better model-data agreement close to shore and near the canyon, enables deeper investigation of dynamics within the canyon, and potential north-south spatial differences within the bay. Additionally, there is an opening in the literature to study wave effects on larval dispersal, which has only been included in a few cases. Near the surface, there is a small net transport in the direction of wave propagation called Stokes drift which can be calculated from the wave spectrum. Stokes drift is relevant for all particles concentrated near the surface, especially over the inner shelf (Monismith and Fong 2004). In northern Norway, there were distinct differences in dispersal patterns between simulations with and without Stokes drift (Röhrs et al. 2014). Off the Australian west coast and surf zone in southern Monterey Bay, modeled dispersal patterns were more consistent with field data when including wave effects (Feng et al. 2011; Fujimura et al. 2014). From the wave spectra measured by Monterey Bay NDBC 46042 from 1987 to 2015, preliminary calculations indicate Stokes drift is stronger than 2 cm/s in 35-50% of the measurements, depending on season. From these calculations, Stokes drift is strongest from April to June, coincident with spring upwelling and larval release for many species. This calculation of Stokes drift is

comparable to late stage larval swimming speeds on the order of a few centimeters, which have a dramatic influence on larval transport and resultant settlement (Drake et al. 2018). In Chapter 3, less than 1% of the floats released recruited to the suitable habitat regions around the Monterey Peninsula; by including Stokes drift, onshore motion comparable in magnitude to late-stage swimming speeds, the number of recruits returning to the Monterey Peninsula (or other suitable habitat regions along the coast) will likely increase. Collectively, these initial calculations provide compelling evidence to continue investigation of wave-effects on larval dispersal off the central California coast.

Finally, in chapter 4, I evaluate fronts near the southern edge of the Monterey Peninsula and their resultant Lagrangian transport. Fronts were characterized by strain squared percentage, which differentiates fronts that accumulate and retain material in the region from those that aid in export by concentrating material and channeling it laterally away from the region. As dynamic, ephemeral features, fronts often shift over their lifecycle which generates a hybrid transport pattern. The Lagrangian transport associated near these fronts have important implications for nutrients, plankton, larvae, pollutants, and potentially search and rescue operations. The next step in this research is to include the vertical dimension in the investigation of Lagrangian transport associated with the front. Including the vertical dimension may show particles subduct at the front, and if true, this subduction may hold larvae in the immediate region for longer, potentially enhancing recruitment. The differences in horizontal and fully-passive Lagrangian transport near a front will further detail the circulation near these biological hotspots.

This suite of research focuses exclusively on transport processes around the Monterey Peninsula (Figure 1), a rather unique environment. The results from Chapter 2 are unique to Carmel Bay, but some of the circulation processes (e.g., headland eddy, canyon upwelling) are found in many other bays. Some of the larval dispersal patterns described in Chapter 3 are likely applicable to nearby MPAs, particularly in eastern boundary upwelling systems. Unequal exchange of larvae between nearby MPAs, particularly ones separated by a headland, and commonalities of particle trajectories of successful recruits compared to non-recruits through bulk particle analysis may show similar results to Chapter 3, but differences in coastline geometry, orientation, and local circulation with make connectivity between MPAs and non-protected suitable habitat regions different in each section of the coastline. I encourage further research on this scale of both the circulation and larval connectivity between other MPAs for comparison. The modeling method and analyses may be used to investigate larval transport to and from small embayments around the world and open sections of the coastline. The types of fronts and their resultant Lagrangian transport described in Chapter 4 are applicable to many other locations off the US west coast and elsewhere that fronts frequently occur in the lee of headlands. This suite of research demonstrates a few ways submesoscale and coastal processes modify the circulation and thereby transport of material in the planktos.

REFERENCES

Drake, Patrick T., Christopher A. Edwards, Steven G. Morgan, and Erin V. Satterthwaite. 2018. "Shoreward Swimming Boosts Modeled Nearshore Larval Supply and Pelagic Connectivity in a Coastal Upwelling Region." *Journal of Marine Systems* 187: 96–110. https://doi.org/10.1016/j.jmarsys.2018.07.004.

Feng, Ming, Nick Caputi, James Penn, Dirk Slawinski, Simon de Lestang, Evan Weller, and Alan Pearce. 2011. " Ocean Circulation, Stokes Drift, and Connectivity of Western Rock Lobster (Panulirus Cygnus) Population ." *Canadian Journal of Fisheries and Aquatic Sciences*. https://doi.org/10.1139/f2011-065.

Fujimura, Atsushi G., Ad J H M Reniers, Claire B. Paris, Alan L. Shanks, Jamie H. MacMahan, and Steven G. Morgan. 2014. "Numerical Simulations of Larval Transport into a Rip-Channeled Surf Zone." *Limnology and Oceanography*. https://doi.org/10.4319/lo.2014.59.4.1434.

Monismith, Stephen G., and Derek A. Fong. 2004. "A Note on the Potential Transport of Scalars and Organisms by Surface Waves." *Limnology and Oceanography*. https://doi.org/10.4319/lo.2004.49.4.1214.

Röhrs, Johannes, Kai Håkon Christensen, Frode Vikebø, Svein Sundby, Øyvind Saetra, and Göran Broström. 2014. "Wave-Induced Transport and Vertical Mixing of Pelagic Eggs and Larvae." *Limnology and Oceanography*. https://doi.org/10.4319/lo.2014.59.4.1213.

Storlazzi, Curt D., and Dana K. Wingfield. 2005. *Spatial and Temporal Variations in Oceanographic and Meteorologic Forcing along the Central California Coast, 1980-2002*. US Geological Survey.

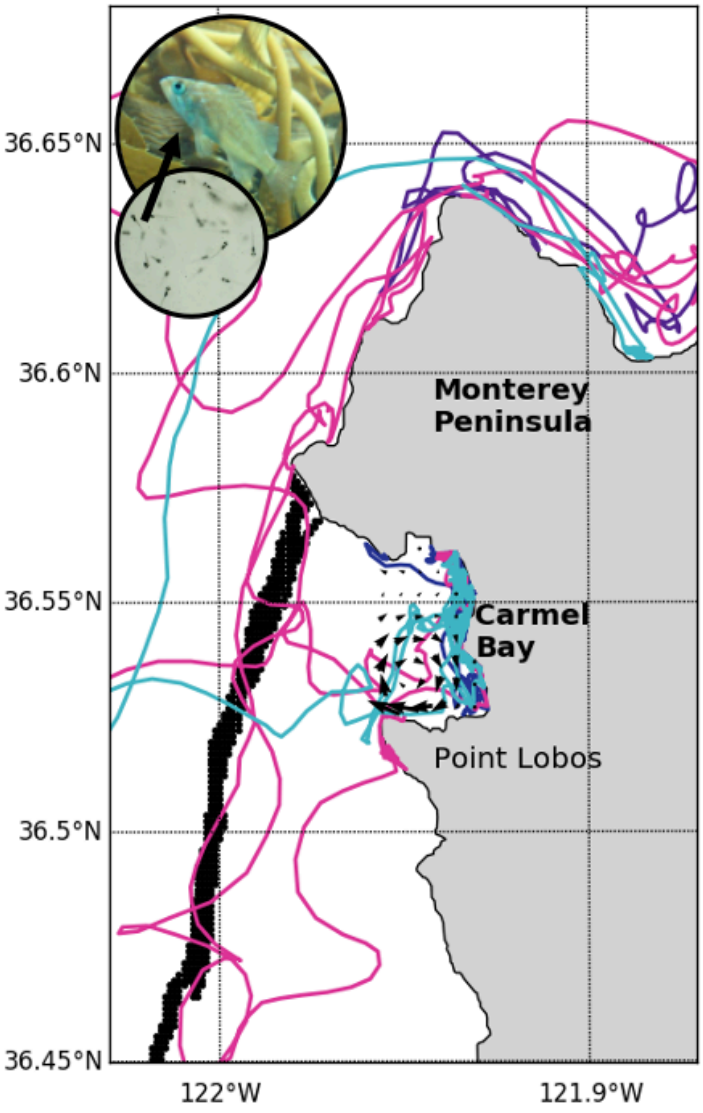

Figure 1. Summary cartoon of the research contained within this dissertation: (1) small black vectors in Carmel Bay represent the circulation described in chapter 2, (2) the colored lines depict a sample of larval trajectories that were investigated in chapter 3, and (3) the thick black line marks one instance of a long front off the southern edge of the Monterey Peninsula characterized in chapter 4.